Ailan Phan

Immunohistochemical and morphological characterization of GABAergic cells in LEC

Master`s thesis

Faculty of Medicine

Department of Neuroscience

2015

Supervisors:

Menno Witter and Bente Jacobsen

Table of Contents

Table of Contents 1
Abbreviations 3
Acknowledgements 4
Abstract 5
1. INTRODUCTION 6
2. MATERIALS AND METHODS 18
2.1. Animals 18
2.2. Perfusion 18
2.3. Immunohistochemical characterization of the GABAergic cells in LEC 19
2.3.1. Immunohistochemistry against CA^{2}+ binding proteins and neuropeptides 20
2.3.2. Image acquisition 22
2.3.3. Data analysis 22
2.4. Somatodendritic morphology of GABAergic cells in LII / L III of LEC 24
2.4.1. Intracellular injections 24
2.4.2. Confocal image analysis 26
2.4.3. Morphological analysis 26
3. RESULTS 28
3.1. Morphological properties of interneurons in L II and L III 28
3.1.1 Small multipolar cell 29
3.1.2 Big multipolar cell 31
3.1.3 Pyramidal like cell 32
3.1.4 Bow tie neuron 34
3.1.5 Bipolar cell 35
3.1.6 Small bipolar spindle cell 37
3.1.7 Triangular neuron 38
3.1.8 Radial neuron 40

3.2 Immunohistochemical characterization of GABAergic subpopulations of LEC 43
3.2.1 Parvalbumin....46
3.2.2 Calbindin....53
3.2.3 Calretinin....61
3.2.4 Vasoactive intestinal peptide....67
3.2.5 Somatostatin....74
3.2.6 Cholecystokinin....80
3.2.7 Neuropeptide Y....86
3.3 Double immunohistochemistry....91
3.3.1 VIP – CR....91
4 METHODOLOGICAL CONSIDERATIONS....97
5 DISCUSSION....99
5.1 Morphological characterization of interneurons in LEC L II/II....99
5.1.1 Morphological cell types in LEC L II / III....99
5.2 Immunohistochemical characterization of GABAergic cells in LEC....101
5.2.1 Immunoreactivity of Ca2+ binding proteins and neuropeptides in LEC 102
5.2.2 Distribution of GABAergic cell populations across LEC....103
5.2.3 Functional implications of the distribution of GABAergic cell groups 104
5.2.4 Overlapping distributions of immunoreactive cell types....106
5.2.5 Co- expression of calcium binding proteins and neuropeptides with GABA 107
5.2.6 Neurochemical markers and cell types in LEC....108
5.2.7 Interneuron heterogeneity and LEC....111
5.3 Future Directions....112
6 CONCLUSION....115
REFERENCES....117

Abbreviations

EC - Entorhinal cortex

GABA – Gamma amino butyric acid

MEC - Medial entorhinal cortex

LEC - Lateral entorhinal cortex

PV - Parvalbumin

CB - Calbindin

CR - Calretinin

VIP - Vasoactive intestinal peptide

NPY - Neuropeptide Y

SST - Somatostatin

CCK - Cholecystokinin

INs - Interneurons

Acknowledgements

This study was carried out at the Kavli Institute for Systems Neuroscience and Centre for Neuronal Computation (CNC) at the Norwegian University of Science and Technology (NTNU), under the supervision of Dr. Menno Witter and Bente Jacobsen.

I would especially like to thank Bente Jacobsen for taking me under her wing, for always being happy to answer questions and teaching me the technical skills needed for this work. I also want to thank Menno Witter for taking time out of his busy schedule to answer questions.

I would also like to thank the cheerful group of people in the Witter group, for sharing your knowledge and advice on technical and academic matters.

Finally, I would like to thank my family and Patrick for cheering me on and support during my studies.

Abstract

The two subdivisions of the entorhinal cortex, the medial and the lateral entorhinal cortex have been implicated a crucial role in spatial cognition but appear to be functionally distinct. To understand the functional contribution of the lateral entorhinal cortex basic knowledge about the neurons constituting the system is needed.

In this study, the GABAergic cell population in LEC was immunohistochemically and morphologically characterized. For this purpose, the transgenic mouse line GAD 67 – GFP was used for immunohistochemical investigation of co-localization of GABA with Ca^2+ binding proteins and neuropeptides. A morphological study of GAD positive cells in L II / III of LEC was additionally performed by intracellular injections of Alexa Fluor Hydrazide 568 in fixed brain slices. The results indicate that the GABAergic cell population in LEC is neurochemically and morphologically diverse. The pattern of distribution across LEC for all immunoreactive cell groups, suggests that a diverse cell population is present across all areas of LEC but display a speficic pattern of distribution across LEC laminae.

1. INTRODUCTION

The entorhinal cortex (EC) is a key structure in the hippocampal memory system, where it functions as a major gateway for the interchanging streams of cortico-hippocampal information. In this system, several lines of evidence have shown that EC is actively engaged with processing of spatial and non - spatial information about the world. These two types of information appear to be distinctly processed in the two subdivisions of EC, the lateral entorhinal cortex (LEC) and the medial entorhinal cortex (MEC). The MEC has shown to be involved in spatial processing and contains complex cells known as grid cells (Hafting, Fyhn et al. 2005). In LEC cells are functionally different, and show little spatial modulation but appear to encode for objects and the location of objects, these cells are known as object place cells (Hargreaves, Rao et al. 2005, Deshmukh and Knierim 2011). Taken together, these findings suggests that LEC is involved in encoding information about w*hat* is in the environment, whereas MEC encodes information about *where*.

How these processes come about in MEC and LEC is largely unknown, as little is known about the cells present in the EC network. Principal neurons in LEC and MEC have been well characterized when it comes to their electrophysiological and morphological properties (Canto 2011, 2011), but little is known about the interneuronal population, the GABAergic cells. To fully understand how EC encodes spatial and non-spatial information, an investigation into the cell types constituting the system and their connectivity is essential.

THE HIPPOCAMPAL- PARAHIPPOCAMPAL REGION

The hippocampal formation lies enclosed by the parahippocampal region and consists of the dentate gyrus, cornus ammonis subfields; CA1, CA2, CA3, and the subiculum (Fig 1). The hippocampus was early implicated in learning and memory (Scoville and Milner 1957). A further investigation into the workings of the hippocampus, led to the discovery of neurons known as place cells. These cells fire at specific places in the environment when an animal is moving freely around in it. Collectively, the place cells' firing fields from different locations are believed to provide an internal map of the environment (O'Keefe and Dostrovsky 1971). Taken together, these findings point to a particular role for the hippocampus in spatial memory, and provided a substrate for investigating learning and memory in animals.

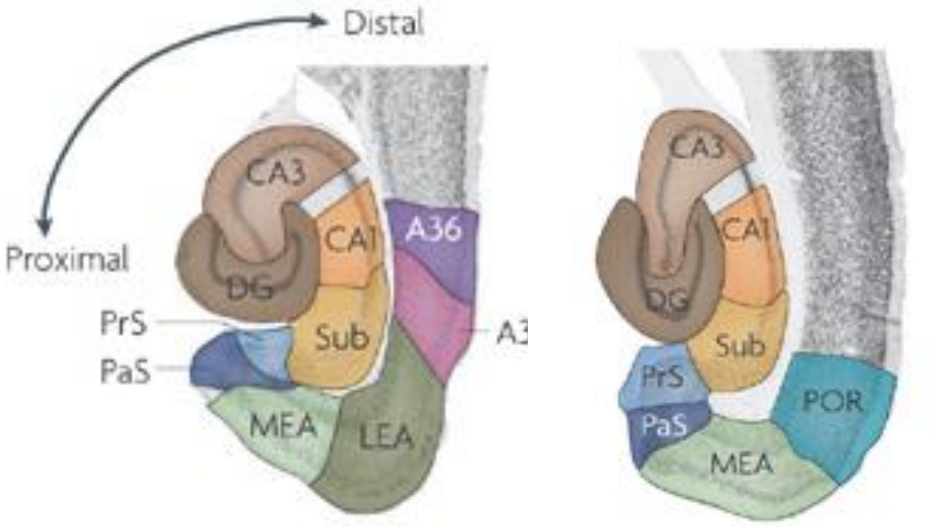

Figure 1: The hippocampal and parahippocampal region.Horizontal sections of the hippocampal parahippocampal region. Figure from Van strien, Cappaert and Witter. 2009.

Neuroanatomical data show that the hippocampus is strongly and reciprocally connected with EC. A major input to the hippocampus arises from the superficial layers of EC via the perforant path, whereas the hippocampal output is targeted towards the deep layers of EC (Witter, Wouterlood et al. 2000) The parahippocampal region consists of EC, the perirhinal cortex, the post rhinal cortex, and pre- and parasubiculum (Van Strien, Cappaert et al. 2009). Both perirhinal and postrhinal cortices are reciprocally connected with EC. The pattern of connectivity with EC suggests that the postrhinal cortex is involved with spatial processing. This is related to the fact that the postrhinal cortex receives heavy visuo-spatial input from other brain areas, and projects to the MEC preferentially. Lesion studies do however not support this anatomical inference, but instead suggest that the postrhinal cortex is involved with contextual learning (Furtak, Wei et al. 2007).The perirhinal cortex, which receives heavy inputs from the olfactory and insular cortices, has been implicated in object recognition as well as object discrimination (Bartko, Winters et al. 2007). Previous findings from studies on the pre and parasubiculum revealed that both areas contained an abundance of spatially modulated cells, similar to MEC (Boccara, Sargolini et al. 2010).The connectivity pattern of these structures showed that EC receives presubicular input preferentially in L I and III in MEC, and that parasubicular input innervates mainly L II of both LEC and MEC (Caballero-Bleda and Witter 1993). The pre- and parasubiculum receive reciprocal projections from LEC and MEC. On the whole, these data show that the parahippocampal and hippocampal regions form an intricate system, where information can be processed in parallel among the structures involved.

THE ENTORHINAL CORTEX

The EC is a six layered cortex that traditionally is subdivided into two main areas, MEC and LEC. MEC and LEC can be further subdivided into five regions where MEC comprises a medial entorhinal region and a caudal entorhinal region, and LEC; a dorsal lateral entorhinal region (DLE), dorsal intermediate entorhinal region (DIE) and ventral intermediate entorhinal region (VIE) (van Groen, Miettinen et al. 2003) . These subdivisions of MEC and LEC do not only show differences in their cytoarchitectonics, but also in the pattern of connectivity to and from cortical and subcortical areas (Insausti, Herrero et al. 1997).

The first layer of EC appears almost cell free and is relatively homogeneous. Neurons in this layer are embedded in fibers from the olfactory bulbs, and apical dendrites from principal cells in other layers (Witter and Wouterlood 2002). It also harbors small horizontal and multipolar neurons that have been shown to be glutamatergic or GABAergic cells. L II, is packed with pyramidal and atypical principal cells, called stellate cells in the MEC and fan cells in the LEC (Canto 2011, Canto and Witter 2012, Canto and Witter 2012).This layer has previously been described to contain the interneuron types; the basket and chandelier cells ((Jones and Bühl 1993, Soriano, Martinez et al. 1993). L III contains mostly pyramidal cells, but also multipolar neurons (Canto, LEC paper). Chandelier cells have also been reported in this layer (Soriano, Martinez et al. 1993), as well as pyramidal-like interneurons, which have only been described in MEC (Gloveli, Schmitz et al. 1997, Canto, Wouterlood et al. 2008). The principal cells in L II and III have axons that project via the perforant pathway and target various subfields of the hippocampal formation (Witter, Wouterlood et al. 2000). L IV; also known as the lamina dissecans, contains in general a low number

of cells, a few pyramidal and interneuron cells can be found in this layer. L V consists of pyramidal cells and multipolar neurons, as well as horizontal and bipolar cells that are situated mainly superficially in the layer (Canto, Canto LEC MEC papers). In L VI, there are spiny spherical multipolar neurons and pyramidal cells, the latter has only been reported in MEC.

As I will primarily focus on the lateral entorhinal cortex in this thesis, descriptions for the laminar, subregional and anterior- posterior connectivity will be mainly described for LEC below.

CORTICAL and SUBCORTICAL connectivity of LEC

LEC connectivity with other cortical and subcortical structures is quite intricate and differs across layers, subregions and along the anterior – posterior axis. For the laminar connectivity of EC, the standard view is that the superficial layers II and III are more involved with mediating hippocampal input, and that the deep layers are considered to be involved in mediating hippocampal output back to the cortex. This distinction is however not strict, as intrinsic connectivity between the layers allows for cross laminar integration of information (Witter and Wouterlood 2002). In the superficial layers of LEC, the main cortical input arrives from the perirhinal, olfactory and insular cortices. The perirhinal cortex preferentially target superficial L I and III, while the olfactory cortex sends projections to L I and insular cortex targets L III. Subcortical input to these layers arrives in L III from hippocampal (CA1 and subiculum) and amygdaloid areas. Projections from the hippocampus and the amygdala additionally target L V. The deep layers V and VI receive mainly input from the pre and infra limbic

cortices, as well as the anterior cingulate cortex. Main output from LEC to cortical areas arises from L V, while L II and III targets the hippocampal formation particularly, and L VI provides output to the thalamus(Fig. 2**Error! Reference source not found.**) (Shepherd and Grillner 2010).

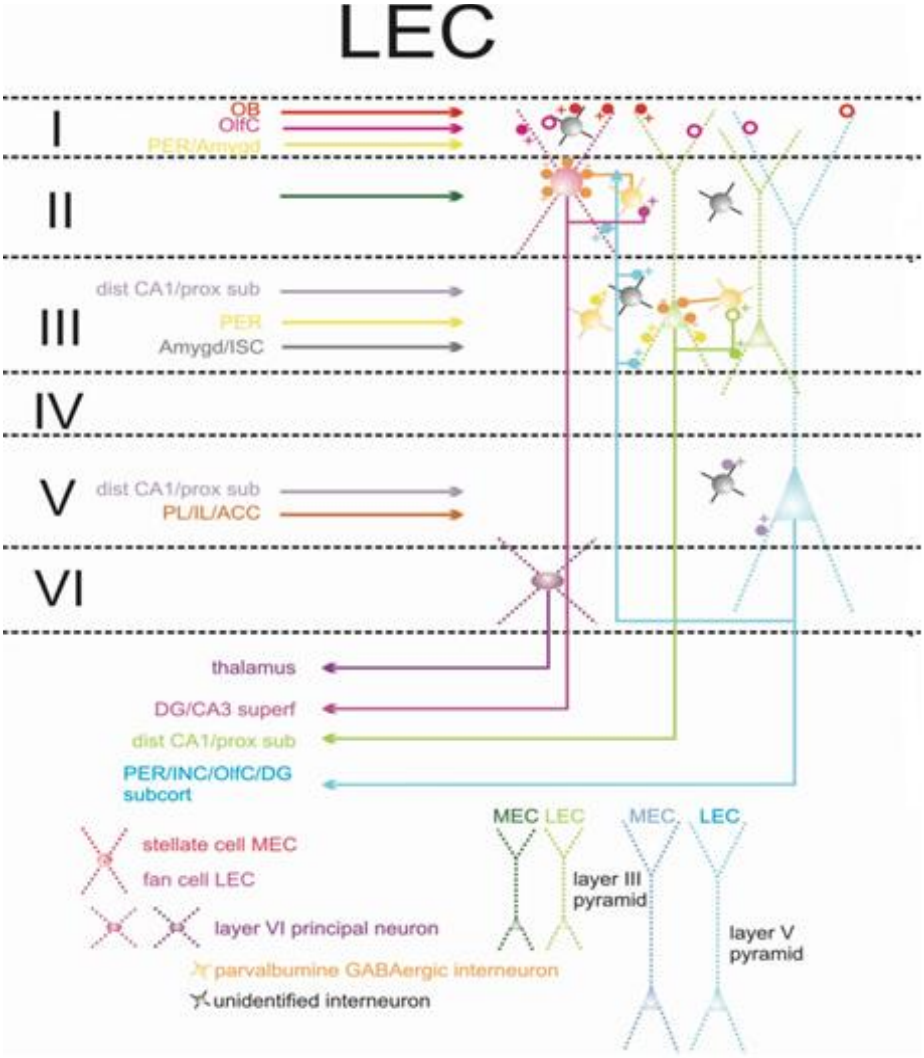

Figure 2: Main cortical and subcortical connectivity with LEC across laminae. Figure from Moser et al. 2010.

There are also subregional and anterior-posterior differences in the connectivity pattern of LEC with subcortical and cortical areas. The pattern

of connectivity between subdivision DLE, DIE and VIE is quite extensive. Most of the subregions, not always VIE, provide extensive projections to perirhinal, insular, pre and infra limibic, temporal, frontal, occipital and even parietal areas (Insausti, Herrero et al. 1997). There are in addition reciprocal connectivity between all subregions of LEC with CA1 and subiculum (Naber, Lopes da Silva et al. 2001), as well as the amygdaloid complex (Pitkänen, Pikkarainen et al. 2000). With regards to the anterior-posterior differences of the connectivity in the EC not much data exists. However, two recent tracer studies, show that both insular and orbitofrontal projections (Kondo and Witter 2014, Mathiasen, Hansen et al. 2015) have a characteristic distribution across the anterior-posterior axis.

INTERNEURONS AND INHIBITION

Interneurons (INs) are local circuit neurons, which mainly modulate activity within a cortical area. Most of these cells express GABA (γ-aminobutyric acid), and thus provide inhibition in the network (Markram, Toledo-Rodriguez et al. 2004). These cells predominantly modulate principal cells activity, but there are reports of interneuron groups preferentially targeting other INs (Acsady, Görcs et al. 1996, Gulyás, Hájos et al. 1996). Findings of both inhibitory and excitatory synapses on the cell body of INs confirms that they receive input from both principal neurons and INs.

In an inhibitory network, these cells are shown to participate in feed forward and feedback inhibition, as well as lateral inhibition (Markram, Toledo-Rodriguez et al. 2004, Isaacson and Scanziani 2011). Feed forward inhibition is a process in which an interneuron receives excitatory output

and exerts inhibition on to another cell (Mittmann, Koch et al. 2005) while, feedback inhibition is considered as a self- regulatory mechanism, in which the activity of a cell can be modulated indirectly in connection with another cell (Bacci, Huguenard et al. 2003). The last kind of inhibition, lateral inhibition, is a mechanism that has been shown to sharpen or tune a response, where the activity of a cell depresses the response of cells surrounding it (Blakemore and Tobin 1972) (Fig 3).

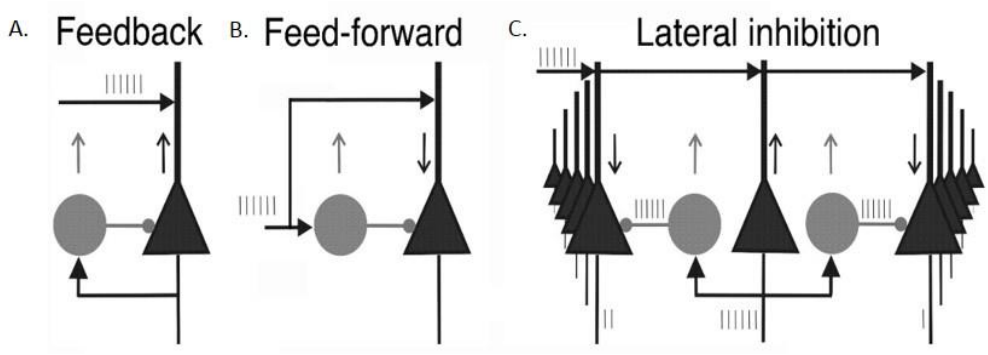

Figure 3: (A) Feedback inhibition in an principal cell (black) by reciprocal connection to an interneuron (grey) (B) Feedforward inhibition, a process where excitatory input to an interneuron leads to inhibition to another cell (C) Lateral inhibition, a process where the activity of a principal cell in connection with interneuronscan depress the activity of other cells nearby. Figure from Jonas and Buzsaki (2007).

Classifying INs has proven to be a challenging task as the cell group is highly heterogeneous. Nonetheless, classifications based upon several properties of the cells such as the morphology, electrophysiology and expression of molecular marker have proven useful in distinguishing groups of INs (Fig 4). For determining the morphological characteristics of a cell, the structural elements: the soma, dendrites, axon and synaptic connectivity can be considered. Certain cell types display a distinct cell morphology which makes them easily recognizable. An example is the chandelier cells, these cells display a peculiar form as their axonal tree forms vertical rows of boutons, making them resemble a chandelier (Howard, Tamas et al. 2005). Another type are the basket cells, which display pericellullar baskets of axonal fibers onto their target cell (Markram, Toledo-Rodriguez et al. 2004, Freund and Katona 2007). The electrophysiological properties of cells are important in understanding what kind of role these cells play in a circuit. The molecular features of a cell include a variety of molecules that can be categorized into several groups, among these are calcium binding proteins, such as parvalbumin (PV), calretinin (CR) and calbindin (BC). Neuropeptides are also useful markers for cell classification, these include neuropeptide Y (NPY), cholecystokinin (CCK), vasoactive intestinal peptide (VIP), somatostatin (SST), neurotransmitters and structural proteins can also be used for cell classification(Markram, Toledo-Rodriguez et al. 2004, Ascoli, Alonso-Nanclares et al. 2008).

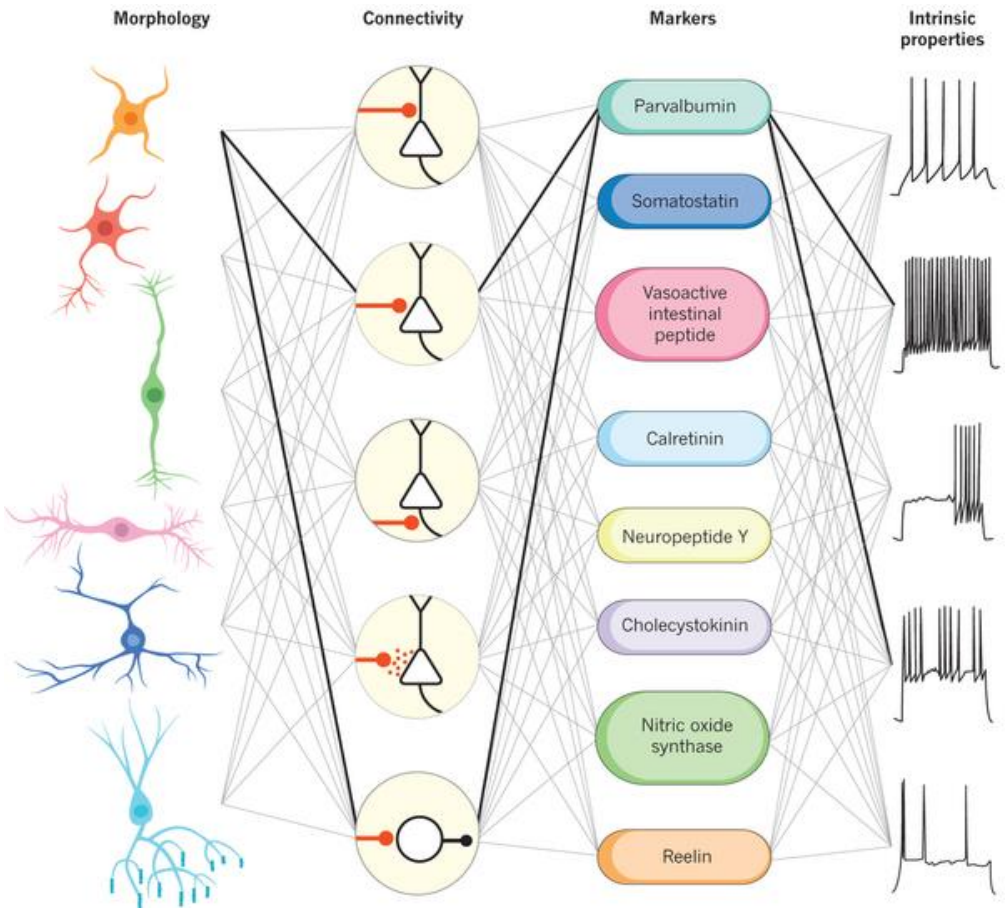

Figure 4: Interneurons are commonly defined by a combination of criteria based on morphology, connectivity, molecular markers and intrinsic properties (i.e electrophysiology). Figure from Kepecs and Fishell (2014).

Characterization by molecular identity can be somewhat unambiguous as the molecular profile of a cell is quite diverse. Nevertheless, certain molecular markers have proven to be expressed only in specific cell groups. As an example, the calcium binding protein PV has been demonstrated in fast spiking cells, and is often found in basket and axo-axonic cells. Taken together, these findings show that INs are diverse, but can be distinguished by their morphology, electrophysiological properties and molecular profiles.

LEC CELL POPULATION

Several populations of neurons in LEC have been recognized by immunoreactivity against different molecular markers, these markers include the calcium binding proteins and neuropeptides. The distribution of these cells is widespread and covers most of LEC in an inhomogeneous manner. The expression of the markers often overlaps with each other (Rogers 1992, Fujimaru and Kosaka 1996) and has additionally shown to co-express partially or completely with GABA or GAD 67/ 65 ((Miettinen, Koivisto et al. 1996, Wouterlood and Pothuizen 2000). In the case of PV (Miettinen, Koivisto et al. 1996), a complete overlap has been seen with GABA, while for the neuropeptide somatostatin (SST) only sparse co-localization has been reported (Wouterlood and Pothuizen 2000). Cells in LEC have additionally been characterized by their electrophysiological and morphological properties (Jones and Bühl 1993, Canto and Witter 2012). Intracellular recordings from principal cells in LEC have for instance revealed a population of pyramidal cells, which differs somewhat in their morphology but show the same overall electrophysiological properties (Canto and Witter 2012). As mentioned earlier, LEC layer II also comprises principal cells known as fan and multipolar cells. These two cell types can be distinguished by their morphology, where the first type, displays an apical dendritic tree that fans out from the soma, and the second, the multipolar neuron, shows resemblance to a stellate cell (Canto and Witter 2012). These populations of principal cells are distributed across LEC layers in a varying degree (Canto and Witter 2012). The population of INs in LEC is however not well characterized. Nonetheless, previous findings have revealed a population of fast-spiking basket cells in L II and axo-axonic cells in L II- III (Jones and Bühl

1993, Soriano, Martinez et al. 1993). Furthermore, based on reports of co-expression with GABA or GAD, there are also CR, PV and SST expressing interneurons in LEC distributed across most layers (ref).

AIMS

In this project I aim to investigate which GABAergic cell populations are present in LEC by immunohistochemical and morphological characterization. In addition, I will describe the distribution of the different cells groups across LEC. For this purpose I will use the GAD 67 -GFP knock-in mouse line for co-localization of neuro chemical markers.

2. MATERIALS AND METHODS

2.1. Animals

A total of 21 animals of the GAD67-eGFP knock-in mouse line (Tamaki et al.2003) aged 3-12 months were used for this study. Of these, 14 were used for obtaining the somatodendritic morphologies of interneurons in LEC LII, while the remaining animals were used for immunohistochemical studies. All animals involved in this study were raised and handled in line with the Norwegian laws and regulations concerning animal welfare and animal research (the Norwegian Animal Welfare Act §§ 1 – 28 and the Norwegian Regulations on Animal Research §§ 1- 26).

2.2. Perfusion

For both immunohistochemical and morphology experiments animals were anaesthetized with isofluorane and injected with a lethal dose of pentobarbital (brand name/company + concentration) intraperitoneally. Subsequently, they were perfused transcardially, first with ringer solution (145 mM NaCl, 3 mM KCl, 2 mM NaHCO3, pH 6.9; 37 °C) and afterwards with a solution of 4% freshly depolymerized paraformaldehyde (Merck, Darmstadt, Germany) (PFA) in 0.125M phosphate buffer (PB, pH 7.4) 3x 30 ml. After the perfusion, brains intended for immunohistochemical studies were retrieved from the skull and placed in the same fixative at 4°C overnight and after this stored in 10-% dimethyl sulfoxide (DMSO, Merck KGaA, Darmstadt, Germany) in PB with 20% glycerol. For cell morphology studies, brains were kept in 4% PFA at 4 °C for 3 hrs and then stored in PB overnight.

2.3. Immunohistochemical characterization of the GABAergic cells in LEC

For uncovering the distribution of different groups of interneurons across LEC, immunohistochemistry was performed against the calcium binding proteins parvalbumin (PV), calbindin (CB) and calretinin (CR) as well as the neuropeptides somatostatin (SOM), vasoactive intestinal peptide (VIP), cholecystokinin (CCK) and neuropeptide Y (NPY). To further define discrete populations of interneurons in LEC double immunohistochemistry against VIP and CR was additionally performed. This was performed as data obtained from the VIP and CR immunostaining displayed cells with similar morphology.

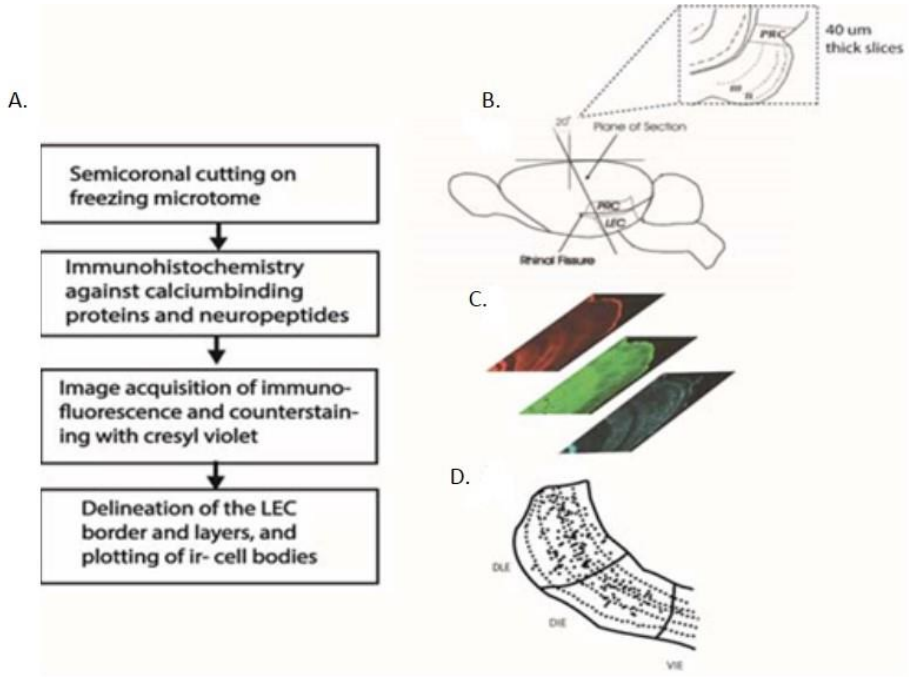

Figure 5: Acquisition of immunohistochemical data (A) Work flow diagram for the entire procedure. (B) Cutting plane for semicoronal section. (C) Image acquisition of the immunostain, GFP expression and counterstained sections. (D) Delineation of LEC and plotting of immunoreactive-cell bodies.

The expressions of these markers were investigated in a transgenic mouse that expressed a green fluorescent marker for GAD 67. This enzyme is involved in the production of GABA and therefore taken to be a good marker for GABAergic neurons in the brain. Neurons that showed fluorescent labelling are therefore regarded as GABAergic.

2.3.1. Immunohistochemistry against CA^{2}+ binding proteins and neuropeptides

Perfused brains were cut into 40 µm thick sections on a freezing microtome (Microm HM430, Thermo Scientific, Waltham, USA) in a semi coronal plane (Fig 5. B). Sections were washed in PB, and then heated in PB at 60 °C for 2 hrs for antigen unmasking. Unmasking was performed on all immuno except from the parvalbumin and calbindin stains. Next, sections were washed with PB containing 1 % Triton- x 100 (Merck Millipore, Damstadt, Germany; PBT) for permeabilizing the tissue. Sections were incubated in a blocking solution containing 10% Goat (Abcam, Cambridge, UK) or Donkey (Sigma) serum in PBT at room temperature for 3 hrs. Afterwards, sections were incubated with a primary antibody in PBT over 1 or 2 nights (depending on the antibody) at 4 °C. After the primary antibody incubation, sections were washed with PB for 3 x 15 min, and incubated with secondary antibodies in PBT at room temperature for 3 hrs**.** Secondary antibodies were used without cross reactivity with the primary antibodies. Finally, sections were washed in PB, and afterwards mounted on Superfrost plus microscope slides (Gerhard/Menzel GmbHm Braunscweig, Germany) in Tris- HCL (Merck, Darmstadt, Germany, Ph 7.6) before being left to dry overnight. The following day, sections were cover slipped with toluene and entellan (Prolabo VWR chemicals and Merck, Darmstad, Germany). After acquisition

of immunofluorescence results, the coverslipped were removed and sections were rehydrated in an increasing alcohol and xylene solution (50-70-80-90-100 %) then counterstained with cresyl violet and coverslipped with xylene (Prolabo VWR chemicals and Merck, Darmstad, Germany) and entellan before being left to dry overnight.

2.3.2. Image acquisition

Immunostained LEC sections were scanned with a fluorescent digital slide scanner (Carl Zeiss, Jena, Germany, model Mirax Midi BF/FL v 1.12) equipped with an Axiocam digital camera (Carl Zeiss, Jena, Germany) and filter sets 43 (PB 545/25) and 38(BP 470/40) (Carl Zeiss, Jena, Germany) for detecting the emission spectra of the fluorophores used in the immunostaining. Images were also acquired by use of a confocal microscope (Zeiss 510 LSM meta live, Carl Zeiss, Jena, Germany) equipped with a DPSS 561- 10 laser for exciting AF546, HENE 633 laser for AF633/647 and an Argon 488 laser for exciting fluorophore GFP/488. The filters used for detecting the emission spectra were a BP 575- 615 (Carl Zeiss, Jena, Germany) filter for the Alexa Fluor 546, LP 650 (Carl Zeiss, Jena, Germany) for the Alexa Fluor 633 and BP 505- 550 (Carl Zeiss, Jena, Germany) filter for detecting the GFP expression. Scans showing the immunofluorescence were later superimposed on the nissl stains in Adobe Illustrator CS6 (Adobe Systems, San Jose, California, USA), this allowed for delineation of LEC borders as well as layers (Fig 5. C).

2.3.3. Data analysis

Images containing fluorescent immunostaining from anterior, intermediate and posterior sections were used for analyzing the distribution of immunoreactive cells in LEC. For this purpose, immunoreactive cell bodies were quantified from the subregions DLE, DIE and VIE as well as layers I- VI of LEC in the selected sections, this gave us a general overview of the distribution of the different markers across the areas (Fig 5. D).

Overlap between immunoreactive cell bodies from sections containing antibody against one or two molecular markers and GFP+ cell bodies was assessed to obtain an estimate of overlap between the expression of specific molecular markers and the GFP expression. Size and shapes of immunoreactive cell bodies and processes, along with descriptions of the extent of the processes emanating from cell body, and orientation of the cells were included as well in this analysis.

2.4. Somatodendritic morphology of GABAergic cells in LII / L III of LEC

To describe the various morphological subtypes of GABAergic cells in LEC LII, somato-dendritic morphology of interneurons in LEC LII was obtained by intracellular filling. Confocal images of the filled cells were later used for reconstructing the cells in 3D, which could be used for further analysis later (Fig 6. A).

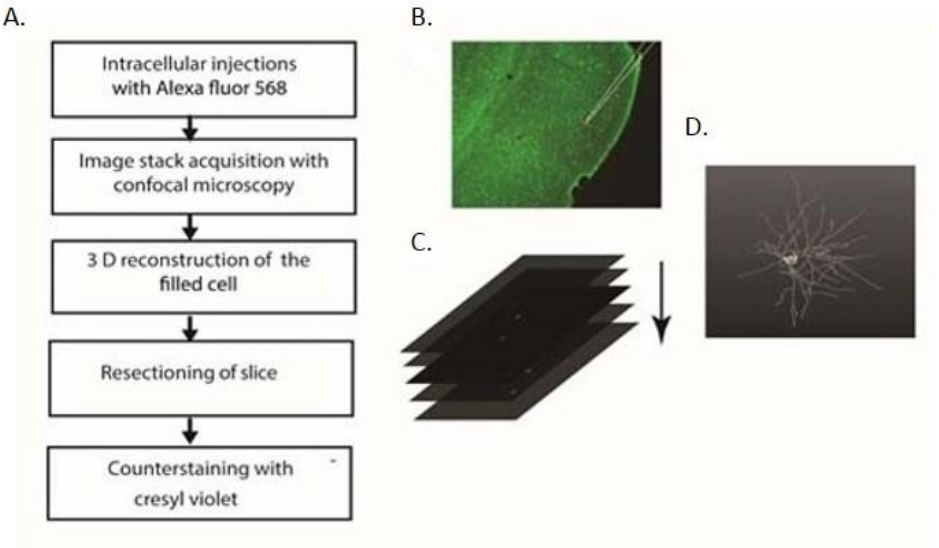

Figure 6: Procedure for intracellular filling of cells and 3D reconstruction. (A) Work flow diagram for the entire procedure (B) Targeting of GFP cells in a section obtained from GAD67 mouse. (C) Confocal image stack acquisition of filled cells. (D) 3 D reconstructed cell.

2.4.1. Intracellular injections

Brains from GAD 67 mice were obtained following the described perfusion protocol above. After perfusion, brains were lightly fixed for 3 hrs at 4 °C, and then sectioned on a vibratome (Leica VT1000S; Nussloch Germany) into 400 µm thick sections in a semicoronal plane. While cutting, the brain was

submerged in PB solution. Intracellular injections were performed on a Zeiss Axiovision Examiner D.1 microscope (Carl Zeiss, Jena, Germany) with a dual filter for detection of GFP and Alexa fluor 568 and a simple electrophysiological set up for filling the cells (homemade appliance). GFP positive cells in LEC LII were impaled with a sharp glass micropipette pulled on a micropipette puller (Sutter Instruments co., California, USA). The micropipettes were back filled with the fluorescent dye AlexaFluor 568 fluorhydrazide (100mM in 200Mm KCl,Invitrogen-Probes, California, USA) in the tip, and KCl (200mM solution) filled the rest of the pipette. Targeting of cells and intracellular filling was executed by controlling and moving an electrode holder with a micro manipulator (Luigs & Neumann SM-5, Ratingen, Germany) holding the sharp glass pipette. The electrode holder`s silver wire tip was inserted into the glass capillary`s solution, and a 2 pA current was applied during injection. Cells were randomly selected in the LEC region close to the rhinal fissure and targeted by their GFP expression (Fig 6. B), before being filled with the fluorescent dye for up to 15 minutes depending on the size of the cell. After intracellular filling, slices were post – fixed in PFA overnight at 4 °C. The following day, slices underwent a dehydration process in which they were placed in increasing concentrations of ethanol; 30-50-70-90-100 % for 10 minutes in each step. The final wash was an ethanol wash at 100% concentration for 40 minutes, after this slices were put into a 50/50 mixture of 100% ethanol and methyl salicylate (Sigma Aldrich, St.Luis, USA) solution for 10 minutes, before finally being placed in methyl salicylate for tissue clearing.

2.4.2. Confocal image analysis

Sections containing the filled cells were analysed using a confocal microscope. Filled cells were detected by use of a DPSS 561-10 laser and a BP 575- 615 filter. To check for co-localization with GFP, the Argon 488 laser and BP 505-550 filter were additionally used. Optical z-stacks of each intracellularly filled cell were taken with a 40x oil objective N/A Plan achromat 40x/ 1.3 oil DIC (Carl Zeiss, Jena, Germany) to obtain a 3D rendering of the cell (Fig 6. C).
For an overview of the cells position in LII and orientation of their dendritic tree, additional images of the slice containing the filled cells were taken with a 10x objective N/A Plan achromat 10x/ 0.45 NA air (Carl Zeiss, Jena, Germany).

2.4.3. Morphological analysis

Three-dimensional reconstruction was performed on cells with good filling of cell bodies and dendritic trees with the use of AMIRA (FEI Visualization Sciences group, Berlin Germany). All measurements of soma, dendritic tree and dendrites were performed in the AMA software. Soma size was obtained by measuring the perimeter of the soma at the largest circumference. The extent of the dendritic tree was measured, by using the radial distance from soma to the end point of the dendritic tree. Dendrite size was measured by taking the diameter. To measure arbor complexity of the dendritic tree a Sholl analysis (Sholl, 1953) was performed on the reconstructed cells, with dendrite crossing measured with intersections of 1 um intervals from the soma. Radial distribution and orientation of dendrites was explored by tracing the dendrites of filled cells in 3D in Neurolucida

(MBF Bioscience, VT, USA). Data analysis of the traced cells was performed in Neurolucida explorer (MBF Bioscience, VT, USA) where the 3D traced dendrites for each cell were reduced to a 2D polar histogram. The 2D polar histograms included information about the dendritic length and orientation from the soma, which was used to describe the overall preferred direction of the dendritic tree.

Classifications and descriptions of GABAergic cells were done in accordance with the Petilla nomenclature (Ascoli et al. 2008). Cells were classified by their dendritic arbor into cells with a unipolar, bipolar, bitufted or multipolar configuration. For the description of soma shape, the terms fusiform, polygonal, globular and triangular were used. Additional terms for soma shapes which were not covered by these terms such as" pear shaped" were also used. The dendritic morphology was described by the shape and fine structure which included descriptive terms as irregular or regular, spiny or aspiny, and beaded.

3. RESULTS

3.1. Morphological properties of interneurons in L II and L III

Interneurons (INs) are known to exhibit a diverse variety of morphological features. Here, the morphology of INs in the LEC has been investigated through intracellular filling of identified GABAergic cells. For the analysis of the somato-dendritic morphology of LII/III INs in the LEC, we acquired confocal image stacks of the filled cells, and they were classified according to the criteria for INs classification made by the Petilla group (Ascoli, Alonso-Nanclares et al. 2008). 3D reconstructions were made for representative cells from each group, and the reconstructions formed the basis for Sholl analysis as well as polar plot analysis. A descriptive analysis was also applied to the morphology, along with measurements taken from soma, dendrites and dendritic trees. Out of 109 filled cells, 54 were considered for the morphological classification. Cells that had been insufficiently filled, severely cut, or proved not to be GABAergic were excluded from the investigation. All but two cells had their cell bodies located in LII, the other two were located in LIII. The analyzed cells were either multipolar or bipolar neurons. Cells in these two classes were analyzed in more detail such that eight morphological IN cell types were found in LII/III of the LEC, these were: small and large multipolar cells, bipolar cells, small bipolar spindle cells, a cell type described as a bow tie neuron , pyramidal like cells, triangular neurons and radial neurons. Figure 7 shows an overview of the different morphological cell types.

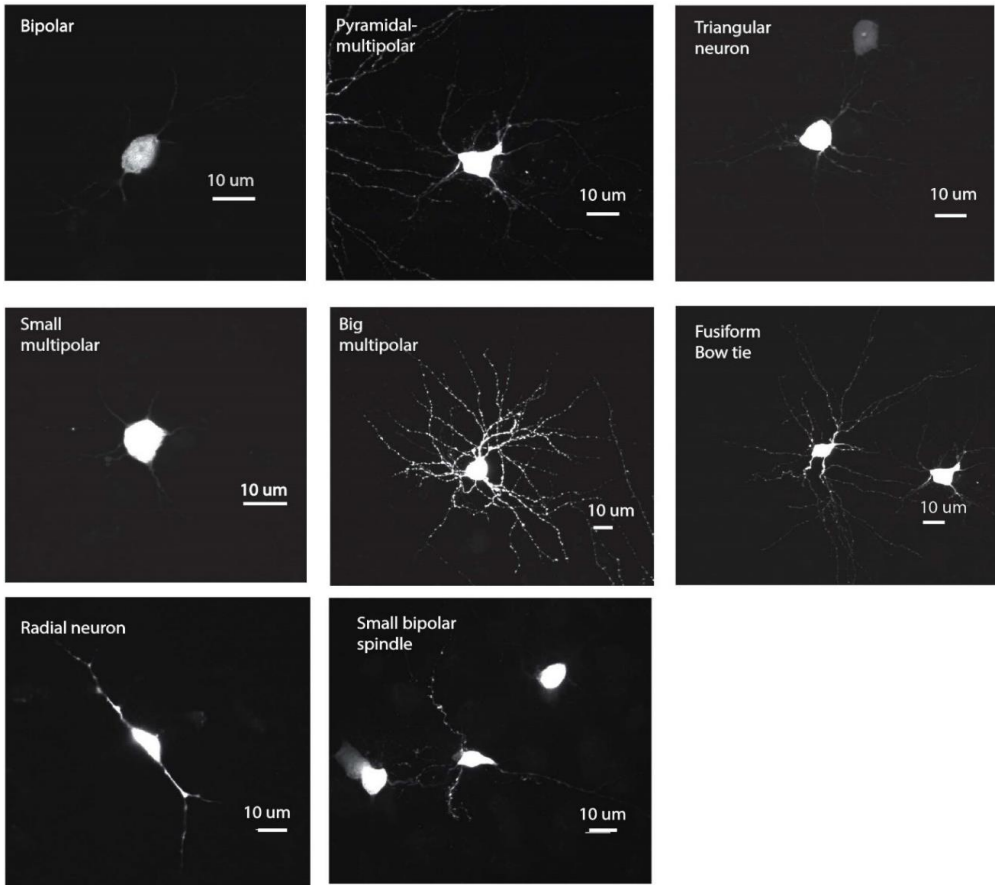

Figure 7: Morphological cell types of LEC L II/III. A Bipolar cell B Pyramidal multipolar cell C Triangular neuron D Small multipolar cell E Big multipolar cell F Bow tie neuron G Radial neuron H Small bipolar spindle cell.

3.1.1 Small multipolar cell

The small multipolar cells (Fig 8. A) exhibited small somata, the reconstructed example cell measured 23.38 µm around its perimeter. Eight primary dendrites, on average, radiated in all directions from the cell body forming a sphere like shape around it. Due to the large number of dendrites spreading in all directions, the soma shape was rounded, but star-like in its form. The dendrites of small multipolar cells were observed to be spine free, smooth, regular and thin (Fig 8. C) with a branch diameter ranging from

0.27 - 0.35 µm. Both the cell body and dendritic tree were confined within L II (Fig 8. E). A polar plot showing the extension of dendrites around the soma of the reconstructed cell, revealed a strong tendency for dendrites to orient toward one particular direction (Fig 8. B). The Sholl analysis revealed that the radius of the dendritic tree measured 35.15 µm from the soma, and that the peak dendritic complexity occurred at a distance of 20 µm from the soma (Fig 8.D). The cell was confirmed GFP positive (Fig 8. F).

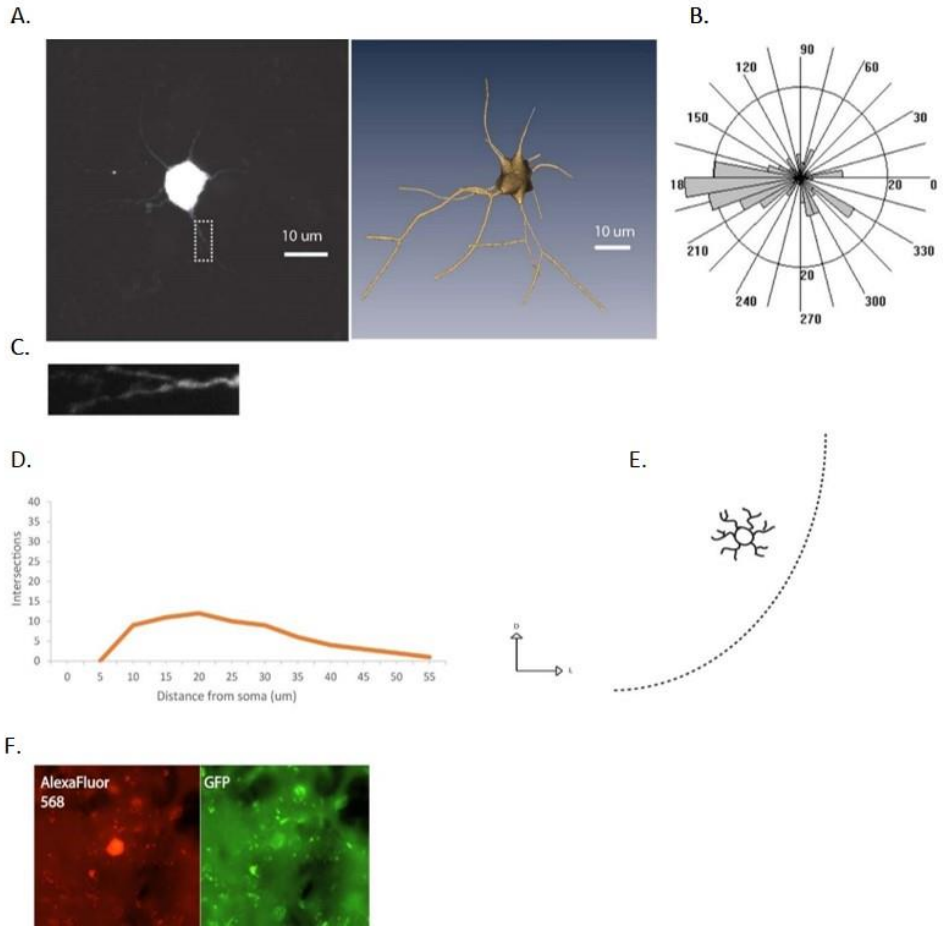

Figure 8: Morphological properties of the small multipolar cell. A Photomicrograph of cell and 3D reconstructed cell B Polar plot of dendritic tree C Enlarged image of dendrite from marked area in A D Sholl profile of dendritic tree with number of intersections with dendrites.

3.1.2 Big multipolar cell

The big multipolar cells had a large oval shaped soma (perimeter of 30.11 µm), and similar to the small multipolar cells featured eight primary dendrites projecting in all directions from the soma (Fig 9. A). The dendritic arbor of the big multipolar cell was however much more complex as seen by the higher number of intersections with dendrites from the Sholl analysis of the reconstructed cell (Fig 9. D).The general size of the dendritic tree was much larger, extending for 86.58 µm from the reconstructed cell soma. In

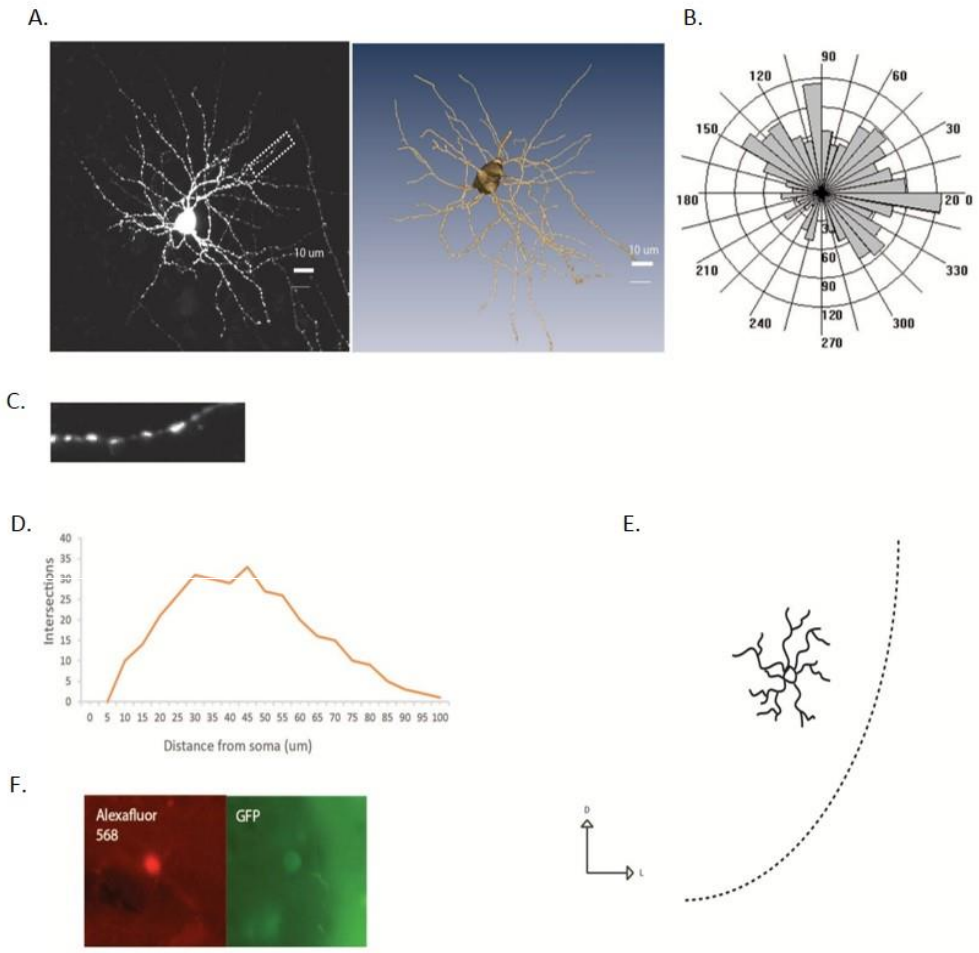

Figure 9: Morphological properties of the big multipolar cell. A Photomicrograph of cell and 3D reconstructed cell B Polar plot of dendritic tree C Enlarged image of dendrite from marked area in A D Sholl profile of dendritic tree with number of intersections with dendrites.

addition, dendrites were observed to branch into LII and LIII while the cell body was located in LII (Fig. 9.E). Polar plot analysis of the big multipolar cell`s dendrites showed medium to long arbors covering ¾ of the area around the cell, leaving one quadrant relatively free of dendrites (Fig 9. B). Dendrites exhibited a spine free and beaded appearance with a diameter ranging from 0.45-142 µm (Fig 9. C) The big multipolar also expressed GFP (Fig 9. F).

3.1.3 Pyramidal like cell

A third type of multipolar cell featured a thick apical dendrite and triangular soma, similar to a pyramidal cell (Fig 10.A). The soma of the reconstructed cell from this class had a perimeter of 27.57 µm and displayed seven primary dendrites which were intermediate to long, branching out around the soma reaching a maximal distance of 69.17 µm. Sholl analysis revealed that the peak dendritic complexity occurred at a distance of 25 µm from the soma (Fig 10.D). Polar plot analysis showed dendritic outgrowth all around the soma and branching of medium to long dendrites in four basic directions (Fig 10.B). Most of these medium to long dendrites were observed to be oriented towards the pial surface (Fig 10.E). Dendrites were measured to have a diameter ranging from 0.37- 0.55 µm and showed a beaded appearance (Fig 10.C), some spines were observed on dendrites proximal to the soma. GFP expression was confirmed in this cell type as well (Fig 10. F).

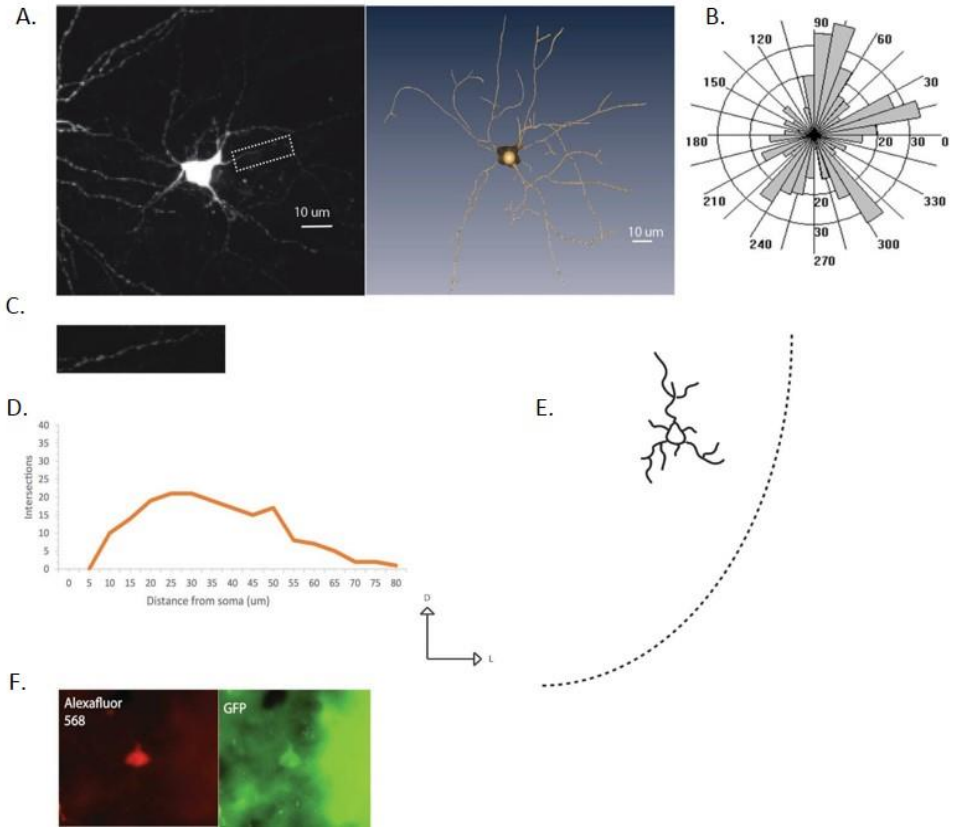

Figure 10: Morphological properties of the pyramidal multipolar cell. A Photomicrograph of cell and 3D reconstructed cell B Polar plot of dendritic tree C Enlarged image of dendrite from marked area in A D Sholl profile of dendritic tree with number of intersections with dendrites.

3.1.4 Bow tie neuron

A fourth multipolar cell type displayed a spindle shaped soma (25.82 µm in perimeter) with four thick dendrites branching out from each of the two poles of the soma, making the cells resemble the shape of a bow tie (Fig 11 .A). In total there were nine primary dendrites, most of these were long, branching out in all directions surrounding the cell body. Dendrites had mostly a beaded appearance and the diameter varied between 0.47-0.63 µm (Fig 11. C). A few of the primary dendrites displayed a smooth and regular appearance proximally, that turned in to a beaded surface in distal segments. The cell was located and confined to L III where the dendritic tree was horizontally oriented, parallel to the pial surface (Fig 11. E).The dendritic tree covered a large area and extended a distance of 75.65 µm from soma. Polar plot analysis showed dendritic radiate from the soma in all directions, with most dendritic extensions occurring in two directions (Fig 11.B). Sholl analysis showed a high overall dendritic complexity of the cells, and that the peak of complexity occurred at 30 µm from the cell body (Fig 11.D). GFP expression was present in the cell (Fig 11 .F).

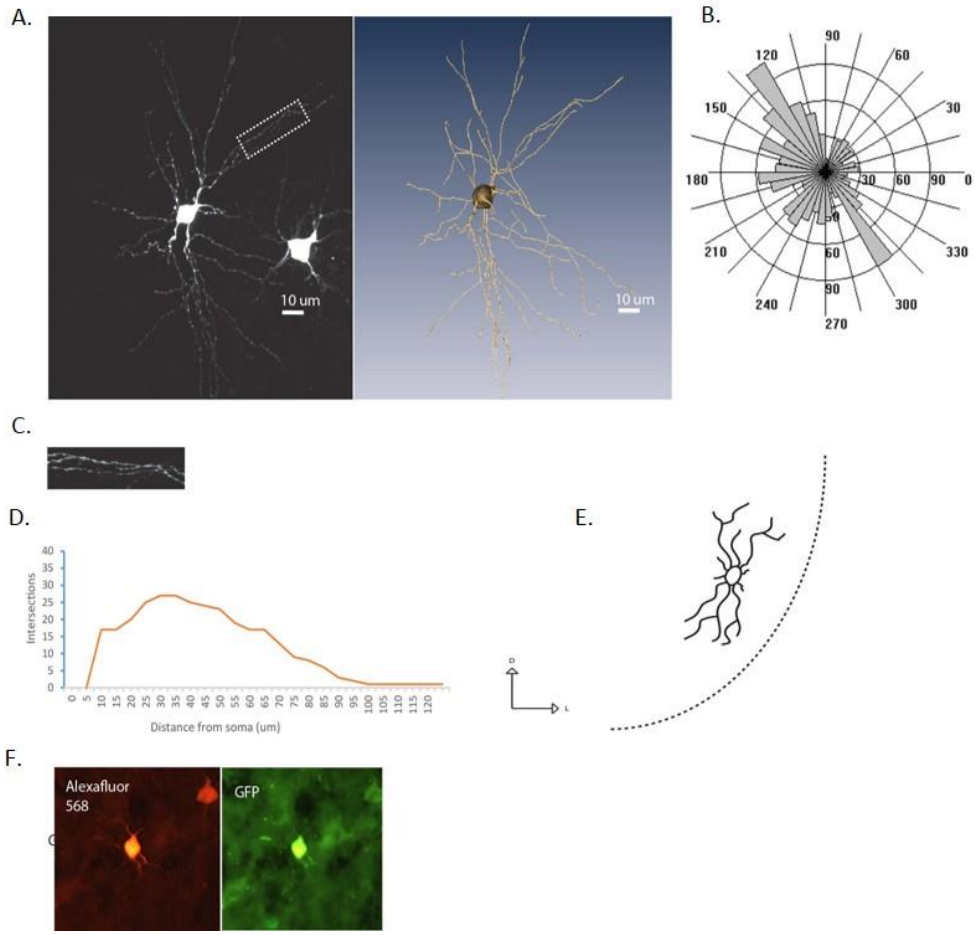

Figure 11: Morphological properties of the bow tie neuron. A Photomicrograph of cell and 3D reconstructed cell B Polar plot of dendritic tree C Enlarged image of dendrite from marked area in A D Sholl profile of dendritic tree with number of intersections with dendrites.

3.1.5 Bipolar cell

The bipolar cells featured two primary dendrites and had oval somata. The reconstructed bipolar cell measured 26.28 µm around the perimeter (Fig 12. A), and dendrites were observed to be thin (0.33 - 0.55 µm), smooth and regular in shape (Fig 12.C). Both the cell body and the dendritic tree were located in LII. The dendritic tree of bipolar cells was measured to reach out

as far as 55 µm from the soma, and it was radially oriented within L II (Fig 12. E). Sholl analysis of the dendritic arbor revealed a low overall complexity, with the peak occurring at 35 µm from the soma (Fig 12. D). Furthermore, the polar plot analysis showed that dendritic extensions occurred mainly into two directions (Fig 12. B). In addition, longer dendrites were observed at one pole and these were oriented towards the deeper layers. GFP expression in the bipolar cell was confirmed (Fig 12. F).

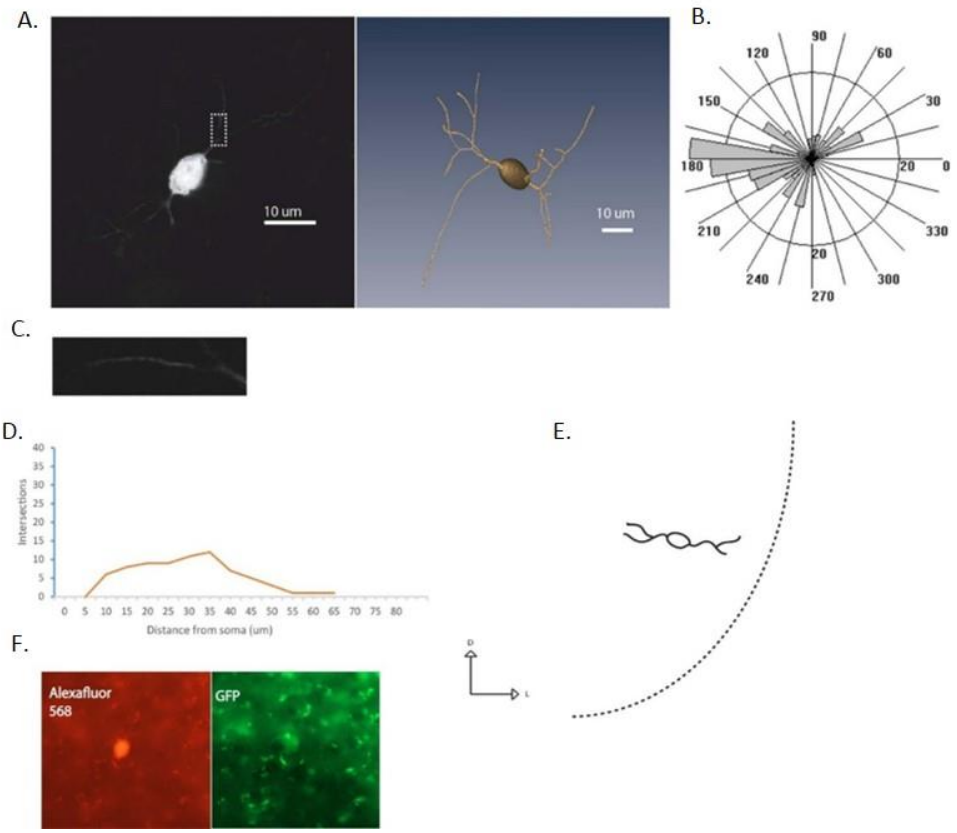

Figure 12: Morphological properties of the bipolar cell. A Photomicrograph of cell and 3D reconstructed cell B Polar plot of dendritic tree C Enlarged image of dendrite from marked area in A D Sholl profile of dendritic tree with number of intersections with dendrites.

3.1.6 Small bipolar spindle cell

The small bipolar spindle cells showed a small spindle shaped soma (reconstructed cell soma perimeter: 24.16 µm) and thin (0.27- 0.55 µm) regular dendrites (Fig 13. A, C). The dendrites initially exhibited a regular shaped appearance and were tortuous at short distances from the soma. The dendritic tree branched out from the poles of the soma and maximally extended for a distance of 26.24 µm. The polar plot analysis revealed that most of the branch points occurred in two regions (Fig 13.B).Furthermore, the cell showed a radial orientation within L II and longer dendritic branches were observed at the pole oriented towards LI (Fig 13. E). Data from the Sholl analysis also showed an overall low complexity, where the maximum occurred at the distance of 10 µm from soma (Fig 13. D). Co- expression of GFP was detected in this cell as well (Fig 13. F).

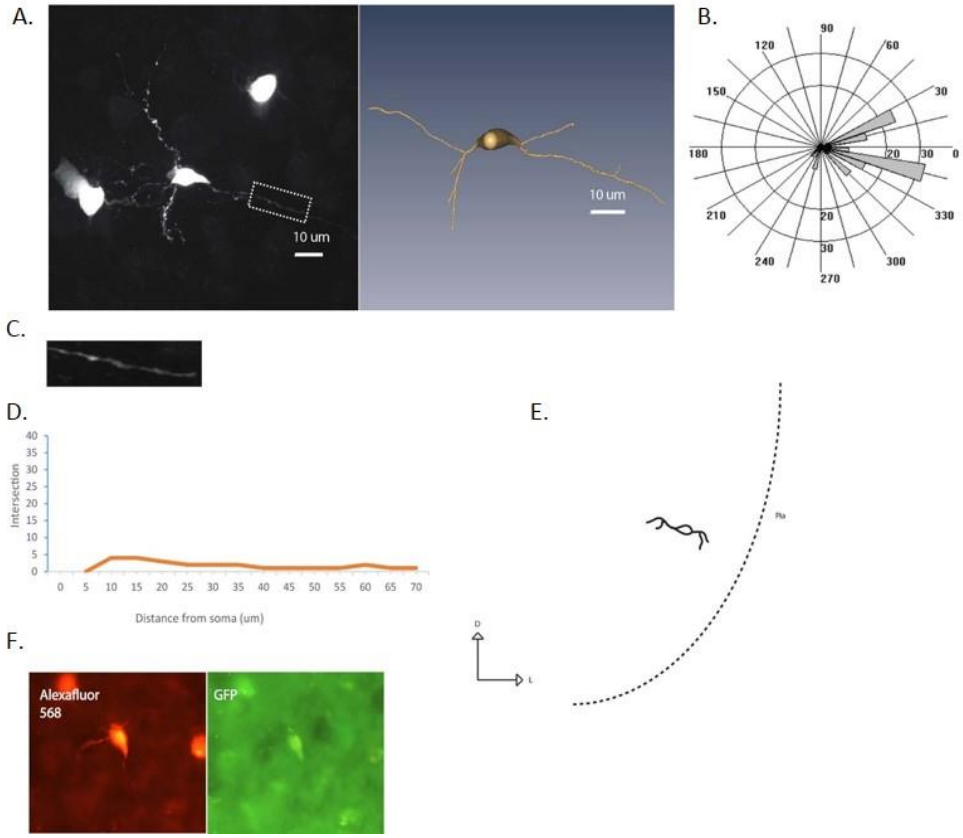

Figure 13: Morphological properties of the small spindle bipolar cell A Photomicrograph of the cell and 3D reconstructed cell B Polar plot of dendritic tree C Enlarged image of dendrite from marked area in A D Sholl profile of dendritic tree with number of intersections with dendrites.

3.1.7 Triangular neuron

The triangular neurons had an oval triangular shaped soma (reconstructed cell: 27.42 µm in perimeter) and featured long dendrites which branched out in three main directions, giving a slight triangular shape to the dendritic tree as well (Fig 14. A). Seven primary dendrites protruded from the soma giving rise to mainly long branches which all had smooth and regular shaped appearances (Fig 14.C). Dendrite diameter ranged from 0.25-0.91 µm. Polar plot analyses of the dendritic tree revealed that dendrites extended in all

directions from the soma, and that there were three regions around the cell where most dendrites branched out (Fig 14. B). Sholl analysis revealed the highest complexity at 25 µm from the soma, and that the overall complexity of the dendritic tree was intermediate compared to the other cell types (Fig 14. D). Both cell body and dendritic tree were located and confined within LII (Fig 14. E). Co- expression of GFP was confirmed (Fig 14. F)

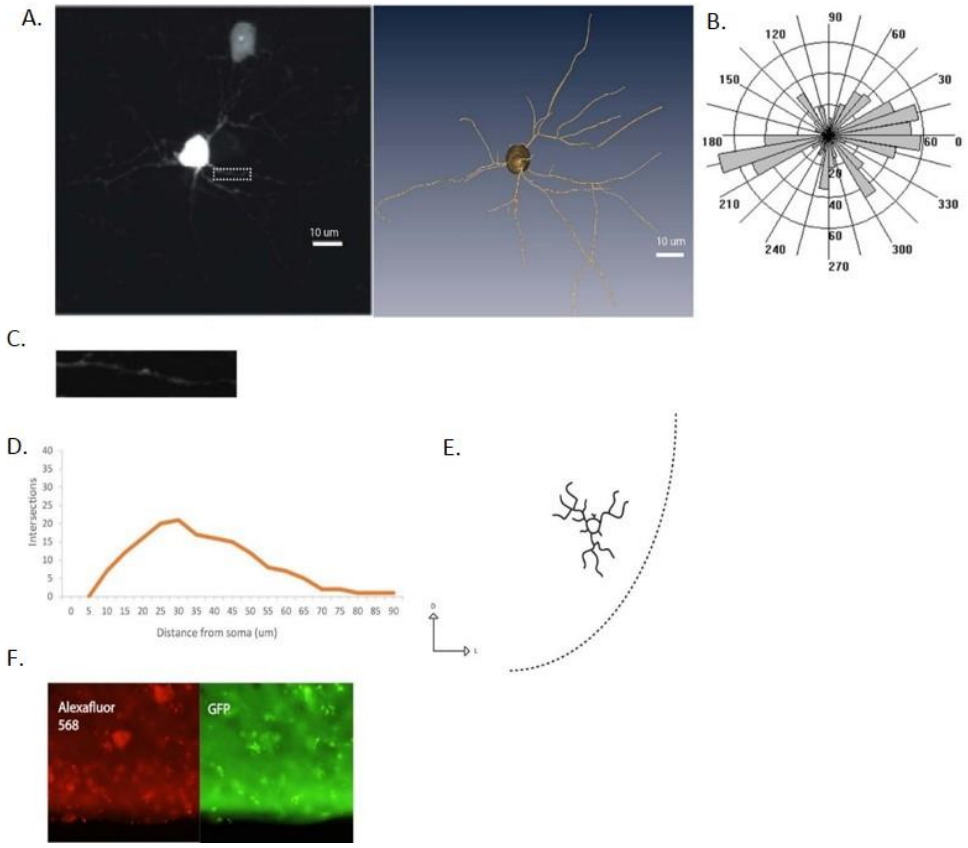

Figure 14: Morphological properties of the triangular neuron. A Photomicrograph of cell and 3D reconstructed cell B Polar plot of dendritic tree C Enlarged image of dendrite from marked area in A D Sholl profile of dendritic tree with number of intersections with dendrites.

3.1.8 Radial neuron

The radial neurons exhibited three to four primary dendrites, and had triangular somata (reconstructed cell: 28.93 µm in perimeter) (Fig 15.A). The cell morphology was distinct having two to three smooth, thick and straight primary dendrites extending into thinner and more irregularly shaped dendrites (Fig 15.C). The remaining primary dendrites were thinner and had a similar appearance to the distal portions of the thicker primary dendrites. Branch diameter was measured 0.95 µm at the thickest and 0.36 µm at the thinnest. Sholl analysis and measurements taken from the dendritic tree showed a low dendritic complexity, (Fig 15.D) but long extensions of branches from the soma (85.16 µm). The soma and dendritic tree were both confined within LII, with the two thick primary dendrites oriented radially within the layer (Fig 15.E). Polar plot analysis showed a preferred direction of longer dendrites in one region (Fig 15. B,D) and GFP expression was present (Fig 15. F).

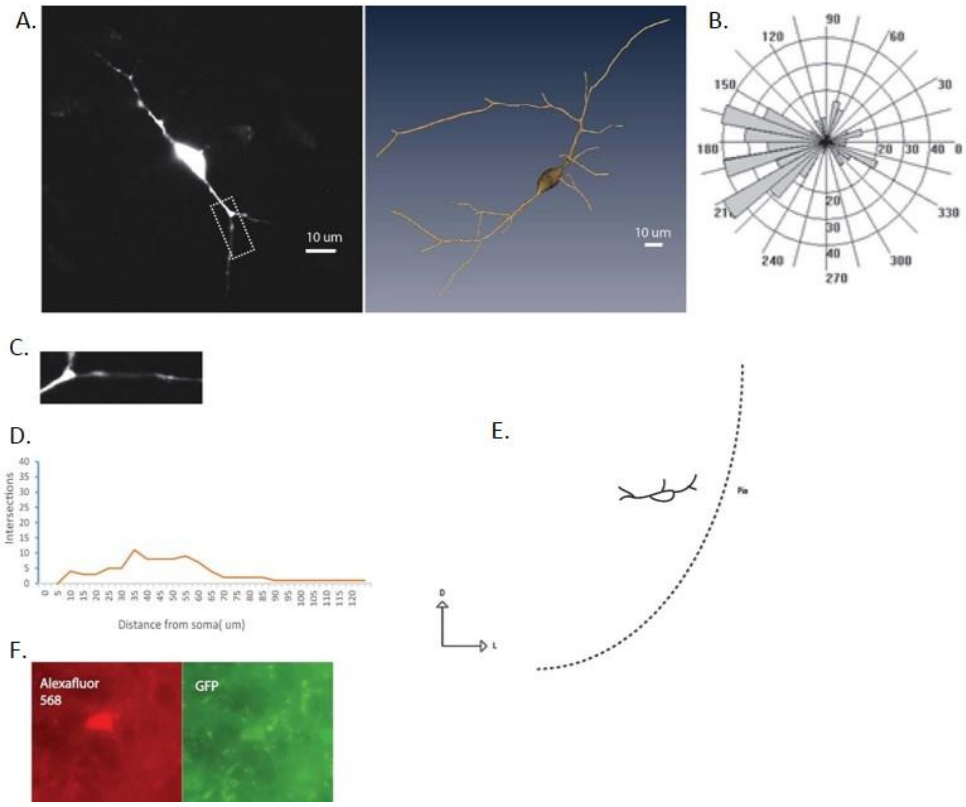

Figure 15: Morphological properties of the radial neuron. A Photomicrograph of cell and 3D reconstructed cell B Polar plot of dendritic tree C Enlarged image of dendrite from marked area in A D Sholl profile of dendritic tree with number of intersections with dendrites.

Altogether the targeted cells displayed a variety of somato-dendritic morphology in size, shape and complexity of the dendritic tree. Soma shapes included fusiform, round, oval and triangular forms, while the soma size was measured to range between 24.16 - 28.93 µm. Measurements of soma size showed that the small bipolar spindle cell had the smallest soma, while the radial neuron exhibited the largest soma. The bipolar cell was observed to have the lowest number of primary dendrites while the bow tie and multipolars cells featured the highest number of primary dendrites. The dendritic arbors of the different cell types were multipolar, bipolar or

triangular, and the dendritic morphology was straight, beaded, irregular or regular, smooth or varicose. The branch diameter of dendrites ranged from 0.25 - 1.95 µm. The thickest dendrites were observed in the bigger cell types, the radial, big multipolar, bow tie and pyramidal cells. While the thinnest, smooth and regular dendrites were mostly observed in the smaller cell types; the bipolar, small multipolar and triangular cells. In most cell types dendrites were at their thickest proximal to cell body before tapering to form thinner dendrites at further distances from the soma.

The Sholl analysis revealed a highly variable arbor complexity across the different morphological cell types, at the lower extreme was the small bipolar spindle cell, this cell featured a small dendritic tree and very low dendritic complexity. The big multipolar cell at the other end featured a highly complex dendritic tree, and branches stretching out covering a large area. Furthermore, the Sholl analysis revealed that most cells displayed the highest dendritic complexity at a distance of around 20-35 µm from the soma (Fig 16). A great variation in how far the dendritic tree extended was also seen, with the most local dendritic branching observed in smaller cell types such as the bitufted, bipolar and small multipolar cell, and the largest dendritic trees observed in the pyramidal like cell, bow tie, big multipolar, radial and triangular cells.

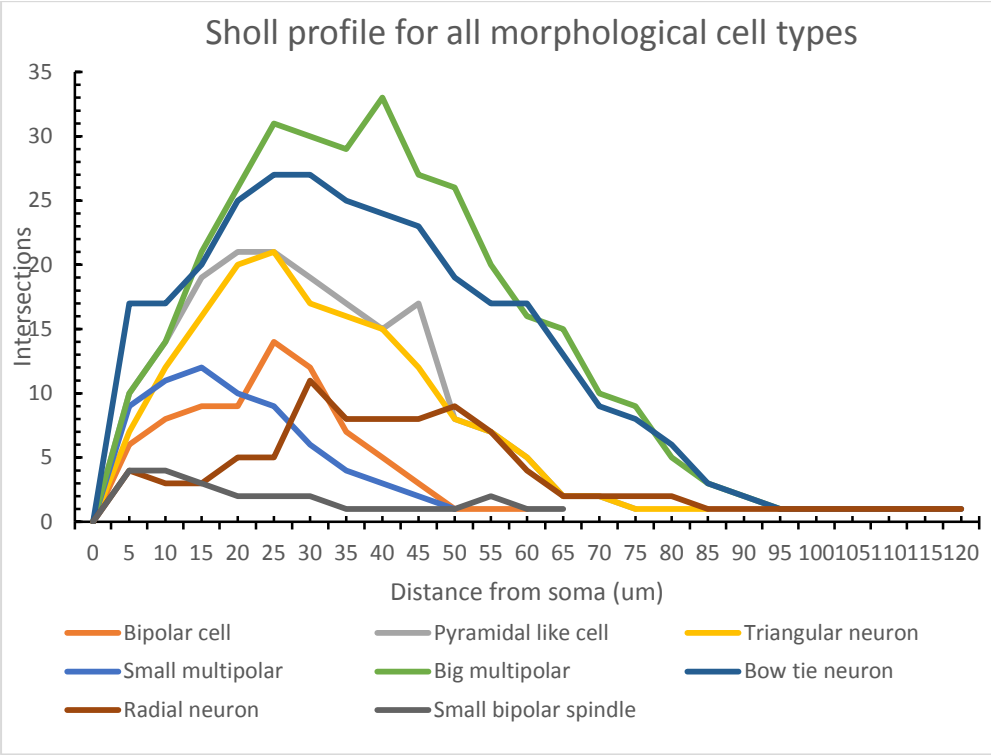

Figure 16: Sholl profiles for all cell types.

3.2 Immunohistochemical characterization of GABAergic subpopulations of LEC

Studies using immunohistochemical methods for investigating subpopulations of GABAergic cells have revealed a range of neurochemical markers present in various types of inhibitory neurons. To further investigate IN groups in the LEC, immunohistochemistry was performed against the calciμm binding proteins parvalbμmin (PV), calbindin (CB), and calretinin (CR), as well as against the neuropeptides; cholecystokinin (CCK), neuropeptide Y (NPY), vasoactive intestinal peptide (VIP), and somatostatin (SOM) in GAD67-GFP mice. An overview of cells co-expressing GFP and the molecular markers of interest was made by mapping out and counting GFP

immunoreactive cell bodies across layers and regions (DLE, DIE and VIE) in anterior, intermediate and posterior sections of the LEC. Cell counts also included cells which showed no GFP expression but immunoreactivity for a specific marker, as well as cells expressing only GFP. The cell count of double (GFP-immunoreactive cells) and single labeled (GFP or immunoreactive) cells were then later used to estimate the expression of a specific molecular within the GABAergic population, and the proportion of immunoreactive cells expressing GFP. Cell count data was also used to estimate the number of immunoreactive cells present in layers, regions and sections obtained along the anterior-posterior extent of the LEC. As chemical subtypes of GABAergic cells have been shown to correlate with certain morphological cell types ((Markram, Toledo-Rodriguez et al. 2004), a descriptive analysis of the morphology of the immunoreactive – GFP cells for each stain was also performed.

To investigate regional, layer and anterior - posterior differences in the distribution of GFP immunoreactive-cells in the LEC, immunostained sections were counterstained with a Cresyl violet stain after obtaining confocal images of each immunostain. The entorhinal cortex is subdivided into the LEC and MEC; the two areas can be distinguished from each other by the different appearance of L II, L III and L VI. L II and L III of MEC feature a denser, thicker and darker stained appearance than L II and L III of the LEC. To delineate the LEC from the adjacent PER 35, the presence of L IV, the cell sparse layer lamina dissicans, in the LEC and the presence of the darker L II and L III stained cells in the LEC were used to identify the border. The LEC can be further divided into three subregions; the dorsal lateral entorhinal area (DLE), dorsal intermediate entorhinal area (DIE) and the ventral

intermediate entorhinal area (VIE). Delineation of borders, layers and subregions; was performed following the cytoarchitectural descriptions of Insausti et al. (1997). Delineation of the regional areas, the DLE, DIE and VIE of the LEC was performed by identifying differences in layer appearance. The border between the DLE and DIE was identified by differences in L II cytoarchitectonics and the presence of an acellular space between L II and L III, which has been described to be present in the DIE but not the DLE. Cytoarchitectonically, L II in the DIE has been described to be homogenous and cell dense, while L II cells of the DLE are more spread out and invade L I to a much greater extent. The DIE and VIE regions were distinguished from each other by the darker stained layer V cells in the VIE and the disappearance of the lamina dissecans (L IV) between L III and L V.

For delineation of L I – VI, the following descriptions were used to identify the borders; L I (the molecular layer) is the outermost layer and exhibits very few cell bodies, L II features dark and densely packed elongated cells which tend to cluster. L III is a broad layer with cells arranged more loosely than L II and it contains cells of various sizes and shapes. L IV separates L III and L V, and is not always very apparent in the LEC, the cells in this layer are irregularly distributed. L V features medium to large darkly stained cells, and a deep layer with cells that are more densely packed together. L VI is more compact then LV and displays cells of different sizes and shapes.

In this study, immunohistochemical data from the calcium binding proteins (PV, CB and CR) will be presented first, followed by data on the neuropeptides (VIP, NPY, SOM and CCK). To ensure that the immunostain was specific, additional immunostaining batches were made on tissue obtained from other animals. Secondary antibodies with different

fluorophores were tested to find the optimal fluorescent signal and specificity. Secondary antibodies conjugated with Alexa Fluor 546 were found to be the most optimal, and were thus used for the cell counting experiments.

3.2.1 Parvalbumin

Distribution of immunoreactive fibers

Immunohistochemistry against PV showed strong labeling in cell bodies as well as neurites in the LEC. The distribution of immunoreactive fibers across layers, subdivisions and the anterior-posterior axis was inhomogeneous, and the PV stain revealed a very conspicuous dense plexus of immunoreactive fibers in the area of LEC bordering PER 35. The PV fiber network was denser and more intense in areas where there were many PV stained cell bodies.

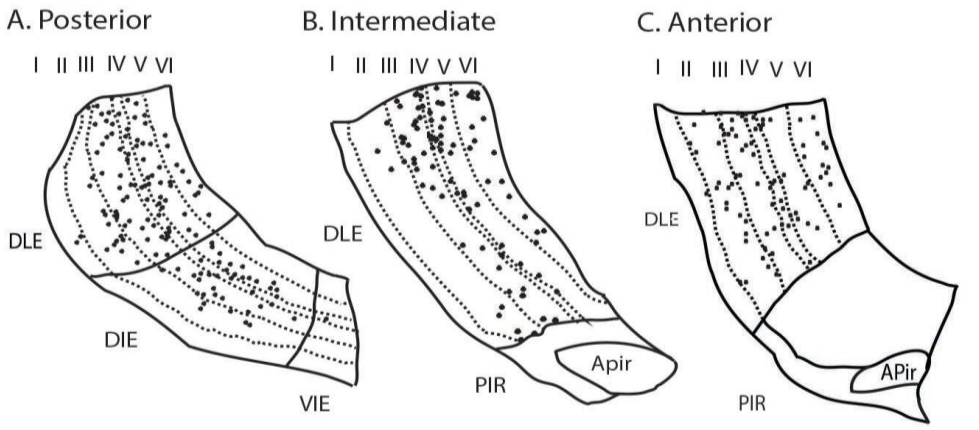

Figure 17: Schematic drawings of posterior (A), intermediate (B) sections with PV cell body distribution plotted across layers and subdivisions.

In the posterior section, which contained portions of the DLE, DIE and VIE, the fiber plexus was especially apparent in subregion DLE L II and L III. Here, fibers were particularly dense and exhibited a high intensity of immunofluorescence. The deep layers L IV- VI displayed a slightly fainter and a less dense fiber network compared to the superficial layers. The fiber network present in the DIE covered all of L III and parts of LII and L IV. In the VIE, the immunoreactive fibers were present in L II – LIV but appeared less dense and more faint compared to the other subdivisions. The intermediate section, comprising only the DLE, displayed a similar pattern of fiber distribution across layers, where the fibers decreased in numbers and

intensity as they approached the amygdalo-piriform transition area. In the anterior section, which included only the DLE, fibers were mainly detected in L II- III, and contrary to the posterior and intermediate sections the density and intensity increased towards the border of the amygdalo-piriform transition area. A difference in immunofluorescence intensity across the anterior, intermediate and posterior sections was also detected, where the immunofluorescence was more intense in the posterior and anterior sections.

Cell distribution

A high number of PV cells were distributed across all layers and regions in the anterior, intermediate and posterior sections from the LEC. An overview of the PV cell distribution in schematic figures of each section (Fig 17 A-C) reveals a relatively scattered population of PV cell bodies. The distribution of PV cells differed somewhat along the anterior-posterior axis across the laminae and subregions. In the anterior section, PV cells spread out across

all layers. An analysis of the laminar distribution of PV cells in the section revealed that most PV cells were located in LII and LIII while the lowest number of cells appeared in L I. In addition, some clusters of PV- cells were observed in L II- III in the area close to the border of PER 35.The remaining layers showed comparable cell numbers of PV cells (Fig 17. C, 18). The intermediate section featured a slightly different pattern. In this section, clustering of PV cells was also observed in the area bordering PER 35, particularly in L III - IV. The highest number of PV cells was discovered in L III, while the deep L V- VI showed low numbers of PV cells and the remaining L II and IV had even fewer PV cells. None were observed in L I (Fig 17. B, 18) In the posterior section, PV cells were scattered across all layers (Fig 17. A)but showed a high number of PV cells in L II and L V. L III and L IV showed comparable intermediate numbers of PV cells and L VI low numbers of PV cells, followed by L I which showed the lowest number (Fig 18). The distribution across subregions was very uneven (Fig 19) with most PV cells located in DLE and DIE and only a pair in VIE.

Laminar distribution

The laminar distribution of PV cells across the anterior- posterior axis showed that L III and LV of the posterior section stands out with the highest cell counts. L IV and VI showed moderate cell numbers along the anterior-posterior axis. While L I featured the lowest number of cells, and LIII the highest number of cells across all sections (Fig 18). An analysis of the total number of PV cells across layers in all sections, showed that the highest portions of PV cells were found in L III (32. 8%) and L V (22. 3%), while the lowest number of PV cells were found in L I (1 %). The deep layers L IV and L

VI displayed similar portions of immunoreactive cells (13. 6%) and L II contained the remaining 16. 7 % (Table 1).

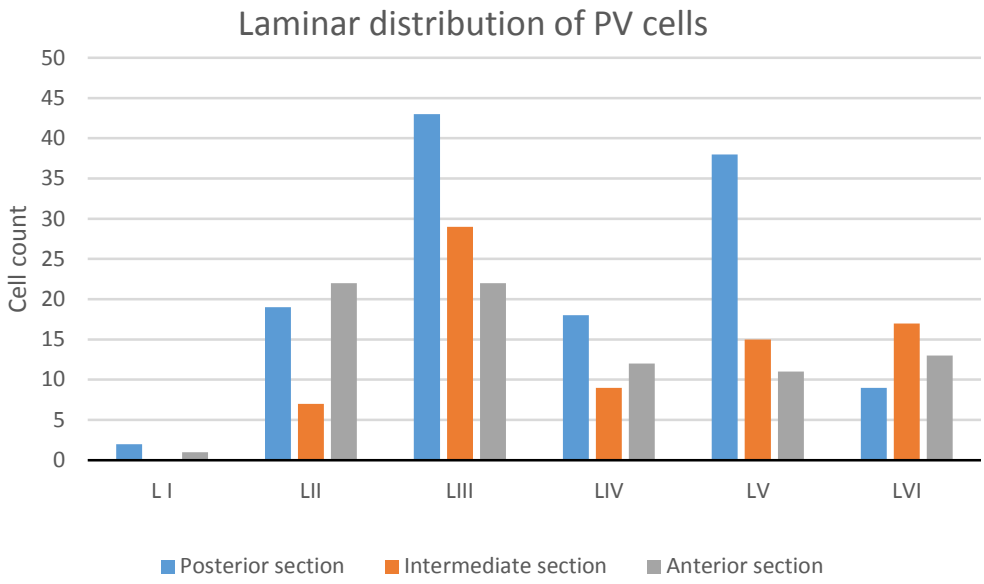

Figure 18: Distribution of PV positive GAD cells across, layers, areas and sub regions in the LEC. Cells counted in the different sub regions across the anterior-posterior axis.

Subregional and Anterior – posterior distribution

With regards to the subregions, a comparison of the PV cell count data from all sections showed that the highest numbers of PV cells were found in DLE for all sections (86. 8 %), while only a small portion of PV cells was found in the DIE (12. 9%) and VIE displayed close to zero PV cells (0.3 %) (Fig 19, Table 1).

For an investigation of anterior-posterior differences in the distribution of PV cells, the total number of PV cells was compared across the analyzed sections. This showed that the majority of PV cells were located in the

posterior section (44.9%) while cells in the intermediate section represented 26.8 %, and PV cells in the anterior section 28. 2 % of the total counted PV cell population (Table 1).

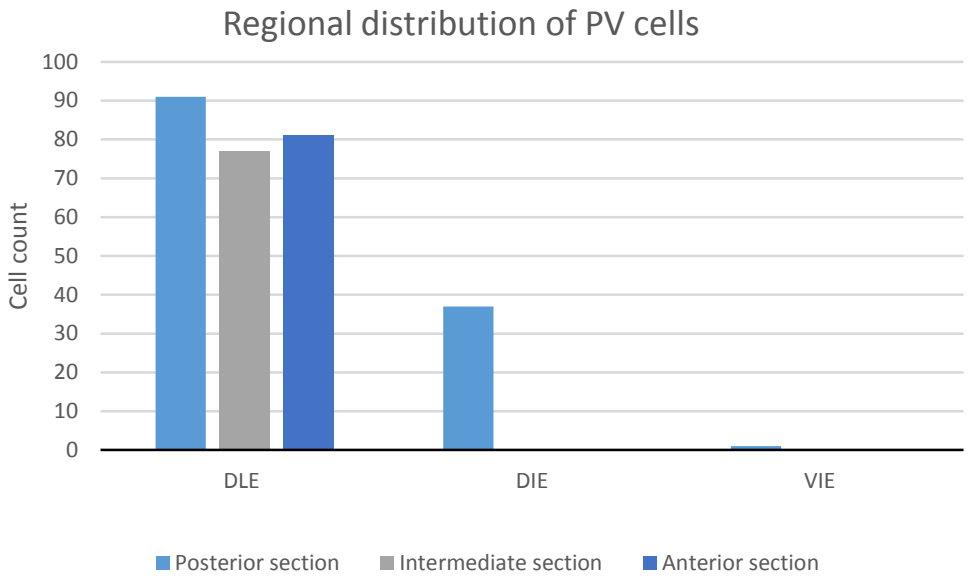

Figure 19: Distribution of PV positive GAD cells across sub regions in LEC. Cells counted in the different sub regions along the anterior-posterior axis.

Table 1: Overall distribution of cells across layers, sub regions and areas

Layer	PV cells (%)	Sub regions	PV cells (%)	Area	PV cells (%)
LI	1,0 %	DLE	86,8 %	Anterior	28,2 %
LII	16,7 %	DIE	12,9 %	Intermediate	26,8 %
LIII	32,8 %	VIE	0,3 %	Posterior	44,9 %
LIV	13,6 %				
LV	22,3 %				
LVI	13,6 %				
Total	**100,0 %**	**Total**	**100,0 %**	**Total**	**100,0 %**

Co-localization with GABA and morphological cell types

An analysis of the overlap between PV stained cells and GFP expressing cells (Fig 20), revealed that all PV cells expressed GFP and that 58 % of all GFP cells co- expressed PV.

The PV cells displayed great morphological variability. Soma shapes included globular, polygonal, oval and triangular forms, while the dendritic trees were observed to feature bipolar, multipolar or triangular configurations. An investigation of the PV cells in the different layers revealed that several morphological cell types were present within each layer and that certain morphological cell types seemed to be layer specific.

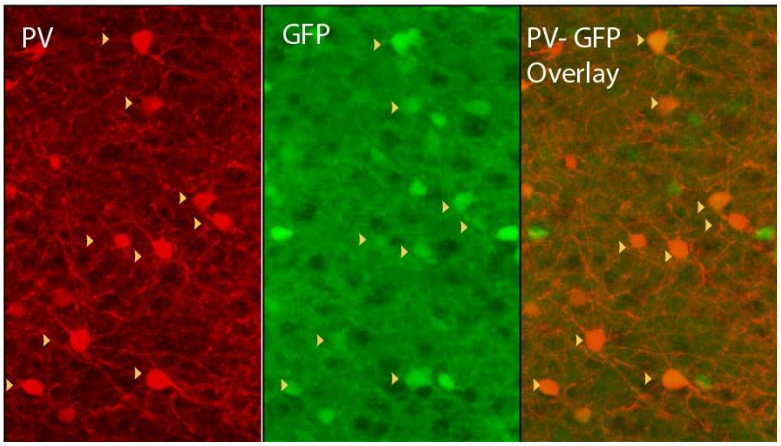

Figure 20: Co-expression of PV and GFP in immunostained cells. Yellow arrows indicate double labeled cells.

In LI, the few PV cells observed had oval somata, the dendrites of these cells were not visible. LII and LIII harbored most of the larger cell types (Fig 21. F), these had oval, fusiform or triangular somata and displayed a multipolar configuration. The dendritic trees of these cells were complex and frequently showed long dendritic branches, which extended into adjacent layers. In L II, medium sized polygonal multipolar cells were observed. One of these cells (Fig 21. C) had thick primary dendrites which tapered off and extended into L III and L IV. Small bipolar cells with spindle shaped somata and thin dendrites, such as the one depicted in Fig 21. C, were also found in L II. These cell were mainly confined within the layer. In L III medium sized triangular shaped cells (Fig 21. E) were also found, these had dendritic trees extending into three main regions and were confined mainly within L III. Layer IV and LV harbored small and medium sized multipolar cells with triangular, round, oval or polygonal cell bodies. The dendritic trees of these cells were mainly confined within the layer. In L IV, triangular cells similar to the ones in L III were additionally observed, these cell displayed dendrites which could branch into L III and V. L V typically featured small cells, but also

contained some medium sized cells and a few large cell bodies. The small cells often displayed a globular or oval cell body and a multipolar dendritic tree with thin straight and smooth dendrites (Fig 21. A). These cells were mostly confined within the layer. L VI contained cells similar to that in LV, consisting mainly of small multipolar cells of different soma shapes, and a few medium sized multipolar cells.

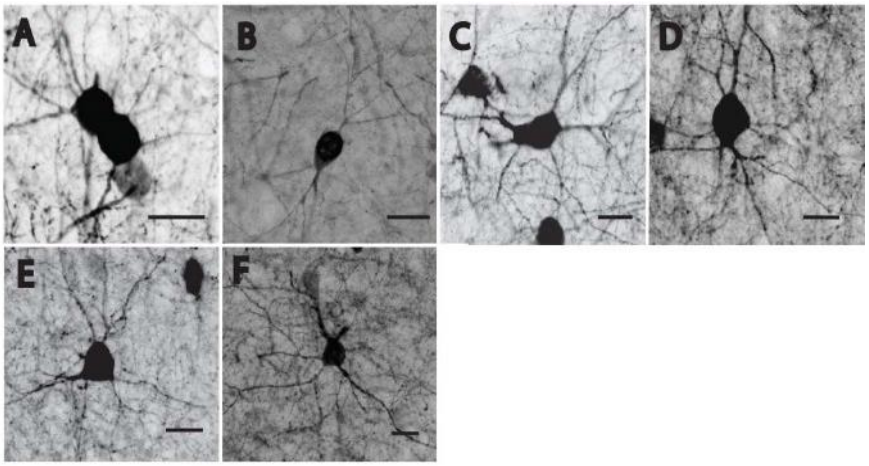

Figure 21: Morphological cell types of PV stained cells A Small globular cells B Bipolar cell C Polygonal multipolar cell D Fusiform multipolar cell E Triangular shaped neuron F Oval large multipolar cell.

3.2.2 Calbindin

Distribution of immunoreactive fibers

CB immunoreactivity was detected in cell bodies and fibers across the LEA in all sections. The CB stain shared some similarities with the PV stain, as they both displayed an immunoreactive fiber network that covered different layers and regions of the LEC in the anterior, intermediate and posterior sections. In the posterior section, which comprised the DLE and VIE, the CB

fibers were present in L II and L III of the DLE and most of L III of the VIE. The intermediate section, which contained portions of the DLE, DIE and VIE, displayed immunoreactive fibers mainly in L III, CB fibers were also present in L IV and L V but were less dense. The overall fiber density was inhomogeneous across the subdivisions, and appeared denser in the DIE and VIE compared to the DLE. The anterior section, which comprised the DLE only, featured a relatively homogenous fiber distribution across the region and throughout layers II – V, with the exception of a slightly denser fiber plexus in the area close to PER 35.

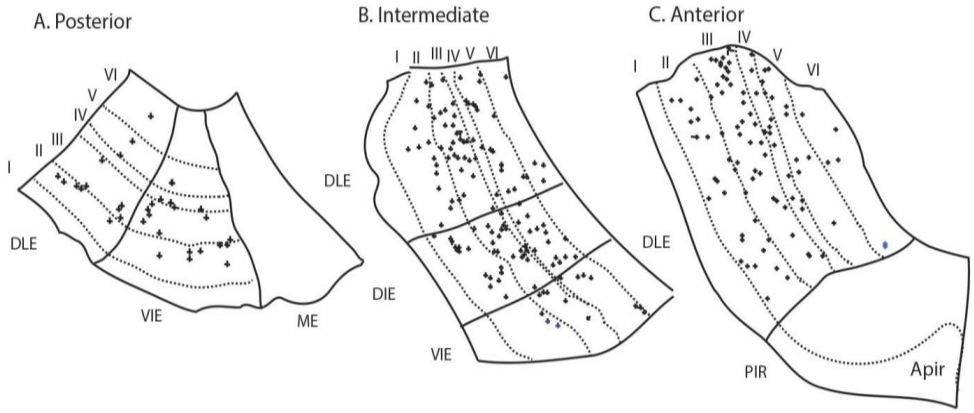

Figure 22: Schematic drawings of posterior (A), intermediate (B) sections with CB celll body distribution plotted across layers and subdivisions.

Cell distribution

In general, a high number of CB cells was observed throughout the LEC. The distribution of CB cells across LEC was mostly scattered but did show an inclination for cells to cluster in certain areas. A general characteristic for all sections was additionally a CB cell free L I (Fig 22. A- C).

The anterior section (only DLE) displayed the most scattered CB cell distribution among the three sections, clusters of CB cells did however

appear near the border of area PER 35. CB cells were present throughout L II- VI, where CB cell numbers were highest in L II and III, while the remaining layers IV- VI showed lower numbers of CB cells (Fig 22. C, 23). In the intermediate section (DLE, DIE, VIE), clusters of CB cells were found in subregions DLE and DIE, and mainly in L III. A few clusters of cells were adduitionally observed in L II, IV and V (Fig 22). PV Cell count from all layers in this setion revealed that the highest number of cells in L III, followed by L II and LV. L IV and VI contained low numbers of CB cells (Fig 23). The cell distribution across the subregions DLE, DIE and VIE showed a preference for DLE and the least for VIE (Fig 24). The posterior section displayed a few clusters of 3-4 cell bodies at the border between L II/ III as well as in L III (Fig 22. A). The cell numbers across laminae and subregions showed that L II and III harbored the majority of CB cells, while the deep layers contained lower numbers of CB cells (Fig 23). The CB cell counts in the two subregions were similar (Fig 24).

Laminar distribution of cells across all sections

A comparison of the laminar distribution of CB cells in all sections along the anterior-posterior axis showed that the anterior and intermediate sections displayed high numbers of CB cells in L II and III. The remaining layers showed comparable low numbers of CB cells, with the exception of L V in the intermediate section which stood out from LV in the posterior and anterior sections (Fig 23).The total number of CB cells across layers in all sections showed that most CB cells were observed in the superficial layers II and III. In total, L II - III was estimated to account for 66.1 % of the entire CB cell population. LV also showed a high number of CB cells (20. 9 %) while the

remaining layers contained lower portions of the CB cell population (L IV 8.7 % and LVI 4.3 %) (Table. 2).

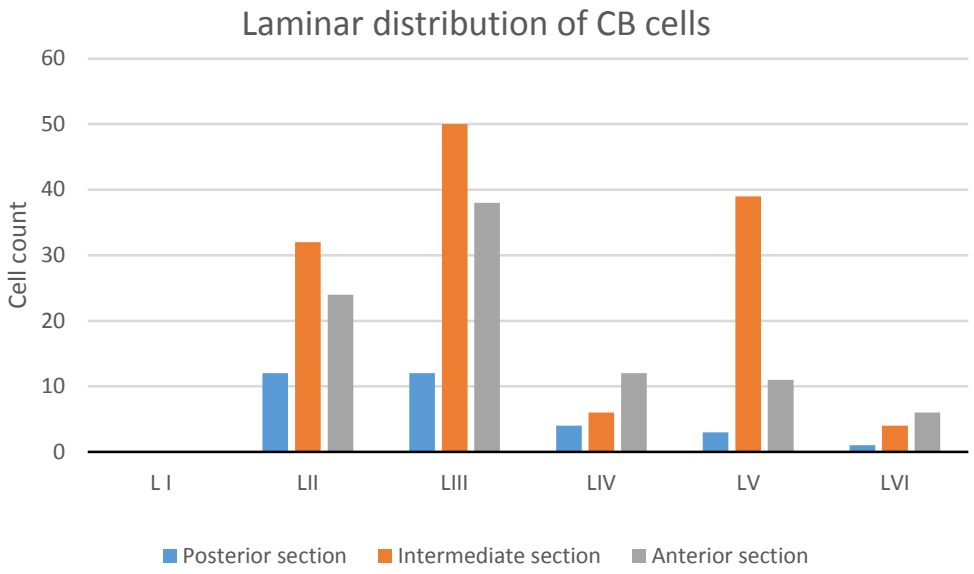

Figure 23: Distribution of CB positive GAD cells across, layers, areas and sub regions in the LEC. Cells counted in the different sub regions across the anterior-posterior axis.

Subregional and Anterior- posterior distribution

For the regional distribution, CB cells along the anterior-posterior axis revealed similar numbers of cells present in the VIE for the posterior and intermediate sections. An increase in CB cell numbers in the DLE along the posterior – anterior axis was also detected (Fig 24). An analysis of the total CB cell numbers from the DLE, DIE and VIE along the anterior-posterior axis showed that 66. 9 % of all CB cells were located in the DLE, 18. 5 % were found in the DIE and VIE contained 14. 6% of all CB immunoreactive cells (table 2).

CB cell counts from the posterior, intermediate and anterior sections indicate an uneven distribution of CB cells across the anterior- posterior axis of the LEC. 51.6% of all CB cells were counted in the intermediate section, which represented the region with the highest number of CB cells. The lowest percentage of CB cells appeared in the posterior section (12.6%), while the anterior section contained 35.8 % of all counted CB cells (Table 2).

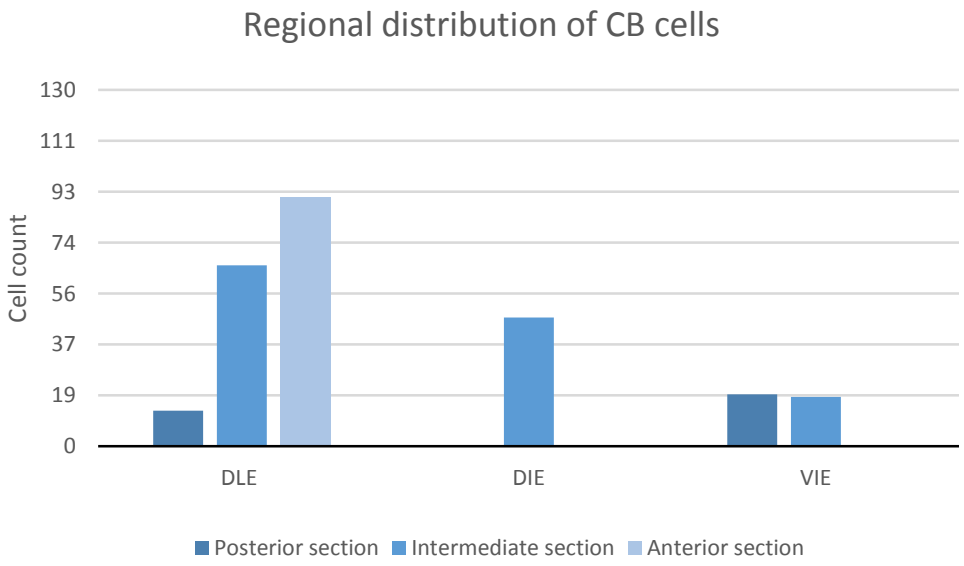

Figure 24: Distribution of CB positive GAD cells across sub regions in LEC. Cells counted in the different sub regions along the anterior-posterior axis.

Table 2: Overall distribution of cells across layers, sub regions and areas.

Layer	CB cells (%)	Sub regions	CB cells (%)	Area	CB cells (%)
LI	0,0 %	DLE	66,9 %	Anterior	35,8 %
LII	26,7 %	DIE	18,5 %	Intermediate	51,6 %
LIII	39,4 %	VIE	14,6 %	Posterior	12,6 %
LIV	8,7 %				
LV	20,9 %				
LVI	4,3 %				
Total	**100,0 %**	**Total**	**100,0 %**	**Total**	**100,0 %**

Co-localization with GABA and morphological cell types

A closer look at the co -expression of CB and GFP revealed that CB is widely expressed in the GABAergic cell population (Fig 25). Approximately half of the CB cell population in our sections (53. 3 %) co-expressed GFP, and 43.2% of the GFP cell population proved to be CB positive cells.

Similar to the PV cells, CB cells also featured a variety of different morphological cell types. An analysis of the CB cells morphology revealed medium sized multipolar cells, radially oriented bipolar cells , small bitufted cells, small polygonal multipolar cells, small globular cells, big polygonal cells, unipolar cells with pear shaped cell bodies, and spindle shaped cells with long dendrites (Fig 26. A-H).

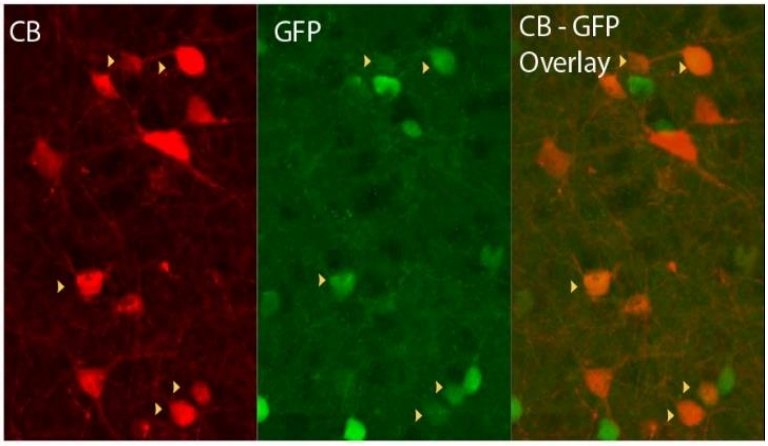

Figure 25: Co-expression of CB and GFP in immunostained cells. Yellow arrows indicate double labeled cells.

While L I was devoid of CB cells, L II featured cells of various shapes and sizes. Most of these cells were multipolar cells of medium or small size with oval or polygonal cell bodies (Fig 26. D). A few CB cells with large dendritic trees which branched into other layers were also found in this layer. One such type displayed a polygonal multipolar appearance with dendrites branching into L III (Fig 26. F), another type was a bipolar cell with a fusiform cell body and dendrites extending radially across layers (Fig 26. B). L III harbored most of the larger cell types, these cells displayed a triangular or oval cell body and a multipolar dendritic tree which stretched out across the layer (FIG 26. I). A few small round cells with short straight dendrites were also observed in LIII, these cells were entirely confined within the layer (Fig 26.A). L IV featured a mixture of strongly and faintly stained cells which had small and medium sized oval, triangular or round cell bodies. Many of these cells featured multipolar dendritic trees, which branched close to the soma. Bitufted cells with dendrites reaching into L III and LV were also found in L IV (Fig 26.C). These cells were radially oriented within the layer and displayed a

fusiform soma. L V featured a variety of smaller cell types, which displayed a weak CB expression, these cells had triangular, oval or globular cell bodies, and multipolar configurations (FIG 26.E). The layer also contained several cells of medium size, which exhibited a triangular shaped cell body (Fig 26. B, left cell) the dendritic tree of these cells appeared to mainly be confined within the layer. L VI was very homogenous, and most cells observed were small multipolar neurons with round or oval cell bodies, similar to the round cells in Fig 26. E.

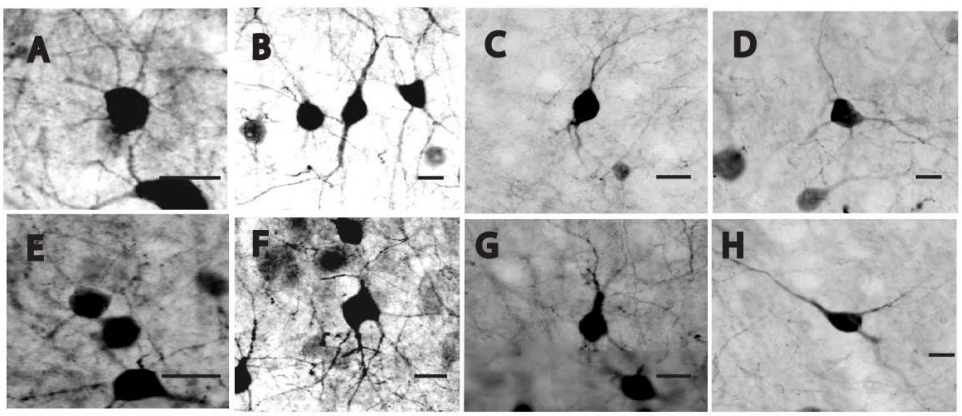

Figure 26: Morphological cell types of CB stained GAD cells. A Small round cells B Bipolar cell C Bitufted cell D Polygonal multipolar cell E small globular cells F Large polygonal multipolar cell G Unipolar cell H Oval shaped neuron.

3.2.3 Calretinin

Distribution of immunoreactive fibers

Immunoreactivity against CR was observed in cell bodies and fibers across LEC in all sections. The distributional pattern of CR fibers was uneven across subregions as well as layers for each section. For all sections, L I was observed to show a high intensity in staining. In the posterior section which includes all subregions, fibers were present throughout L II- VI. In L II, fibers were radially oriented and sparse compared to L III – V which displayed a denser fiber network. The distribution across the subregions showed that fibers were slightly denser in DIE and VIE compared to DLE. The intermediate section displayed a similar distribution across layers but had an even distribution of fibers across all subregions. The anterior section which consists of DLE, displayed less CR fibers than the intermediate and posterior sections. Most CR fibers were found in L III- V while none were found in L I and L VI contained few CR fibers.

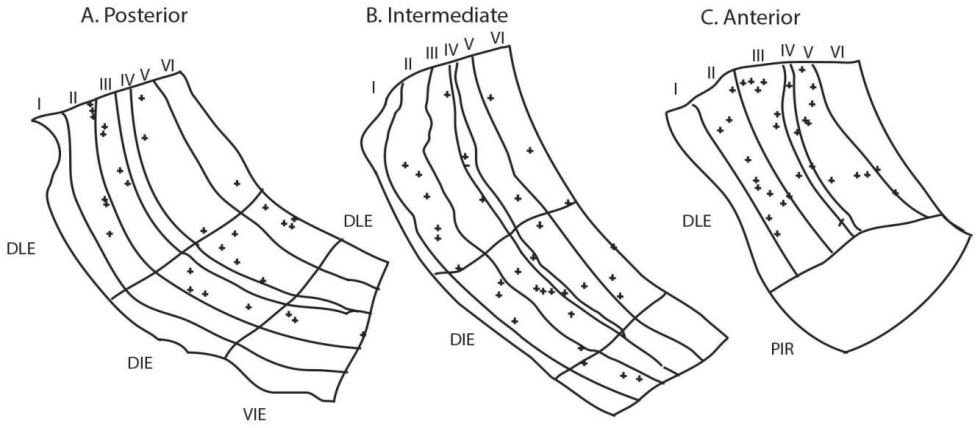

Figure 27: Schematic drawings of posterior (A), intermediate (B) sections with CR cell body distribution plotted across layers and subdivisions.

Cell distribution

CR cell bodies were present in all layers and regions except for L I. An analysis of the CR cell distribution in the posterior, intermediate and anterior sections showed no apparent pattern or clustering of CR cell bodies emerging across the LEC. CR cells were in general observed to be widely scattered across L II – L VI, and present in all sub regions (DLE, DIE and VIE) (Fig 27. A-C).

In the anterior section, CR cells were evenly distributed across LII-V, while Layer VI had a sparse number of CR cells (Fig 27. C, 28). The intermediate section showed similar results. However, there were more CR cells present in LVI as compared to the anterior section. The intermediate section comprised portions of both the DLE, DIE and VIE. There did not seem to be any real preferences for either area, except for an obvious lower cell number in area VIE, probably due to the significantly smaller size of this region as compared to the others (Fig 27. B, 29). The posterior section featured a similar pattern distribution of CR cells as the intermediate and anterior sections (Fig 27. A, 28, 29).

Laminar distribution of cells across all sections

The general laminar distribution of CR cells across all sections, revealed that the highest number of cells was located in L II (32. 3 %) and in L III (26.8 %). Only a small proportion of the counted CR cells was observed in L IV (7.5% of all CR stained cells counted), while L V and L VI contained 19.4% and 14 % of the total stained CR cell population respectively (Table. 3). A comparison of the CR cell numbers from all layers in the anterior- posterior sections,

revealed that the anterior and intermediate sections showed the highest cell numbers in L II (Fig 28).

Subregional and Anterior-posterior distribution

CR cell numbers from all subregions showed that the CR cell distribution in DLE, DIE and VIE was uneven (Fig 29). The majority of CR stained cells were located in the DLE (and accounted for 63.4 % of all CR cells), while the DIE featured 30.1 % and the VIE only 6.5 % of all counted CR cells (table 3). Along the anterior-posterior axis, the DLE of the anterior section stood out with a high number of cells, whereas the remainder of the subregions showed comparable cell numbers along the A -P axis (Fig 20. B).

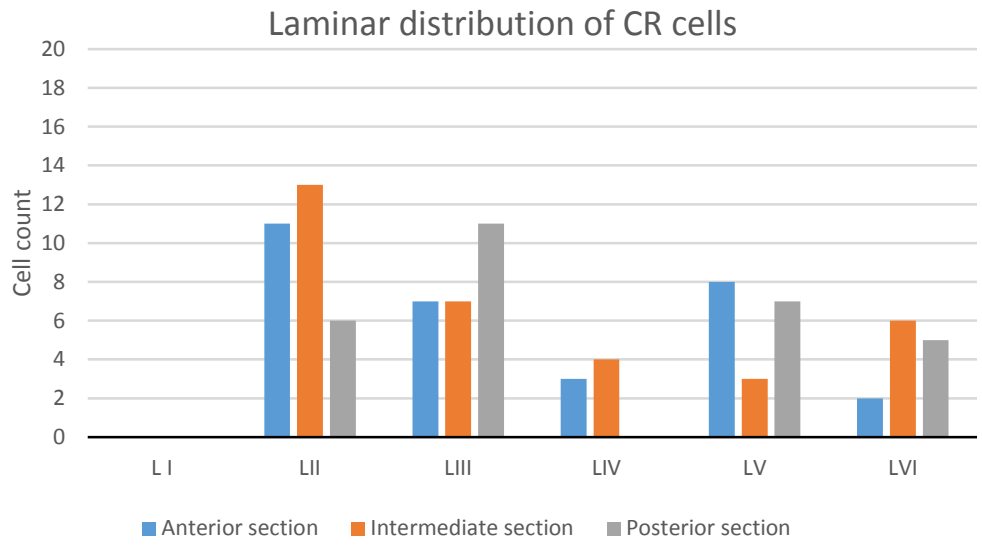

Figure 28: Distribution of CR positive GAD cells across, layers, areas and sub regions in the LEC. Cells counted in the different sub regions across the anterior-posterior axis.

Subregional and Anterior- posterior distribution

The overall CR cell distribution across layers and subregions along the anterior posterior axis showed that all sections contained similar portions of CR cells (33. 3 % anterior section, 35. 5 % intermediate section and 31. 2% posterior section) (Table 3).

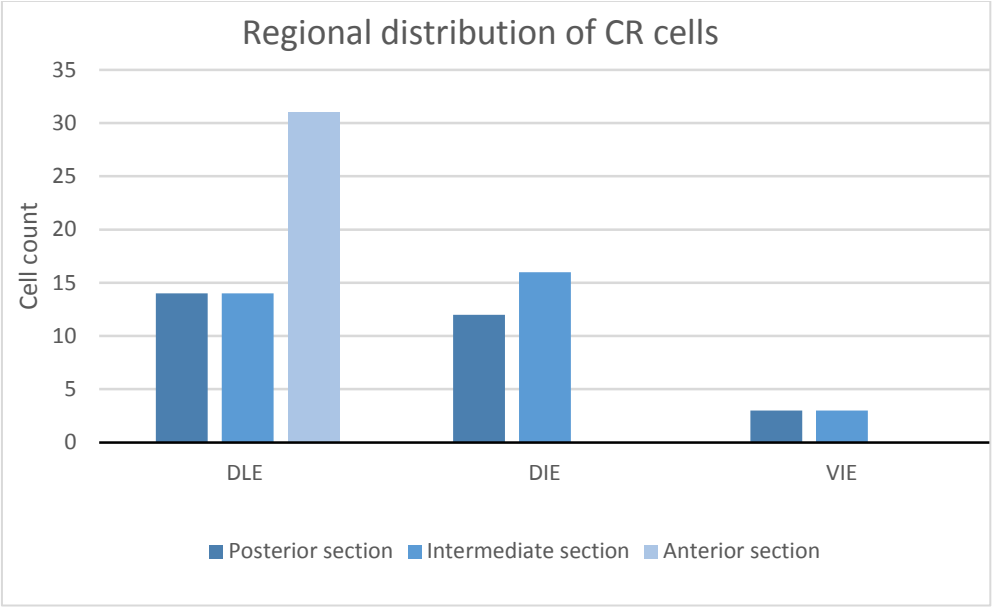

Figure 29: Distribution of CR positive GAD cells across sub regions in LEC. Cells counted in the different sub regions along the anterior-posterior axis.

Table 3: Overall distribution of cells across layers, sub regions and areas.

Layer	CR cells (%)	Sub regions	CR cells (%)	Area	CR cells (%)
LI	0,0 %	DLE	63,4 %	Anterior	33,3 %
LII	32,3 %	DIE	30,1 %	Intermediate	35,5 %
LIII	26,8 %	VIE	6,5 %	Posterior	31,2 %
LIV	7,5 %				
LV	19,4 %				
LVI	14,0 %				
Total	**100,0 %**	**Total**	**100,0 %**	**Total**	**100,0 %**

Co-localization with GABA and morphological cell types

CR co-localized with both GFP positive and negative cells (Fig 30). Cell counts indicate that a majority of CR cells express GABA (60. 49%), while CR expression in the GFP population was limited and estimated to 16.61%.

In the CR stain, several cell types were seen, and bipolar cells were observed to be prevalent in all sections. These cells featured an oval or fusiform cell body, and bipolar dendritic configurations, which either were horizontally or vertically oriented. Other observed cell types were round multipolar cells, fusiform bitufted cells, small triangular cells, and unipolar cells with short dendrites (Fig 31. A-E).

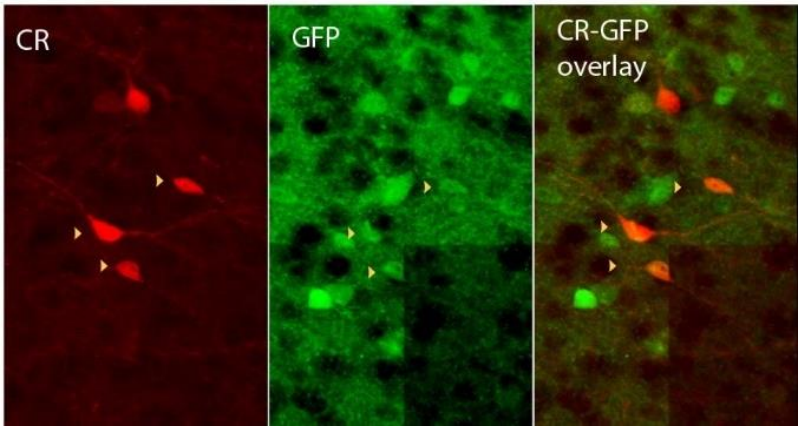

Figure 30: Co-expression of CR and GFP in immunostained cells. Yellow arrows indicate double labeled cells.

Various cell types could be observed within different layers of the LEC. LI was free of CR cells, hence no morphological subgroups were described. In L II, most cells were either small or medium sized, bipolar or multipolar cells with an oval, round or fusiform cell body (Fig 31. A-D).The multipolar cells were usually confined within the layer, while bipolar cells frequently displayed long dendrites extending into L I and III. L III also contained bipolar cells which extended across layers, these cells were radially oriented and had oval cell bodies and dendrites that often branched into LII and L III. Medium sized triangular cells with multipolar configurations (Fig 31. B) were additionally seen in L III. L IV had vertically oriented bipolar cells as well as round medium sized cells, while L V and L VI mainly contained small to medium sized oval or round cell bodies (Fig 31.E).

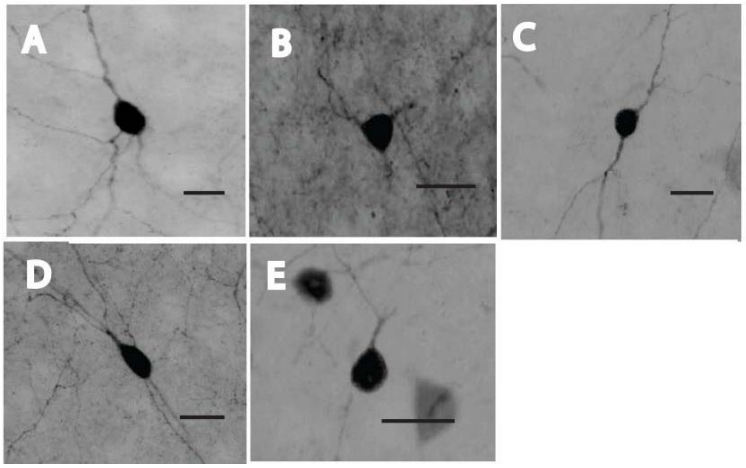

Figure 31: Morphological cell types of CR stained GAD cells. A Round multipolar cell B Small triangular multipolar cell C Bipolar cell D Bituftted cell E round unipolar cell.

3.2.4 Vasoactive intestinal peptide

Distribution of immunoreactive fibers

VIP immunoreactivity was observed in cell bodies as well as dendrites and fibers. In VIP immunostained sections immunoreactive fibers were present in all areas of the LEC. A difference in fiber density was especially prominent between the anterior section (DLE only) and the other two sections, where the intermediate (DLE and DIE) and posterior sections (DLE, DIE and VIE) displayed a denser VIP fiber network. However, the distribution of VIP fibers across subregions for all sections appeared relatively homogenous. For the laminar distribution, there was some variability in where VIP fibers were present as well as in the intensity of the immunostain in each section. In the posterior section, VIP fibers in the superficial L I- II exhibited a more intense immunostain than fibers observed in the deep layers L IV – VI. The opposite could be seen for the anterior section, where fibers in the superficial L I - III displayed a fainter immunofluorescence while fibers in the deep layers IV- VI

had a stronger stain. In the intermediate section, VIP fibers displayed a more homogenous intensity in their immunoreactivity and distribution across the LEC.

Cell distribution

In general, a low number of immunoreactive cell bodies was observed scattered throughout LEC. VIP cells were present across all regions and most layers in all sections (Fig 32. A-C). In the anterior section (only DLE), VIP cells were only present in L II, L V and L VI. Most VIP cells were found in L II, while a low numbers of cells were detected in L V –VI (Fig 32. A). In the intermediate section (DLE, DIE), VIP cells were found in all layers and they were evenly distributed (Fig 32, 33). The regional distribution of VIP cells showed a higher number of cells in the DIE compared to the DLE (Fig 34). The distribution of VIP cells in the posterior section was uneven compared to the previous section. A high number of cells were found in L II compared to L III- LVI (Fig 33).

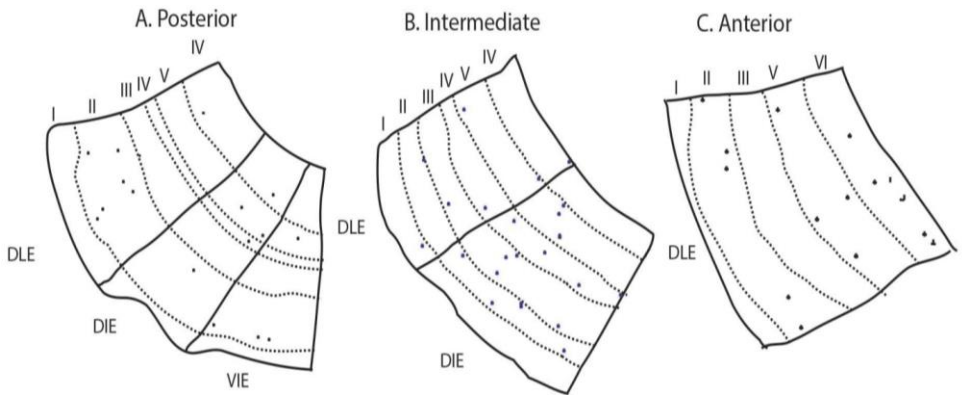

Figure 32: Schematic drawings of posterior (A), intermediate (B) and anterior(C) sections with VIP cell body distribution plotted across layers and subdivisions.

Laminar distribution of cells across all sections

A comparison of VIP cell data from layers in all sections showed that a high number of VIP cells were present in L II for all sections. For the remaining layers, VIP cell numbers differed along the anterior-posterior axis and the distribution followed no specific pattern across the laminae (Fig 33).The laminar distribution of VIP cells from all sections revealed that most cells were found in L II (41. 5%) and L V (20. 7%). The smallest portion of the VIP cell population was observed in L I (1. 7%), while L III and IV contained similar small portions of the remainder of counted cells (L III: 10. 3%, L VI: 15. 5%) (Table 4).

The VIP cell numbers from all sub regions (DLE, DIE and VIE) in the anterior-posterior sections revealed that the highest number of VIP cells was found in the DIE of the intermediate section. The DLE of the anterior section also stood out as an area featuring a high number of VIP cells (Fig 34).

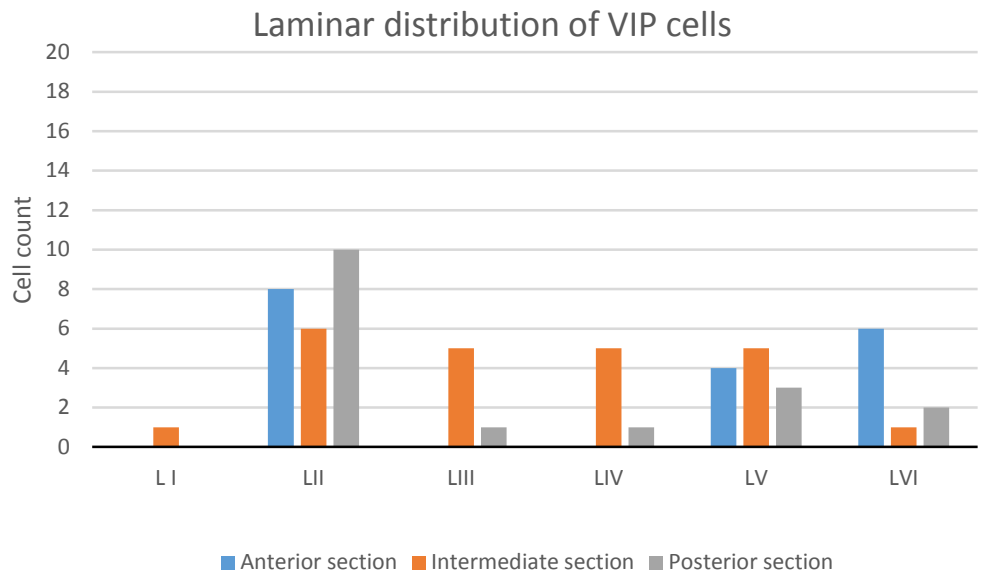

Figure 33: Distribution of VIP positive GAD cells across, layers, areas and sub regions in the LEC. Cells counted in the different sub regions across the anterior-posterior axis.

Subregional and Anterior- posterior distribution

Regional wise, data from the VIP cell count in the DLE, DIE and VIE revealed that more than half of all of VIP immunoreactive cells were located in the DLE (51 .7%) and that the VIE featured the lowest number of VIP cells (12. 1%). A large portion of the VIP cells were also located in the DIE (36. 2%) (Table 4).

To investigate differences in VIP cell distribution across the anterior – posterior axis, cell numbers from the anterior, intermediate and posterior sections were compared. These numbers showed that most VIP cells appeared in the intermediate section (39.7%), whereas the anterior and posterior sections showed smaller proportions of immunoreactive cells (anterior section: 31 %, posterior 29. 3 % , table X- % A- P axis)(Table 4).

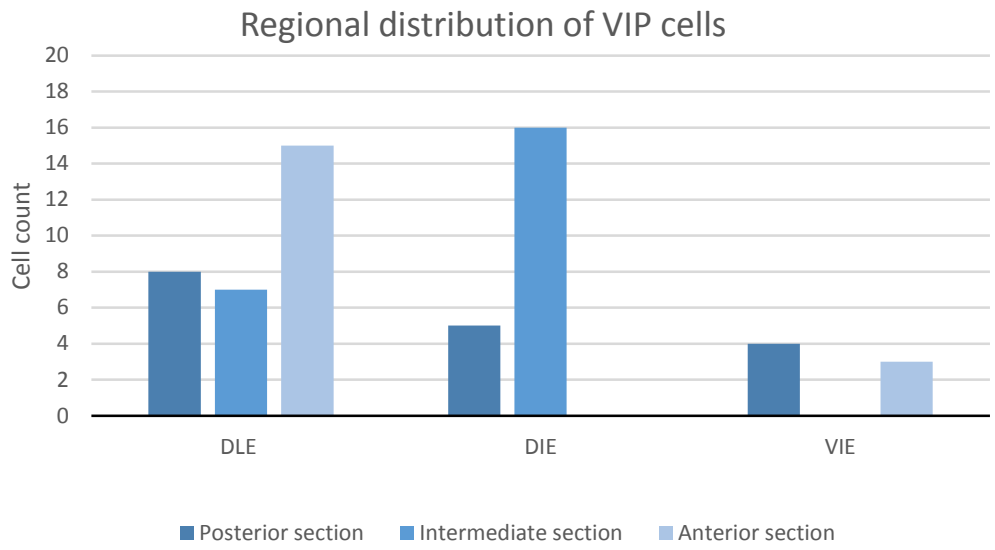

Figure 34: Distribution of VIP positive GAD cells across sub regions in LEC. Cells counted in the different sub regions along the anterior-posterior axis.

Table 4: Overall distribution of cells across layers, sub regions and areas.

Layer	VIP cells (%)	Sub regions	VIP cells (%)	Area	VIP cells (%)
LI	1,7 %	DLE	51,7 %	Anterior	31,0 %
LII	41,5 %	DIE	36,2 %	Intermediate	39,7 %
LIII	10,3 %	VIE	12,1 %	Posterior	29,3 %
LIV	10,3 %				
LV	20,7 %				
LVI	15,5 %				
Total	**100,0 %**	**Total**	**100,0 %**	**Total**	**100,0 %**

Co-localization with GABA and morphological cell types

VIP immunohistochemistry showed that VIP immunoreactivity was present in both GFP expressing cells and non-GFP expressing cells (Fig 35). Cell count numbers of VIP and GFP cells revealed that the majority of VIP cells expressed GFP (75.9 %). VIP co-expression in the GFP population was estimated to 8.6 %.

Immunohistochemistry against VIP showed that VIP was especially expressed in bipolar cells, and these cells were detected in different layers. Most bipolar cells featured round or oval somata and were usually radially oriented within the layer. These bipolar cells displayed dendrites which frequently branched into other layers but could also be confined within the layer. Bipolar cells with tangential orientations were also observed (Fig 36. F), the dendrites of these cells however appeared shorter than the vertically oriented ones and branched mainly within the layer. Pear shaped unipolar cells with simple and complex dendritic trees (Fig 36. A, E) were also observed. Their dendrites were either oriented towards the pia, or towards the deep layers. The pia-oriented cells had dendritic trees that frequently stretched into the adjacent layer. The deep-layer oriented cells on the other hand were confined within their layer. Additional observed cell types were small multipolar cells with globular and triangular somata (Fig 36. C, B). These cells were observed in all layers, but were particularly present in the deeper laminae.

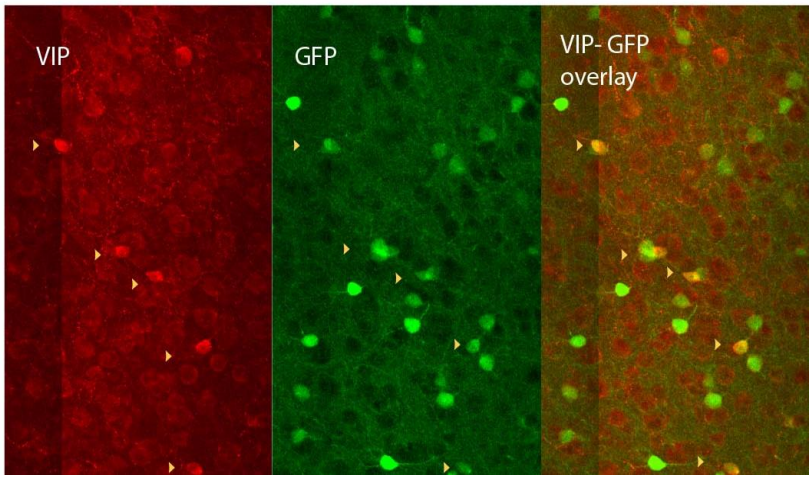

Figure 35: Co-expression of VIP and GFP in immunostained cells. Yellow arrows indicate double labeled cells.

In spite of the majority of VIP immunoreactive cells displaying bipolar morphologies, various cell types were present in each layer. In L I, a single oval cell body was observed, of which the dendrites were either gone or not well stained. In L II, a variety of cell types were detected, these were both radially and tangentially oriented bipolar cells with round or spindle shaped somata, these cells could stretch across layers. There were also triangular shaped cells with dendrites mainly confined within the layer (Fig 36. B, F). A unipolar cell with a complex dendritic tree (Fig 36.E) was additionally

detected in this layer, its dendrites reached into LI. In L III, bipolar cells with a spindle or oval shaped soma and radial orientation were detected. These bipolar cells were observed to have dendrites which were confined within the layer but a few extended into L II and IV. L III additionally contained oval triangular shaped multipolar cells with dendrites branching out to L II (Fig 36. B). In L IV, only bipolar cells were observed, a few of these cells featured long dendrites which extended into L V. L V contained mostlytriangular, oval

and round cells (Fig 36. C, D) while LVI featured bipolar cells and triangular cells of small and medium size. The cell types in L V and VI displayed mainly a local dendritic tree confined to the layer.

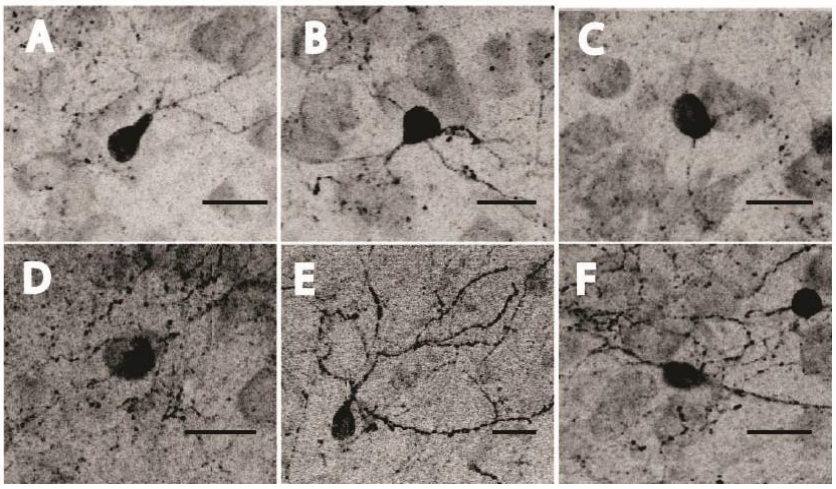

Figure 36: Morphological cell types of VIP stained GAD cells A Unipolar cell B Small triangular cell C oval multipolar cell D round cell E Unipolar cell with complex large dendritic tree F Bipolar cell.

3.2.5 Somatostatin

Distribution of immunoreactive fibers

Immunostaining against SST labeled fibers and cell bodies throughout the LEC. The cell bodies were however often only partially stained. Variations in fiber distribution as well as density were detected for the different sections. The posterior section which comprised the DLE, DIE and VIE, displayed immunoreactive SST fibers in all subdivisions and layers. In the DIE and VIE of this section fibers were especially dense in L I and L II. Besides this, no other regional differences were detected and fibers were moderately distributed across all regions and layers. The intermediate section, similar to the posterior section, displayed immunoreactive fibers in all layers. The SST fiber plexus was however a lot denser, and especially prominent in LI of the

DLE. Apart from that, fibers were observed to be rather homogenously distributed across the subregions and layers. An exception was L VI, which appeared to contain less SST Immunoreactive fibers. In the anterior section, which comprised area DLE only, L I displayed a slightly more dense SST-immunoreactive fiber network than the remaining areas. Fibers were otherwise sparse compared to the intermediate section but evenly distributed throughout L II – L VI. The anterior section in addition displayed a slightly denser SST fiber network in the area close to the amygdalopiriform transition area.

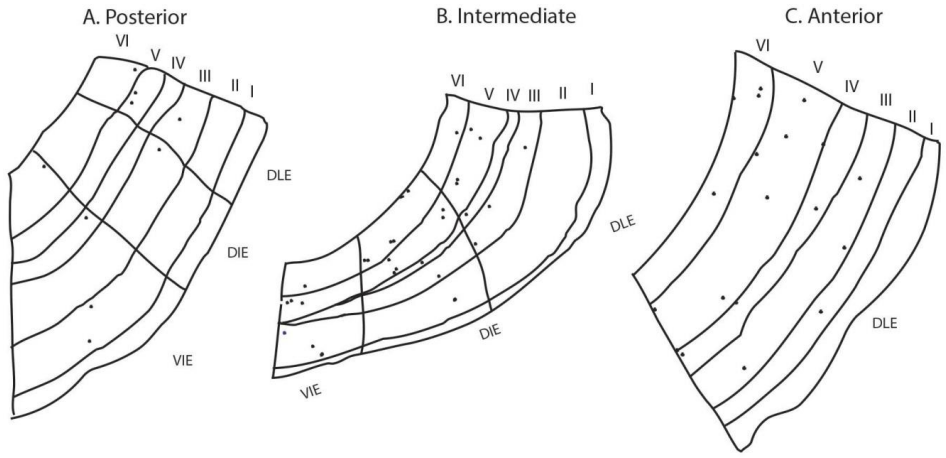

Figure 37: Schematic drawings of posterior (A), intermediate (B) and anterior(C) sections with SST cell body distribution plotted across layers and subdivisions.

Cell distribution

The SST cell distribution in sections obtained from the anterior, intermediate and posterior sections of LEC, revealed an overall low number of SST cells (Fig 37. A-C). SST Cells were in general widely scattered across LEC.

In the posterior section (DLE, DIE VIE), all layers contained SST cells except L I (Fig 37. A). The laminar distribution of SST cells was uneven, and most SST cells were situated in the deep layers V – VI, very few were present in L II- IV (Fig 38). An uneven distribution was also seen across the subregions, where most SST cells were either located in the DLE or VIE (Fig 39). The intermediate section (DLE, DIE, VIE) displayed, similar to the posterior section, a scattered distribution, but did also show SST cells in pairs which were present throughout the DLE, DIE and VIE (Fig 37. B). The SST cells in this section were mainly present in the deep layers V – VI. The subregional distribution showed that most SST cells were found in the DIE, while the VIE and DLE showed similar numbers of SST cells (Fig 39). The anterior section (DLE) displayed a widely scattered population of SST cells (Fig 37. C). SST cells were present in all layers except L I, and displayed a relatively homogenous distribution across the laminae with a few more cells in the deep layers V- VI (Fig 38).

Laminar distribution of cells across all sections

Despite the widespread distribution of SST cells, the overall laminar distribution showed that more than half of the detected SST cells were located in the deep layers L V (36.8%) and L VI (24.6%). A tenth (10,5%) of all SST cells were found in LIV, while L II and L III contained comparable proportions of the SST cell population (L II: 12.3%, L III : 15.8 %) (table. 5). The laminar distribution of SST cells along the A- P axis revealed that the highest number of SST cells was found in the posterior section, particularly in L V and LVI. L II-III of the anterior, intermediate and posterior sections displayed lower but similar numbers of SST cell bodies (Fig 39).

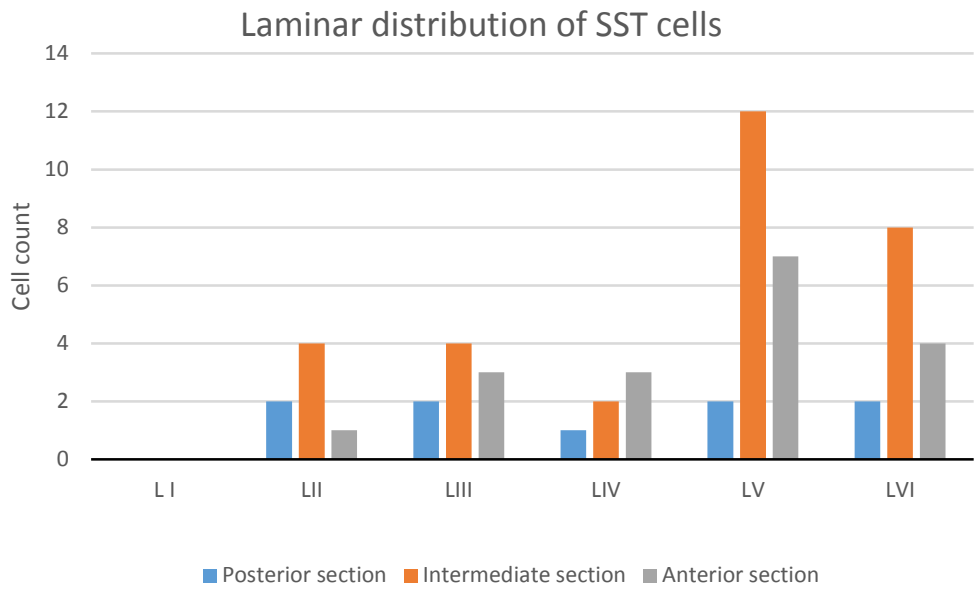

Figure 38: Distribution of SST positive GAD cells across laminae in LEC. Cells counted in the different layers in selected sections along the anterior-posterior axis.

Subregional and Anterior- posterior distribution

A comparison of SST cell distribution across the sub regions along the anterior – posterior axis revealed that the highest number of SST cells was found in the DLE of the anterior section and in the DIE of the intermediate section. The lowest number of SST cells was seen in the DIE of the posterior section (Fig 39). The total regional distribution of SST cells showed that most immuno positive cell bodies were detected in the DLE (54. 4 %) and the least in the VIE (19. 3%). An intermediate number of cells was present in the DIE (26. 3%) (Table 5). Data from the total number of SST cells from the anterior, intermediate and posterior sections showed that the majority of SST cells were located in the intermediate section (52.6 %) while the minority (15.8 %) of SST cells appeared in the section that was obtained from the posterior portion of the LEC. The remaining portion of the SST cells was found in the

anterior section, these accounted for 31 % of the total SST cell population (Table 5).

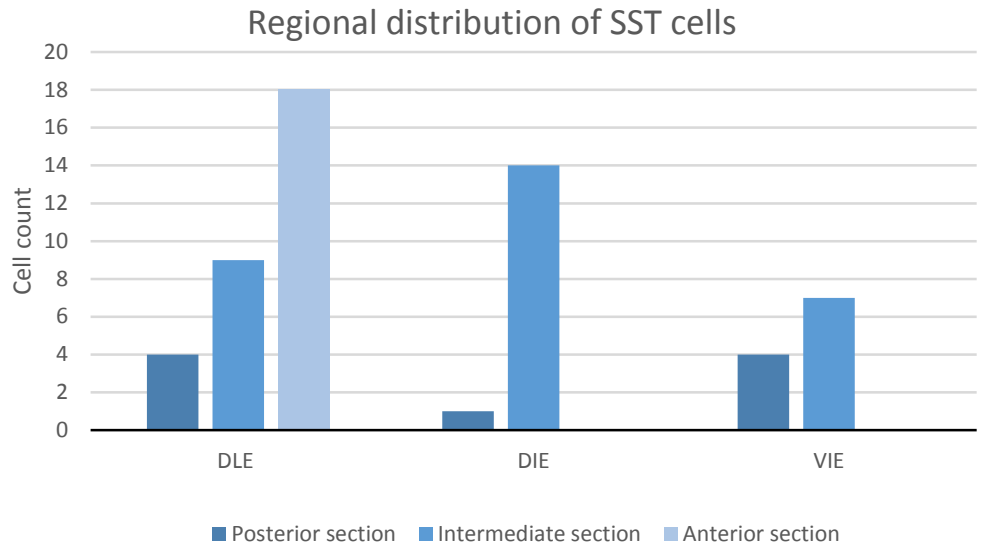

Figure 39: Distribution of SST positive GAD cells across sub regions in LEC. Cells counted in the different sub regions along the anterior-posterior axis.

Table 5: Overall distribution of cells across layers, sub regions and areas

Layer	**SST cells (%)**	**Sub regions**	**SST cells (%)**	**Area**	**SST cells (%)**
LI	0,0 %	DLE	54,4 %	Anterior	31,6 %
LII	12,3 %	DIE	26,3 %	Intermediate	52,6 %
LIII	15,8 %	VIE	19,3 %	Posterior	15,8 %
LIV	10,5 %				
LV	36,8 %				
LVI	24,6 %				
Total	**100,0 %**	**Total**	**100,0 %**	**Total**	**100,0 %**

Co-localization with GABA and morphological cell types

An analysis of the overlap between GFP cells and SST stained cells revealed that SST immunoreactive cells represented 8.1 % of the total counted GFP cells, and that 43.7% of all counted SST cells showed GFP expression (Fig 40). As the SST staining mainly labelled the proximal dendrites of the SST cells, the full dendritic extent was not easy to establish for most cell types. Despite partial staining of SST cells, several morphological cell types were revealed.

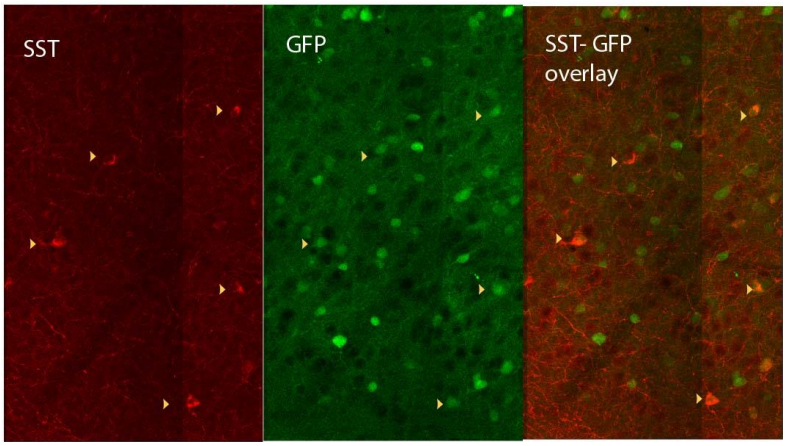

Figure 40: Co-expression of SSTand GFP in immunostained cells. Yellow arrows indicate double labeled cells.

In L II, most cell bodies were of medium size and featured an oval soma, a few of these were observed to be multipolar cells (Fig 41. C). L III contained oval cells as well and a few pear shaped cells (Fig 41. B), a few big multipolar cells did also appear in the stain from this layer (Fig 41. D). L IV, frequently featured oval, elongated SST cells such as the one depicted in Fig 41. A (oval cell to the right), while LV showed several small and a few medium sized oval and round cell bodies (Fig 41.A). In L VI mainly cells with round somata were seen.

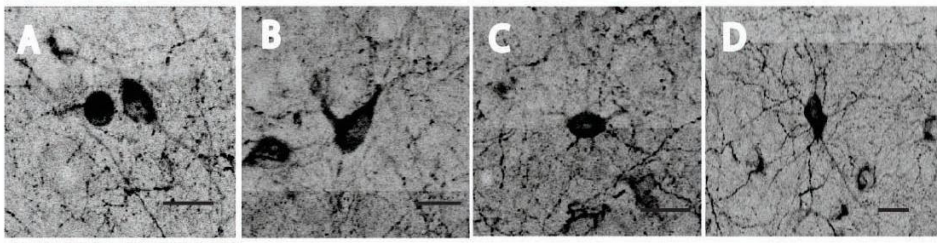

Figure 41: Morphological cell types of SST stained GAD cells. A Small round cell and medium sized oval multipolar cell B Pear shaped cell C Oval shaped multipolar cell D Large oval multipolar cell.

3.2.6 Cholecystokinin

Distribution of Immunoreactive fibers

Immunostaining against CCK labeled fibers and cell bodies in all three sections. The staining was highly variable along the anterior – posterior axis and the distribution of fibers varied across subregions and layers. In the posterior section fibers were sparse and found in L II – VI with no obvious preference for any layer. The distribution of CCK fibers across DLE, DIE and VI showed that there were slightly more fibers in VIE. The intermediate section which comprised subregions DLE and DIE, displayed a slightly denser network of CCK fibers compared to the posterior section. The fiber distribution across layers showed an uneven distribution where most CCK fibers were found in L III, while the remaining layers displayed few and scattered fibers. A slightly higher density of fibers was found in DLE, compared to DIE in this section. The anterior section displayed the highest density of CCK fibers among the three sections. CCK fibers were found at all dorso-ventral levels and showed a slightly higher density ventrally. For the laminar distribution, most fibers were present in L II – IV, while L I contained few and LV –VI displayed moderate density of CCK fibers.

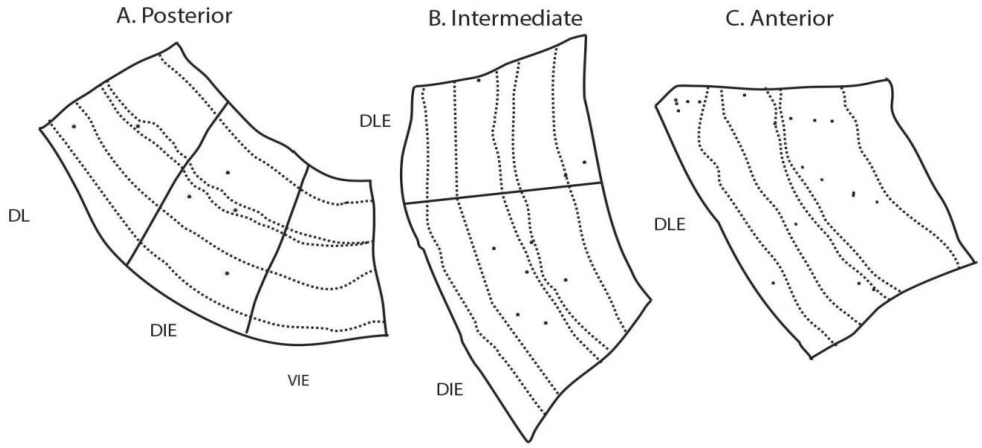

Figure 42: Schematic drawings of posterior (A), intermediate (B) and anterior (C) sections with CCK cell body distribution plotted across layers and subdivisions.

Cell distribution

For this immunostain, cell count included only GABAergic cells and GABAergic CCK cells. No apparent pattern of the CCK cell distribution was detected in the anterior, intermediate, and posterior sections. CCK cells were in general few and widely scattered across all layers and regions in LEC. In the anterior section, comprised of area DLE, the CCK cells were present mainly in layers I, III, and VI showing a preference for L I. In L I, a small cluster of CCK cells could be detected in the region bordering PER 35 (Fig 42. C).The intermediate section, which comprised DLE and DIE, displayed a different laminar distribution (Fig 42. B). CCK cells were found in all layers except from L I and L II and most cells appeared in L III and in subregion DIE . In the posterior section, CCK cells were present in DLE and DIE while VIE was devoid of CCK cells (Fig 42. A).

Laminar distribution of cells across all sections

The majority of CCK cells were distributed in L II, III and L V, these layers contained similar proportions of the CCK cell population (L II: 23 %, L III : 20%, L V:20%). L IV and VI contained smaller populations of cells (L I :10%, IV:10) and L I a moderate proportion (Table 6). A comparison of the laminar distribution of CCK cells along the anterior- the posterior axis showed that the highest occurrence of cells could be found in L I of the anterior section. The remaining layers in the anterior- posterior sections showed comparable cell numbers (Fig 43).

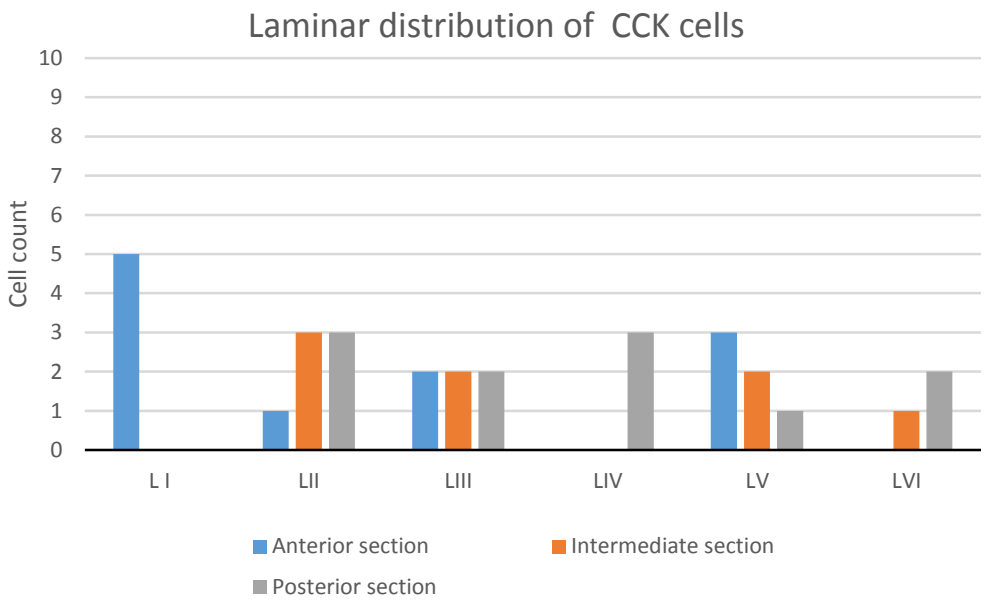

Figure 43: Distribution of CCK positive GAD cells across laminae in LEC. Cells counted in the different layers in selected sections along the anterior-posterior axis.

Subregional and Anterior- posterior distribution

The regional distribution of the CCK population showed that CCK cells were preferentially located in the DLE and DIE (DLE: 70. 6% DIE: 29. 4%), while the VIE contained no cells (Fig 44). The preferred region however changed across the anterior-posterior axis, where the highest number of CCK cells was seen in the DLE of the anterior section. The remaining cells from the intermediate and posterior sections featured comparable cell numbers in regions DLE and DIE.

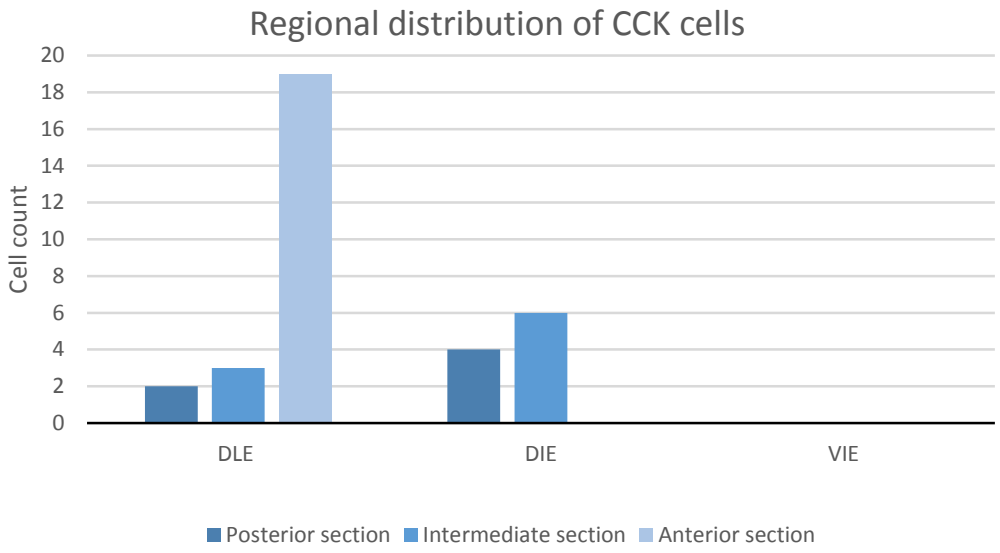

Figure 44: Distribution of CCK positive GAD cells across sub regions in LEC. Cells counted in the different sub regions along the anterior-posterior axis.

Table 6: Overall distribution of cells across layers, sub regions and areas

Layer	CCK cells (%)	Sub regions	CCK cells (%)	Area	CCK cells (%)
LI	16,7 %	DLE	70,6 %	Anterior	36,7 %
LII	23,3 %	DIE	29,4 %	Intermediate	26,6 %
LIII	20,0 %	VIE	0,0 %	Posterior	36,7 %
LIV	10,0 %				
LV	20,0 %				
LVI	10,0 %				
Total	**100,0 %**	**Total**	**100,0 %**	**Total**	**100,0 %**

The total CCK cell count from all sections showed that the anterior and posterior section featured similar proportions of CCK cells. A smaller proportion of CCK cells were present in the intermediate section (table 6).

Co-localization with GABA and morphological cell types

orphological description of CCK cells and co-localization with GAD

A cell count of the CCK immunoreactive GAD expressing cells versus the entire GAD cell population revealed that 5. 74% of all GAD cells expressed CCK.

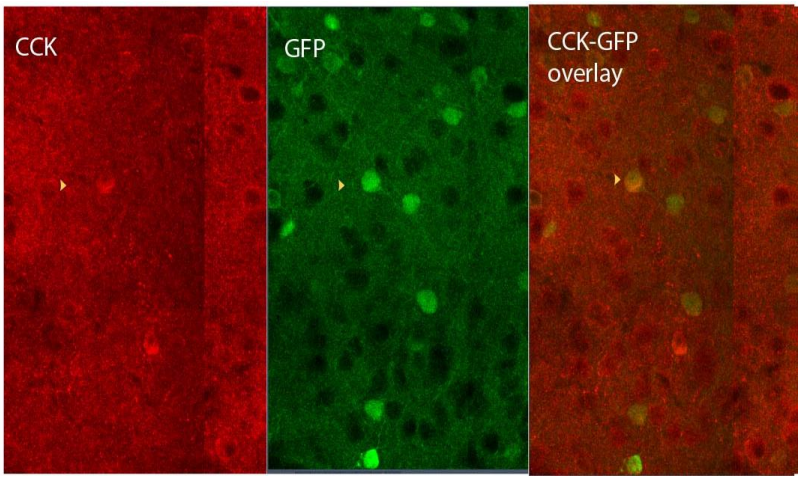

Figure 45: Co-expression of CCK and GFP in immunostained cells. Yellow arrows indicate double labeled cells.

The CCK cells generally displayed an incomplete staining of their cell bodies and often no staining of neurites could be seen (Fig 45). Two complete somato-dendritic morphologies were however detected in deep L V. These were small multipolar cells and a pear shaped unipolar cell (Fig 46. A, B). Most of the stained cells were observed to feature round or oval somata, and they were found across all layers except for L I.

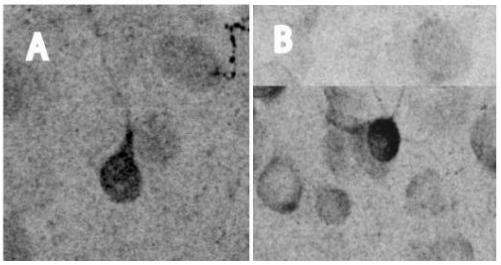

Figure 46: Morphological cell types of CCK stained GAD cells
A Pearshaped unipolar cell B small multipolar cell.

3.2.7 Neuropeptide Y

Distribution of immunoreactive fibers

Sections immune-stained for NPY showed sparsely distributed cell bodies and immunoreactive fibers across all regions and layers throughout the LEC. NPY fibers were observed to be especially prevalent in L I in all sections. Besides this, some variation in the NPY fiber distribution was observed in the anterior, intermediate and posterior sections. More NPY immunoreactive fibers were present in the posterior and intermediate sections compared to the anterior. Apart from this difference, the general pattern of distribution across sections, and the intensity of the immunofluorescence was similar.

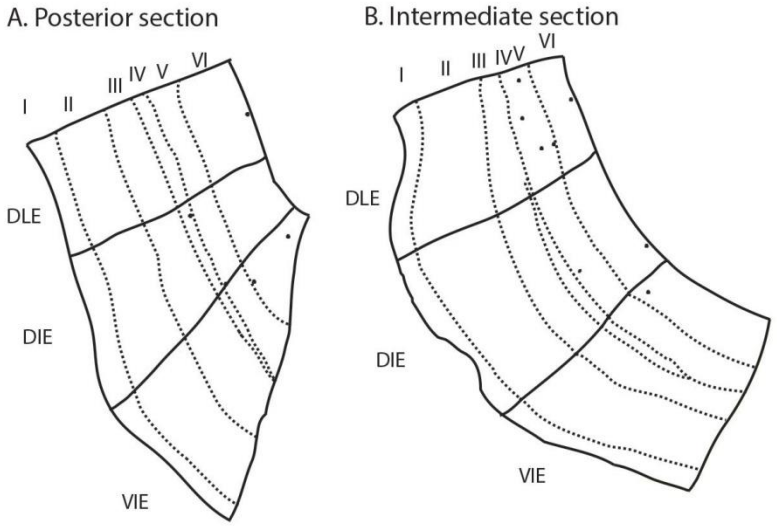

Figure 47: Schematic drawings of posterior (A) Posterior and (B) intermediate sections with NPY cell body distribution plotted across layers and subdivisions. The anterior section did not contain any NPY cells and is therefore not included here.

Cell distribution

NPY stained cells were in general few and only found in the deep layers L IV-VI (Fig 47 A-B). In the posterior section a few more cells were present in L VI

than L V, while the intermediate section displayed more NPY cells in L VI than L V. The regional distribution of cells for both sections showed that NPY cells were present in all subdivisions. No NPY cells were found in the anterior section.

Laminar distribution of cells across all sections

A comparison of the laminar distribution of NPY cell numbers from both sections showed that the highest number of NPY cells was found in L V of the intermediate section (Fig 48). The general laminar distribution of NPY cells showed that 65% were located in L VI, 30 % were present in L V and only 5 % of the cells counted were located in L IV (Table. 7).

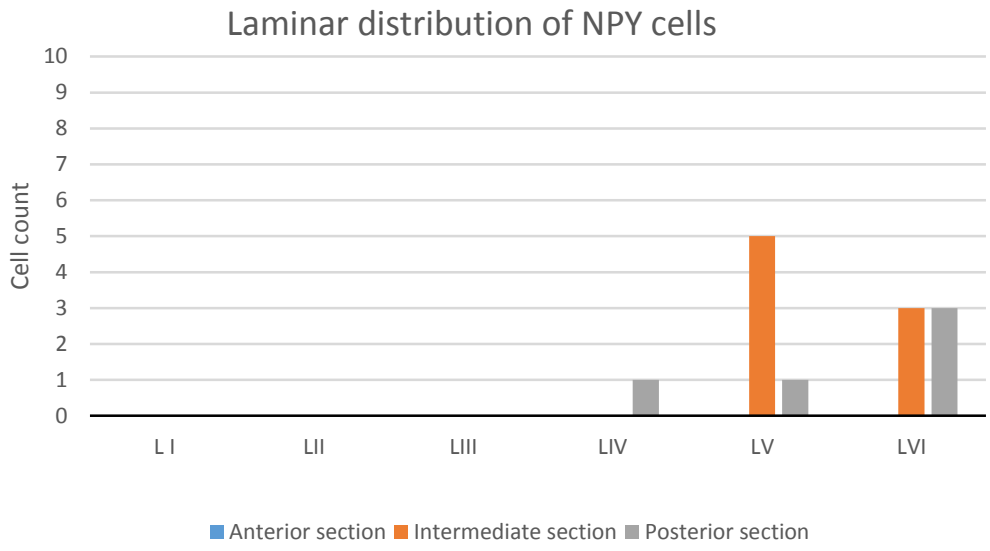

Figure 48: Distribution of NPY GAD cells across laminae in LEC. Cells counted in the different layers in selected sections along the anterior-posterior axis.

Subregional and Anterior- posterior distribution

An analysis of the regional distribution of NPY cells indicated that a major portion (46.2%) of all NPY cells was found in the DLE, while 30.8% were located in the DIE and 23.1% in the VIE (table. 7). In addition, cell numbers from the DLE, DIE and VIE in the posterior and intermediate sections showed that the highest number of NPY cells could be found in the DLE of the intermediate section. The posterior and intermediate sections were observed to contain fewer cells (Fig 49). With regards to the anterior-posterior distribution of NPY cells, we observed that the majority of the NPY cells were in the intermediate section (61. 5 %) (Table 7).

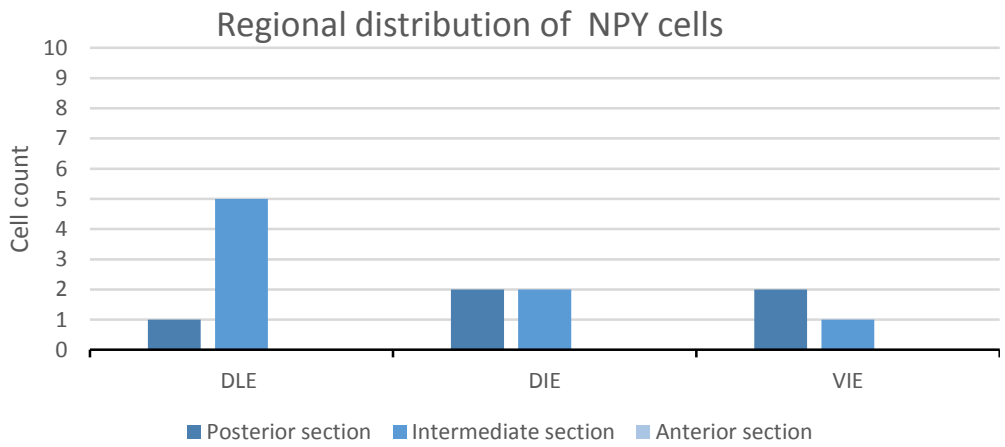

Figure 49: Distribution of NPY positive GAD cells across sub regions in LEC. Cells counted in the different sub regions along the anterior-posterior axis.

Table 7: Overall distribution of cells across layers, sub regions and areas.

Layer	NPY cells (%)	Sub regions	NPY cells (%)	Area	NPY cells (%)
LI	0,0 %	DLE	46,2 %	Anterior	0,0 %
LII	0,0 %	DIE	30,7 %	Intermediate	61,5 %
LIII	0,0 %	VIE	23,1 %	Posterior	38,5 %
LIV	5,0 %				
LV	30,0 %				
LVI	65,0 %				
Total	**100,0 %**	**Total**	**100,0 %**	**Total**	**100,0 %**

Co-localization with GABA and morphological cell types

For the morphological analysis, only cells featuring a complete NPY staining of the soma and proximal dendrites were included (Fig 50). The extent of the dendritic trees of the analyzed cells could not be determined as only the proximal dendrites were visibly stained. Therefore, whether or not dendrites of NPY cells were confined within layers could not be determined. In spite of few NPY cells observed, five different morphological cell types were detected. The first cell type featured a small fusiform soma, and resembled a bipolar cell at first glance. This was due to dendrites extending out from the poles of the cell. A closer look at the cell revealed that it featured three primary dendrites which displayed a regular shape proximal to the soma, and a more irregular form distally.

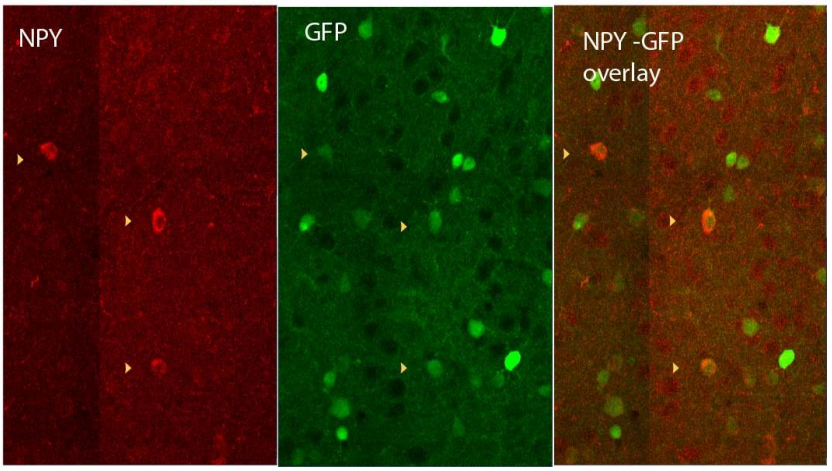

Figure 50: Co-expression of NPY and GFP in immunostained cells. Yellow arrows indicate double labelled.

The second cell type was a round multipolar neuron, with straight smooth dendrites radiating in all directions from the soma. The third cell type, was also a multipolar cell, but it featured a fusiform soma. The fourth cell type, featured a pear shaped soma and a few thin dendrites extending from it (Fig 51. A- D).

An analysis of morphological cell types across the layers revealed a single round big multipolar cell in L IV (Fig. 51. B). In L V, the NPY cells displayed mostly oval or round somata, the bipolar looking cells as well as fusiform multipolar cells (Fig 51. A, C) were also detected in this layer. In L VI, the pear shaped cell (Fig 51. D) was found among small immunostained oval and round cell bodies.

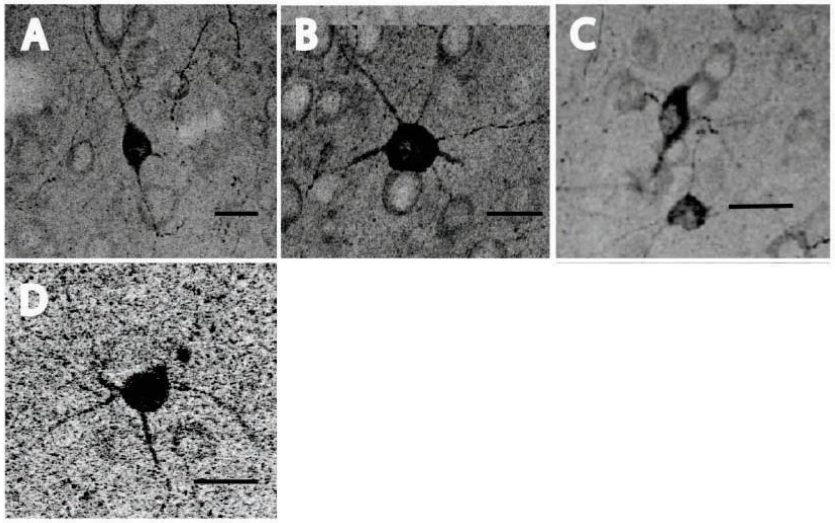

Figure 51: Morphological cell types of NPY stained cells. A Oval multipolar cell B round multipolar cell C Fusiform multipolar cell D pear shaped multipolar cell.

3.3 Double immunohistochemistry

Data from the mono-immunohistochemistry revealed that bipolar cells were especially prevalent in the VIP and CR stains. To investigate whether or not these two molecular markers may be present in the same cells, double-immunohistochemistry was additionally performed. To look at the overlap between the two population confocal images of the two immunostains (CR and VIP) and GFP were analyzed.

3.3.1 VIP – CR

Distribution of immunoreactive fibers

In double immunostained sections from the anterior, intermediate and posterior portions of the LEC, immunoreactive VIP and CR fibers displayed a similar distribution to that previously described in the mono-stained VIP and CR sections. Double labelled fibers were also observed but the distribution

of these overlapping fibers was difficult to see as the immunolabeling of fibers appeared to mainly stain proximal dendrites of both VIP and CR immunoreactive cells. Most double labelled cells were observed to show a complete labelling of the soma, a few cells showed only partial VIP staining but displayed a complete CR stain of the cell body. Cell bodies that displayed immunoreactivity for either CR or VIP were also seen in the double stained sections.

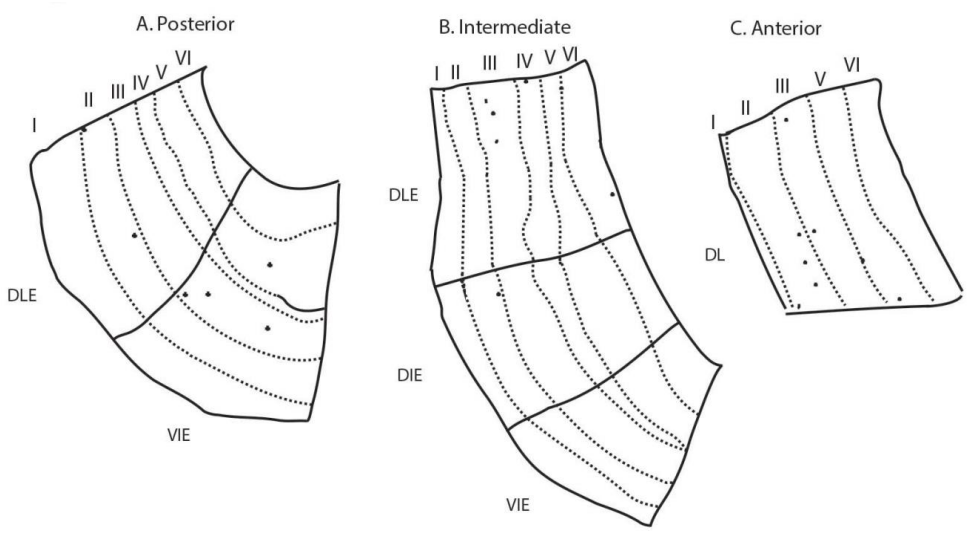

Figure 52: Schematic drawings of posterior (A), intermediate (B) sections with VIP-CR cell body distribution plotted across layers and subdivisions.

Distribution of immunoreactive cell bodies

VIP-CR immunoreactive cells were in general few and scattered, but appeared to show a preference for certain layers and regions in the LEC across the anterior- posterior sections (Fig 52). The posterior section which comprised of DLE and VIE, displayed a few scattered VIP- CR stained cells in L II, III and V. Most of these cells were located in the VIE (Fig 52.A). The intermediate section displayed few VIP- CR cells, which were observed in L II – IV and V. The subregional distribution showed that most VIP- CR cells were

located in the DLE, while one was present in the DIE and none in the VIE (Fig 52.B). In the anterior section, which comprises the DLE, VIP- CR cells were located in L II, III and V (Fig 52.C).

Laminar distribution of cells across all sections

A comparison of the VIP- CR cells laminar distribution in the anterior, intermediate and posterior sections, showed that the highest number of VIP-CR cells were found in L II and L III of the anterior and posterior sections (Fig 53). Looking at the total cell numbers from the laminar distribution across anterior-posterior sections, most VIP –CR cells were found in LII and L III (L II: 33.3%, L III: 44. 4%), while LV had an intermediate portion of cells (16.7%), and only a few cells were found in L VI (5. 6%). No VIP- CR cells were present in L I and L IV (Table 8).

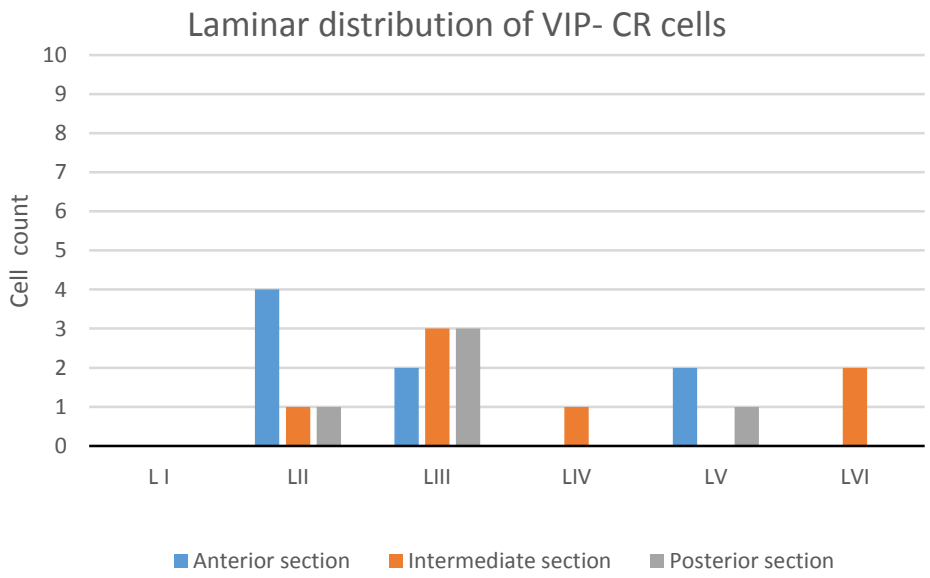

Figure 53 Distribution of VIP-CR double positive GAD cells across laminae in LEC. Cells counted in the different layers in selected sections along the anterior-posterior axis.

Subregional and Anterior- posterior distribution

Across sub regions, most VIP – CR cells in the analyzed sections were found in the DLE (75 %), while the fewest were found in the VIE (5 %) (table. 8) and a moderate proportion were found in VIE (20 %). In the intermediate and posterior sections the preferred region of VIP-CR cells were in the DLE , while in the anterior section most VIP -CR cells were found in the VIE (Fig 54).

An analysis of the total number of VIP- CR Cells present in the posterior, intermediate and anterior sections revealed that the distribution of cells was fairly uniform, with a slightly higher number of VIP-CR cells located in the anterior section(Anterior: 40 %, intermediate: 35 % and posterior slice: 25 %) (Table 8).

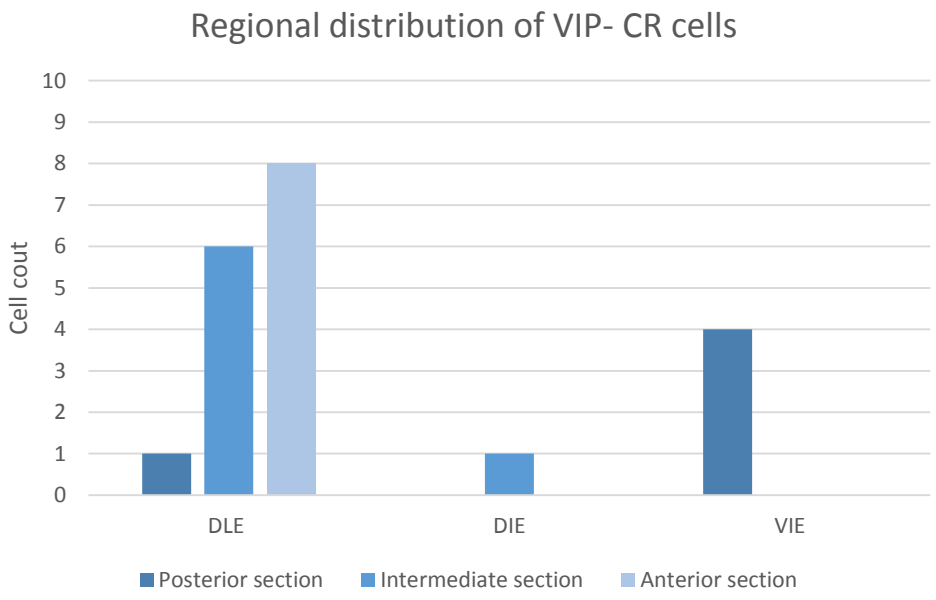

Figure 54: Distribution of VIP-CR double positive GAD cells across sub regions in LEC. Cells counted in the different sub regions along the anterior-posterior axis.

Table 8: Overall distribution of cells across layers, sub regions and areas

Layer	VIP- CR cells (%)	Sub regions	VIP- CR cells (%)	Area	VIP -CR cells (%)
LI	0,0 %	DLE	75,0 %	Anterior	40,0 %
LII	30,0 %	DIE	5,0 %	Intermediate	35,0 %
LIII	40,0 %	VIE	20,0 %	Posterior	25,0 %
LIV	5,0 %				
LV	15,0 %				
LVI	10,0 %				
Total	**100,0 %**	**Total**	**100,0 %**	**Total**	**100,0 %**

Co-localization with GABA and morphological cell types

All VIP-CR cells were GFP positive (Fig 55), and they represented 5.9 % of the GFP population in the analyzed sections. VIP- CR double-labelled cells accounted for 27.8 % of the VIP cell population, while 36.9% of all CR cells co-expressed VIP. In terms of morphology, VIP – CR cells included two morphological types, bipolar cells and small globular multipolar cells. The bipolar cells were detected in L II and were observed to be radially oriented to the pia. They displayed fusiform or oval somata (Fig 56. A-C) and dendrites distributed in L II-III. The small multipolar cells (Fig 56. B) were mainly observed in L VI and occasionally in the superficial L II-III.

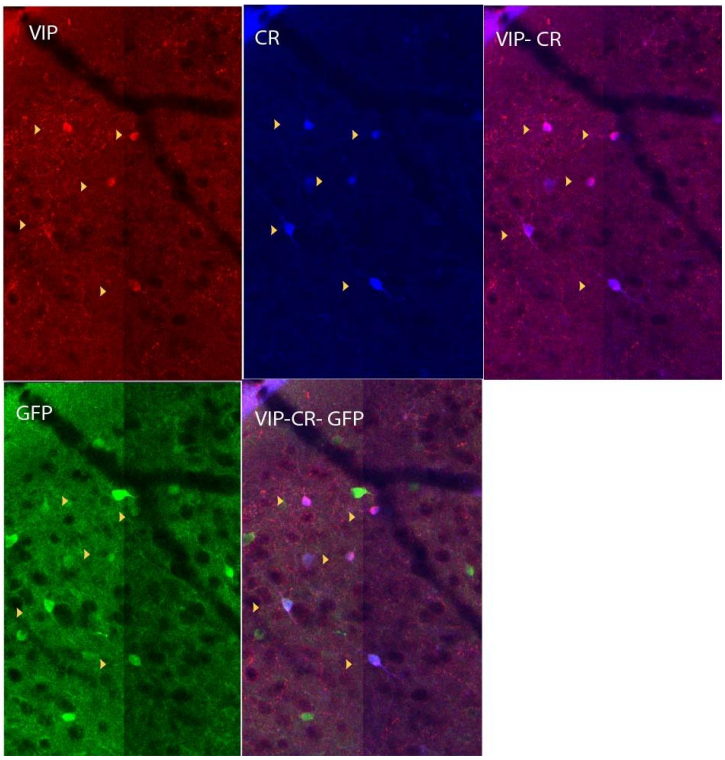

Figure 55: Co-expression of VIP and CR immunostained cells and GFP. Yellow arrows indicate double labeled cells.

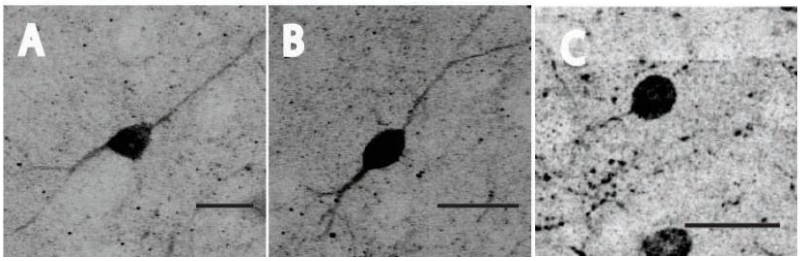

Figure 56 Morphological cell types of VIP- CR stained cells. A Bipolar cell with triangular somata B Bipolar cells with oval somata C Round small multipolar cell.

4 METHODOLOGICAL CONSIDERATIONS

In this study, the aim was to provide an overview of which populations of GABAergic cell types are present in LEC both with regards to morphological and chemical identities. We also aimed to map the distribution of these cell populations in LEC. We obtained these data by intracellular filling of identified GABAergic cells and immunohistochemical methods. A few aspects of the methods need to be discussed in order to interpret the presented data.

First, the morphological data was obtained by intracellular filling of cells in sections that expressed GFP. This procedure was very much random as the cell morphology was not visible. As GFP expression of cells was easier to detect in medium and large sized cells, we tried to aim for both for strongly and weakly GPF expressing cells. As with all slice work, cells are susceptible to cutting which could result in inaccurate data. To ensure that we got a representative sample of cells with more or less complete morphologies, the stacks of confocal images were checked to identify any obvious cuts of dendrites. The cells which showed incomplete filling or that were severely cut were not included in the data analysis.

For the morphological analysis of filled cells, we followed the petilla nomenclature (Ascoli, Alonso- Nanclares L. et al. 2008) and did additional measurements of the cell body, dendrites and dendritic tree in 3D reconstructed cells. Further analysis of the dendritic tree by using polar plots and sholl analysis was also performed to provide more detailed information. Based on these measurements, the eight morphological cell types were distinguished. Previous studies (Markram 2004) using a combination of

measurements and descriptions of cell morphology has shown that these are valid methods for characterizing cell types.

For the confocal analysis, the filled cells were susceptible to photobleaching during the scanning. The fluorescent dye used was however of a high concentration, and as cells were loaded with the dye the effect of bleaching did not seem significant. For our immunohistochemical studies, sections were obtained from anterior- intermediate and posterior portions of LEC. As we did not use sections from all of LEC, there is a possibility of over or underestimation of the number of immuno-reactive cell bodies in the different areas of LEC. The stained sections were also vulnerable to photo bleaching as they were scanned using a confocal microscope. To optimize staining for the confocal scanning we tested several different fluorophores conjugated to the secondary antibody. The fluorphore Alexa Fluor 546 provided the best staining in terms of intensity, and seemed to show minimal bleaching during the image acquisition with the confocal microscope. To ensure specificity in staining against the different primary antibodies, all immunohistochemistry was carried out in different animals, and if available, we tested other primary antibodies against the same antigenes. All data was also cross-checked against previous findings in the literature.

5 DISCUSSION

5.1 Morphological characterization of interneurons in LEC L II/II

Summary

Using intracellular filling of cells in L II/ III of LEC in a GAD 67 eGFP transgenic mouse line, and 3D reconstructions based on confocal images of these cells, we show that GABAergic cells in the superficial layers of LEC are morphologically heterogeneous. Nevertheless, we conclude that there are at least two morphologically different cell groups in LEC: multipolar and bipolar cells. In the multipolar group we find the small and big multipolar, pyramidal like, bow tie, radial and triangular cells, and in the bipolar group the small bipolar spindle and bipolar cells. In total eight different morphological cell types were identified. The cells displayed distinct somatodendritic morphology and differed in both size and complexity of their dendritic trees.

5.1.1 Morphological cell types in LEC L II / III

The GABAergic cells in L II/ III of LEC showed diverse somatodendritic morphologies. These cells were largely aspiny and predominantly multipolar or bipolar. These findings are in line with previous descriptions of cells in LEC (Köhler and Chan-Palay 1983, Köhler, Eriksson et al. 1986, Wouterlood, Härtig et al. 1995, Miettinen, Koivisto et al. 1996), and cells in our own immunohistochemical study. The soma size of the cells did not show any major variability in our study. Previous data (Wouterlood, Härtig et al. 1995, Miettinen, Koivisto et al. 1996, Miettinen, Pitkänen et al. 1997, Wouterlood

and Pothuizen 2000) on cells in LEC however indicate a highly variable soma size. This is most likely related to the type of measurement used, as the circumference of a 3D reconstructed cell was measured in our study rather than the long axis in a 2D image, which can be more susceptible to bias. Our cells displayed several types of cell body shape and a variable number of primary dendrites. These observations are also in line with previous reports of described cells in LEC. In contrast to the soma size, dendrites displayed a relatively great range in thickness. Our observations of the larger cell types displaying thicker dendrites and smaller cells thinner dendrites, along with the highly variable dendrite thickness is in accordance with previous results (Wouterlood, Härtig et al. 1995). The dendritic complexity of cells was highly variable but showed a peak of maximum branching points at the distance of 20-35 µm for all cell types. An analysis of the dendritic tree in terms of branching points has previously not been performed on GABAergic cells in LEC. However, previous descriptions (Miettinen, Pitkänen et al. 1997, Wouterlood and Pothuizen 2000) of GABAergic cells in LEC displaying a variable number of primary dendrites support our findings. As most synaptic input on interneurons is formed on dendrites (Markram, Toledo-Rodriguez et al. 2004), it is tempting to hypothesize that the area with the highest number of dendrites receives the largest proportion of input. This would then suggest that most input to interneurons in L II/ III of LEC occurs within a short distance from the soma. Depending on the extent of dendrites, cells can receive input from one or several layers. These inputs might be from principal cells or interneurons within the layer(s), intrinsic input from other layers in LEC or extrinsic inputs from areas outside LEC (Canto, Wouterlood et al. 2008). The dendritic extent for most cells were mainly found within a layer, an exception was seen for the big multipolar cells which had dendrites

distributed in L II and III. This could indicate that the GABAergic cells in L II/III of LEC mainly receive input from one layer.

To this date, the functional role of the different GABAergic morphological cell types in EC is not well known. Our study provides detailed information about the somatodendritic shapes of cells in L II/ III, but is limited as no information is provided about the axonal tree. The morphological characteristics used in this study can however provide a clue as to which cell types we have encountered. In addition, there are several lines of evidence that have shown that there is a link between cell morphology and firing activity. Phenomena such as back propagation in a cell, a synaptic event where the spread of an action potential propagates back to the dendrites, as well as the regular forward propagation of an action potential have been shown to be influenced by differences in dendritic morphology (Stuart, Spruston et al. 1997, Vetter, Roth et al. 2001). In addition, neuronal models in which the dendritic tree is altered in size and shape, have shown that these differences alone can support a variety of spiking behaviors (Mainen and Sejnowski 1996, Magee 2000, van Elburg and van Ooyen 2010). Taken together, all these findings suggest that L II / III contains a morphologically diverse GABAergic cell group which might be functionally different.

5.2 Immunohistochemical characterization of GABAergic cells in LEC

Summary

In this study, the immunoprofiles of GABAergic neurons in LEC were analyzed in a transgenic GAD 67 eGFP mouse line. This study showed that the GABAergic cells in LEC are neurochemically heterogeneous, and contains

subpopulations of PV, CB, CR, NPY, VIP, CCK and SOM cells, as well as a population of VIP-CR co-expressing cells. These subpopulations displayed distinct but altogether substantial morphological heterogeneity. In addition, the distribution of the different cell types across LEC was variable, but showed a preference for either the superficial or deep layers. The co-expression with GABA for each neurochemical marker showed either a partial or complete overlap.

5.2.1 Immunoreactivity of Ca2+ binding proteins and neuropeptides in LEC

Immunohistochemistry against the calcium binding proteins PV, CB and CR showed a staining pattern comparable to what has been reported in previous studies (Wouterlood, Härtig et al. 1995, Fujimaru and Kosaka 1996, Miettinen, Koivisto et al. 1996, Miettinen, Pitkänen et al. 1997, Wouterlood, van Denderen et al. 2000). For these markers the immunoreactivity was showed high staining intensity in cell bodies and neurites throughout LEC, and the distribution of immunoreactive fibers for each marker was similar to what has been reported before. This was also true for our VIP stain, which yielded a similar pattern of fiber distribution as well as labeling of cell bodies and dendrites (Köhler and Chan-Palay 1983). However, for the neuropeptides CCK, NPY and SST we observed that there was a consistent difference in staining quality between our data and previous reports. In previous reports (Köhler and Chan-Palay 1982, Köhler and Chan-Palay 1983, Köhler, Eriksson et al. 1986, Wouterlood and Pothuizen 2000), the immunostaining for CCK, NPY and SST showed a more complete labeling of cell bodies and proximal dendrites compared to our data. This is most likely

a result of the colchinine pretreatment given to the animals in these studies. This procedure has been shown to increase neuropeptide expression in cell bodies and proximal dendrites by blocking axonal transport in the cells (Dahlström 1968, Aguado, Pozas et al. 1999). As the treatment is done with a significant impact on animal health this was not considered for our project.

5.2.2 Distribution of GABAergic cell populations across LEC

The immunohistochemistry against different molecular markers in the GABAergic population in LEC revealed a widespread distribution of cell groups across the laminae. Nonetheless, most cell types appeared to show a preference for either the superficial layers II- III or deep layers V–VI. Layer I and IV typically showed a low number of immunoreactive cells for all neurochemical markers. The superficial layers II and III were dominated by neurons expressing the calcium binding proteins PV, CB and CR, but cells expressing the neuropeptides VIP and CCK were also observed. The deep layers L V and VI, on the other hand, contained large proportions of the NPY and SST cell populations. These data are in accordance with what has been reported earlier for the different immunoreactive cell groups in LEC (Köhler and Chan-Palay 1982, Köhler and Chan-Palay 1983, Fujimaru and Kosaka 1996, Miettinen, Pitkänen et al. 1997, Wouterlood, van Denderen et al. 2000).

The regional distribution of immunoreactive cells across DLE, DIE and VIE in our study shows a decrease in cell number from DLE to VIE. An important note here is that the size of each LEC subdivision is inherently different. DLE has the largest overall size, DIE shows an intermediate size, and VIE is the

smallest. The cell count numbers from the different subregions in our study are therefore skewed as they do not represent the number of cells per area, but rather the absolute number of cells. Despite this limitation, our data provides an overview of which immunoreactive GABAergic cell groups are present in the different subregions. Our data showed that a diverse cell group of GABAergic cells are present at all dorsoventral levels of LEC. This is In line with previous findings. With regards to the anterior-posterior distribution, no data have so far been reported on the different immunoreactive cell groups in LEC. Moreover, our data indicate that all the different immunoreactive cell groups are present along the entirety of the anterior-posterior extent. An exception was the CCK population of GABAergic cells where none were detected in the anterior section, which suggests that either none or very few CCK cells are found in the anterior portion of LEC.

5.2.3 Functional implications of the distribution of GABAergic cell groups

The laminar distribution of the different GABAergic cell groups in LEC, gives a clue as to which cell types are involved in processing the in- and output information in the different layers. Moreover, LEC contains a variety of principal cells (Canto and Witter 2012) that inhabit the different laminae, these are most likely under the influence of the local GABAergic cells.

In L I we found that small populations of VIP, CCK and PV positive GABAergic cells were present. Considering the connectivity of this layer, these GABAergic cells are possible recipients of olfactory, perirhinal and amygdaloid inputs. These neurons might in turn target cells within the layer and thus indirectly modulate the output to different areas. Layers II and III

contain large populations of immunoreactive, PV, CB, CR and VIP GABAergic cells, which suggest that the cells projecting to the hippocampal formation are under strong inhibitory control of these cell types specifically. These GABAergic cells most likely receive input from neurons within these layers but could also be modulated by incoming input from cells in the deep layers of EC as well as by input from CA1, perirhinal, amygdaloid and olfactory areas (Canto & Witter, 2008). The deep layers V and VI show a different composition of GABAergic cell groups, as large proportions of the SST and NPY population are found in these layers compared to the superficial. This points to a different inhibitory control of the deep layers compared to the superficial layers where NPY and SST cells are sparse. Recordings of synaptic activity in the EC have shown a functional difference in the overall background inhibition between the deep and superficial layers (Woodhall et al. (2005), Greenhill et al. 2014). In line with our findings, these reports confirm the notion of a fundamental difference in inhibition between the superficial and deep layers of LEC.

The distribution of GABAergic cell groups across subregions and along the anterior-posterior axis of LEC, can provide information about which GABAergic cell types take part in modulating information processing in the different areas. As all cell groups were present in all subregions of LEC, our data indicate that the input-output connectivity of these areas are under diverse inhibitory influence,. The same is true for the connectivity of LEC along the anterior- posterior axis. Taken together, our findings indicate that a diverse group of GABAergic cells are involved in modulating streams of input and output LEC across all layers, subregions, and along the anterior-posterior axis of LEC.

5.2.4 Overlapping distributions of immunoreactive cell types

It is common for GABAergic cells to express more than one molecular marker, this has been reported in several areas of the brain (Kawaguchi and Kubota 1997, Markram, Toledo-Rodriguez et al. 2004, Xu, Roby et al. 2010) and is also true for EC. In our study, the PV and CB expressing cells had a highly comparable laminar and regional distribution across LEC. This is in accordance with a previous report (Fujimaru and Kosaka 1996) that revealed that PV and CB overlap in EC neurons was relatively common. As PV is only present in GABAergic cells, these findings suggest that the subgroup of neurons co-expressing PV and CB are GABAergic as well.

In L I we detected populations of VIP, CCK and PV cells. Based on morphological similarity of cells in this layer, the expression of PV and CCK appears to not overlap. Studies reporting a total separation between PV expressing and CCK cells support this notion (Kawaguchi and Kubota 1997, Freund and Katona 2007). In contrast, comparable cell morphology between VIP and CCK cells in this layer suggest possible overlap. Previous reports of CCK and VIP co-expression in cells suggest that there is a small overlap, it is the same could be true for LEC (Kawaguchi and Kubota 1997, Kawaguchi and Kondo 2002). VIP and CR co-expression in cells has previously been demonstrated in the neocortex (Kawaguchi and Kubota 1997), in EC of rats (Rogers, 1992) and is now confirmed by our double-labeling study of VIP and CR cells in mice. According to our study, the VIP and CR containing neurons are all GABAergic, and the majority of these cells are located in superficial layers II - III. Interestingly, the morphological cell types that express both VIP and CR was restricted to two forms, as they were either bipolar or small

globular multipolar cells. In the deep layers L V-VI, we found a high number of NPY and SST cells. There has so far not been any investigation into whether or not these two populations overlap in LEC. However, the morphological similarity of these cells in LEC does suggest that there might be an overlap. A previous study of NPY and SST expression in neurons have reported a high degree of overlap between the two markers (Kawaguchi and Kubota 1997). Furthermore, investigations of the connectivity of the double labeled NPY and SST cells showed that they were GABAergic projection neurons (Tomioka, Okamoto et al. 2005).

5.2.5 Co- expression of calcium binding proteins and neuropeptides with GABA

In our study, the neurochemical markers PV and NPY were exclusively detected in GABAergic cells. Our results in the case of PV neurons are in line with previous findings in LEC, in which a complete overlap between PV and GABA has been reported (Miettinen, Koivisto et al. 1996). For NPY co-expression with GABA in EC, little or no data has so far been reported. Nonetheless, a previous report from Kariagannis et al. 2009 suggests that NPY is mainly expressed in GABAergic cells. The co-expression of CB and CR with GABA in LEC has been previously been demonstrated to show partial overlap (Rogers 1992, Miettinen, Pitkänen et al. 1997, Wouterlood, van Denderen et al. 2000). Comparable to the CB study, we observed a substantial but not complete overlap for CB and GABA. Our results for the overlap between CR and GABA however, differed substantially in that we observed almost doubled numbers compared to what was reported in the previous studies. This could possibly be related to the difference in the

animals used, as immuno histochemical staining in the previous studies was performed in the rat while ours was performed in the mice. For the neuropeptide SST, we saw a significant deviation from a previous study where only sparse co-localization between SST and GABA in EC was detected (Wouterlood and Pothuizen 2000).These discrepancies might result from the use of the GAD 67 mouse model, which might allow for a better detection of GAD positive cells as compared to the immunostaining used in the previous study. Another explanation can be that the selected sections in our study contained a high number of GABAergic SST expressing cells compared to single labeled SST cells. However, unpublished data from our lab shows that in MEC the co-localization of GAD67 and SST is near complete. This is also in accordance with previous findings, which show an almost complete overlap for SST and GABA in the neocortex (Gonchar and Burkhalter 1997). For the markers VIP and CCK co- expression with GABA in EC has not been investigated. However, data on VIP and CCK overlap with GABA from the several areas of the brain (Kosaka, Kosaka et al. 1985, Kawaguchi and Kubota 1997, Gonchar, Wang et al. 2007) indicate partial overlap for both markers. Our studies indicate that this is true for LEC as well.

5.2.6 Neurochemical markers and cell types in LEC

Several lines of evidence have shown that there is an association between cell type and the expression of molecular markers. In our study of GABAergic PV and CB cells displayed great morphological diversity; these results are in line with previous reports of PV and CB cells in LEC (Wouterlood, Härtig et al. 1995, Fujimaru and Kosaka 1996). A number of studies have shown that PV is expressed in fast spiking cells such as basket and axo-axonic cells (Kosaka,

Katsumaru et al. 1987, Kawaguchi and Kondo 2002, Gulyás, Szabó et al. 2010)). Both of these cell types have previously been reported in LEC (Bühl, 1993) and Soriano et al. 1993). Although there is not much known about basket cells in LEC, results propose a role for these cells in modulating principal cell activity by perisomatic inihibition (Freund and Katona 2007).Basket cells have additionally been shown to have a role in synchronizing and coordinating neural activity (i.e network oscilliations) (McBain & Fishan (2001), Freund & Katona (2007)). The axo-axonic cells have demonstrated similar functional roles (Howard, Tamas & Soltesz (2005) but have also proved capable of both inhibiting and promoting spike activity in principal cells (Woodruff, 2011, Howard, 2005). Calbindin is an abundant marker, and it is often co –expressed with other molecular markers (Markram). The CB cell group therefore consists of a variety of cells and includes; basket, axo-axonic, double bouquet cells and bitufted cells as well as Martinotti cells (Markram, 2005). Based on these data, the PV and CB cell populations in LEC might comprise several functional cell types.

Our immunostain against VIP and CR showed a high prevalence of bipolar and small- medium sized round multipolar cells, this was in accordance with previous reports (Köhler and Chan-Palay 1983, Miettinen, Pitkänen et al. 1997, Wouterlood, van Denderen et al. 2000). Several studies of GABAergic VIP and CR expressing cells suggest that they often are providers of disinhibition, as they preferentially target other GABAergic cells (Gulyás, Hájos et al. 1996, Pfeffer 2014) . In LEC, the VIP and CR cells involvement in the circuitry has not yet been described, but it is possible that they might be providers of disinhibition here as well. Previous reports of pericellular basket VIP fibers in LEC, suggest that LEC might also contain a population of small

basket cells, which usually express VIP (Markram 2004). SST is a molecular marker that is associated with large basket cells and Martinotti cells (Markram 2004 and the Kstudy). In the neocortex, Martinotti cells are known to modulate dendritic input and they are involved in cross-columnar inhibition (Markram (2004). Martinotti cells in LEC have so far not been reported, and in our SST stain we did not detect any cells with bitufted dendrite morphology that these cells commonly display. A previous study (wouterlood) reported pericellular baskets of immunoreactive SST fibers in LEC, this suggest a SST positive basket cells might be present as well.

For the NPY stained cells, our findings also fall in line with previous reports of NPY cells with fusiform or ovoid cell bodies and a multipolar or bipolar configuration (Köhler, Eriksson et al. 1986). Little is known about the NPY expressing neurons in LEC. In the neocortex, NPY expression has been demonstrated in basket, bitufted and neurogliaform cells (Markram 2004, Olah (2009). Previous reports of bitufted cells as well as pericellular basket fibers in an earlier NPY study of EC (Köhler, Eriksson et al. 1986) suggest that there are NPY positive basket and bitufted cells in LEC. Not much is known about the bitufted cells but they have often been described to have an axonal tree that ramifies widely within a layer, and that they similar to the Martinotti cells, mainly target dendrites. Neurogliaform cells in LEC have to our knowledge not been described. If they exist in LEC they must be a very small population of cells as seen by the sparse NPY labeling. A high number of NPY cells in a circuit appear not to be necessary as these cells are capable of widespread and unspecific inhibition in large areas (Olah, 2009). Our data on CCK cell types in LEC differs from the previous study by Köhler (1986), where the CCK cells are described to also contain large multipolar cells, as

well as bipolar and bitufted cells. This discrepancy is most likely related to the pretreatment with colchinine in the Köhler study, which result in better staining of soma and proximal dendrites. CCK expression is found in basket cells, but has also been detected in bipolar, bitufted and martinotti cells (Markram, Toledo-Rodriguez et al. 2004).

5.2.7 Interneuron heterogeneity and LEC

The functional role of LEC is still under investigation but it has been implicated in non-spatial processing. By its connectivity, LEC appears to be a site of integration for parallel streams of information coming from both unimodal and polymodal areas (e.g olfactory and amygdaloid areas) which could later be relayed to the hippocampus. Recordings in freely behaving rats indicate that neurons in LEC respond to objects and their position in space, even showing a memory for the previous location of familiar objects (Hargreaves (2005) and Desmukh (2011). How these complex computations come about is largely unknown, but what becomes clear is that the LEC network would need a certain flexibility to regulate the parallel streams of input and the integration of these inputs at the cell, microcircuit and network level (McBain and Fisahn 2001). As information is believed to lie in the temporal and spatial firing patterns of cells (Stevens and Zador 1995), the flexibility to encode information at cell, microcircuit and network levels can be provided by GABAergic cells which can fine tune the system at a small and large scale. The purpose of the highly heterogenous groups of GABAergic cells in LEC as well as other areas in the brain would then most likely be to support and modulate the small and large scale network processes. At a small scale the GABAergic cells can reduce the spike

response of principal cells as well as other GABAergic cells at both dendritic and somatic levels, and thus have an effect on the encoding of input at the single cell. In a microcircuit, GABAergic cells can provide recurrent inhibition to principal cells as well as indirect modulation of these cells by disinhibition, and by these mechanisms they can decide the firing activity of different principal cell assemblies. At a network level GABAergic cells could be involved in coupling information across cortical areas by dynamically creating neuronal assemblies temporally and spatially (Buzsáki and Chrobak 1995). At the same time the INs could play a part in routing information by changing the balance of inhibition and excitation in the network (Akam and Kullmann 2010) such that incoming information can be selected or filtered out. As previously mentioned, the functional implications of different immunoreactive GABA cell groups in LEC are far from known but the diversity itself suggest that the GABAergic cells have multiple roles in the LEC network, and that they can be involved in different levels of information processing in LEC.

5.3 Future Directions

The data presented here gives an introduction to the different morphological and chemical groups of INs present in LEC of mice. The first part of the study showed the morphology of GABAergic cells in L II/ III. Due to the limitations of our methods, we were not able to provide any descriptions of the axonal trees for the various cell types. This would be informative, as describing their complete morphologies would give a better indication of what kind of cell types these are. Mapping the axonal tree would also give a suggestion as to which cells and layers the different cell

type target. For a better understanding of the functional roles of the GABAergic cells in LEC, an investigation of the electrophysiological properties of the different sub populations of GABAergic cells should be carried out. Alongside this, multi-cell recordings to map their connectivity to principal cells would provide more specific information about how the different cell types are involved in the LEC network.

The second part of our study gave an indication of how neurochemically identified interneuron groups are distributed across LEC. A study that includes more sections of LEC and hence covers more of the region would give a more complete picture of the different cell types. In particular, this would be important in order to accurately describe the cell distribution across lamina, subregions and along the anterior-posterior axis. Moreover, in the subregional distribution of cells across DLE, DIE and VIE, the number of cells per surface area should be considered as this could remove the bias when counting absolute cell numbers, as we did in our data.

Our data from the immunostaining of NPY, SST and CCK appeared limited as cells showed partial labeling of cell bodies and proximal dendrites. This difference is however likely due to a general low expression of CCK and NPY in cells. Although overall staining can be boosted by colchinine treatment, this is considered a problem due to serious side effects causing harm to the animal. Transgenic animal models where cells expressing these neurochemical markers are labeled intrinsically might be a good alternative to visualize the neuropeptide expressing cells.

As many studies report co-expression of several markers and we observed overlap in cell distribution and similar cell morphologies, an investigation

into the co- expression of several neurochemical markers in LEC cells might be a powerful tool to further discretize the GABAergic cell population.

6 CONCLUSION

From our morphological and immunohistochemical studies we discovered that the GABAergic cell population in LEC is both neurochemically and morphologically heterogeneous.

The different populations of GABAergic cells were found distributed across most areas of the LEC. The distributional pattern across layers revealed that there was a preference for either the deep or superficial layers of LEC. Based upon observed morphological similarities in our immunostain against VIP and CR, and location of immunoreactive cell bodies, we detected an overlap between the VIP and CR expressing cells. We also suggest there to be further possible overlaps in the LEC between different neurochemical expressing cell populations.

Despite the fact that most immunohistochemical studies in the EC have been performed in the rat, we did not see any remarkable differences in our immunohistochemical and morphological data, for the pattern of distribution and cell types. We did however detect a difference in the co-expression of SST and CR with GABA, which could be a specie difference or a result of the different methodologies used. The minor differences we detected for the neuropeptide stains for CCK, SST and NPY we suspect is due to the colchine treatment administered in previous studies.

Although we do not know what the functional roles are for the different GABAergic subpopulations in the LEC, the expression of the various neurochemical markers and cell morphologies gives us a clue as to which functional cell type they might be. The heterogeniety of GABAergic cells in LEC therefore suggests that a variety of cell types are involved in small and

large scale processes in LEC, much like what is seen in other areas of the brain.

REFERENCES

Acsady, L., T. Görcs and T. Freund (1996). "Different populations of vasoactive intestinal polypeptide-immunoreactive interneurons are specialized to control pyramidal cells or interneurons in the hippocampus." Neuroscience **73**(2): 317-334.

Aguado, F., E. Pozas and J. Blasi (1999). "Colchicine administration in the rat central nervous system induces SNAP-25 expression." Neuroscience **93**(1): 275-283.

Akam, T. and D. M. Kullmann (2010). "Oscillations and filtering networks support flexible routing of information." Neuron **67**(2): 308-320.

Ascoli, G. A., L. Alonso-Nanclares, S. A. Anderson, G. Barrionuevo, R. Benavides-Piccione, A. Burkhalter, G. Buzsáki, B. Cauli, J. DeFelipe and A. Fairén (2008). "Petilla terminology: nomenclature of features of GABAergic interneurons of the cerebral cortex." Nature Reviews Neuroscience **9**(7): 557-568.

Bacci, A., J. R. Huguenard and D. A. Prince (2003). "Functional autaptic neurotransmission in fast-spiking interneurons: a novel form of feedback inhibition in the neocortex." The Journal of neuroscience **23**(3): 859-866.

Bartko, S. J., B. D. Winters, R. A. Cowell, L. M. Saksida and T. J. Bussey (2007). "Perceptual functions of perirhinal cortex in rats: zero-delay object recognition and simultaneous oddity discriminations." The Journal of neuroscience **27**(10): 2548-2559.

Blakemore, C. and E. A. Tobin (1972). "Lateral inhibition between orientation detectors in the cat's visual cortex." Experimental Brain Research **15**(4): 439-440.

Boccara, C. N., F. Sargolini, V. H. Thoresen, T. Solstad, M. P. Witter, E. I. Moser and M.-B. Moser (2010). "Grid cells in pre-and parasubiculum." Nature neuroscience **13**(8): 987-994.

Buzsáki, G. and J. J. Chrobak (1995). "Temporal structure in spatially organized neuronal ensembles: a role for interneuronal networks." Current opinion in neurobiology **5**(4): 504-510.

Caballero-Bleda, M. and M. P. Witter (1993). "Regional and laminar organization of projections from the presubiculum and parasubiculum to the entorhinal cortex: an anterograde tracing study in the rat." Journal of Comparative Neurology **328**(1): 115-129.

Canto, C. B. (2011). "Layer specific integrative properties of entorhinal principal neurons."

Canto, C. B. and M. P. Witter (2012). "Cellular properties of principal neurons in the rat entorhinal cortex. I. The lateral entorhinal cortex." Hippocampus **22**(6): 1256-1276.

Canto, C. B. and M. P. Witter (2012). "Cellular properties of principal neurons in the rat entorhinal cortex. II. The medial entorhinal cortex." Hippocampus **22**(6): 1277-1299.

Canto, C. B., F. G. Wouterlood and M. P. Witter (2008). "What does the anatomical organization of the entorhinal cortex tell us?" Neural plasticity **2008**.
Dahlström, A. (1968). "Effect of colchicine on transport of amine storage granules in sympathetic nerves of rat." European journal of pharmacology **5**(1): 111-113.
Deshmukh, S. S. and J. J. Knierim (2011). "Representation of non-spatial and spatial information in the lateral entorhinal cortex." Frontiers in behavioral neuroscience **5**.
Freund, T. F. and I. Katona (2007). "Perisomatic inhibition." Neuron **56**(1): 33-42.
Fujimaru, Y. and T. Kosaka (1996). "The distribution of two calcium binding proteins, calbindin D-28K and parvalbumin, in the entorhinal cortex of the adult mouse." Neuroscience research **24**(4): 329-343.
Furtak, S. C., S. M. Wei, K. L. Agster and R. D. Burwell (2007). "Functional neuroanatomy of the parahippocampal region in the rat: the perirhinal and postrhinal cortices." Hippocampus **17**(9): 709-722.
Gloveli, T., D. Schmitz, R. Empson, T. Dugladze and U. Heinemann (1997). "Morphological and electrophysiological characterization of layer III cells of the medial entorhinal cortex of the rat." Neuroscience **77**(3): 629-648.
Gonchar, Y. and A. Burkhalter (1997). "Three distinct families of GABAergic neurons in rat visual cortex." Cerebral Cortex **7**(4): 347-358.
Gonchar, Y., Q. Wang and A. Burkhalter (2007). "Multiple distinct subtypes of GABAergic neurons in mouse visual cortex identified by triple immunostaining." Frontiers in neuroanatomy **1**.
Gulyás, A. I., N. Hájos and T. F. Freund (1996). "Interneurons containing calretinin are specialized to control other interneurons in the rat hippocampus." The Journal of neuroscience **16**(10): 3397-3411.
Gulyás, A. I., G. G. Szabó, I. Ulbert, N. Holderith, H. Monyer, F. Erdélyi, G. Szabó, T. F. Freund and N. Hájos (2010). "Parvalbumin-containing fast-spiking basket cells generate the field potential oscillations induced by cholinergic receptor activation in the hippocampus." The Journal of neuroscience **30**(45): 15134-15145.
Hafting, T., M. Fyhn, S. Molden, M.-B. Moser and E. I. Moser (2005). "Microstructure of a spatial map in the entorhinal cortex." Nature **436**(7052): 801-806.
Hargreaves, E. L., G. Rao, I. Lee and J. J. Knierim (2005). "Major dissociation between medial and lateral entorhinal input to dorsal hippocampus." Science **308**(5729): 1792-1794.
Howard, A., G. Tamas and I. Soltesz (2005). "Lighting the chandelier: new vistas for axo-axonic cells." Trends in neurosciences **28**(6): 310-316.
Insausti, R., M. Herrero and M. P. Witter (1997). "Entorhinal cortex of the rat: cytoarchitectonic subdivisions and the origin and distribution of cortical efferents." Hippocampus **7**(2): 146-183.
Isaacson, J. S. and M. Scanziani (2011). "How inhibition shapes cortical activity." Neuron **72**(2): 231-243.

Jones, R. and E. Bühl (1993). "Basket-like interneurones in layer II of the entorhinal cortex exhibit a powerful NMDA-mediated synaptic excitation." Neuroscience letters **149**(1): 35-39.
Kawaguchi, Y. and S. Kondo (2002). "Parvalbumin, somatostatin and cholecystokinin as chemical markers for specific GABAergic interneuron types in the rat frontal cortex." Journal of neurocytology **31**(3-5): 277-287.
Kawaguchi, Y. and Y. Kubota (1997). "GABAergic cell subtypes and their synaptic connections in rat frontal cortex." Cerebral Cortex **7**(6): 476-486.
Kondo, H. and M. P. Witter (2014). "Topographic organization of orbitofrontal projections to the parahippocampal region in rats." Journal of Comparative Neurology **522**(4): 772-793.
Kosaka, T., H. Katsumaru, K. Hama, J.-Y. Wu and C. W. Heizmann (1987). "GABAergic neurons containing the Ca 2+-binding protein parvalbumin in the rat hippocampus and dentate gyrus." Brain research **419**(1): 119-130.
Kosaka, T., K. Kosaka, K. Tateishi, Y. Hamaoka, N. Yanaihara, J. Y. Wu and K. Hama (1985). "GABAergic neurons containing CCK-8-like and/or VIP-like immunoreactivities in the rat hippocampus and dentate gyrus." Journal of Comparative Neurology **239**(4): 420-430.
Köhler, C. and V. Chan-Palay (1983). "Somatostatin and vasoactive intestinal polypeptide-like immunoreactive cells and terminals in the retrohippocampal region of the rat brain." Anatomy and embryology **167**(2): 151-172.
Köhler, C. and V. Chan-Palay (1982). "The distribution of cholecystokinin-like immunoreactive neurons and nerve terminals in the retrohippocampal region in the rat and guinea pig." Journal of Comparative Neurology **210**(2): 136-146.
Köhler, C., L. Eriksson, S. Davies and V. Chan-Palay (1986). "Neuropeptide Y innervation of the hippocampal region in the rat and monkey brain." Journal of Comparative Neurology **244**(3): 384-400.
Magee, J. C. (2000). "Dendritic integration of excitatory synaptic input." Nature Reviews Neuroscience **1**(3): 181-190.
Mainen, Z. F. and T. J. Sejnowski (1996). "Influence of dendritic structure on firing pattern in model neocortical neurons." Nature **382**(6589): 363-366.
Markram, H., M. Toledo-Rodriguez, Y. Wang, A. Gupta, G. Silberberg and C. Wu (2004). "Interneurons of the neocortical inhibitory system." Nature Reviews Neuroscience **5**(10): 793-807.
Mathiasen, M. L., L. Hansen and M. P. Witter (2015). "Insular projections to the parahippocampal region in the rat." Journal of Comparative Neurology.
McBain, C. J. and A. Fisahn (2001). "Interneurons unbound." Nature Reviews Neuroscience **2**(1): 11-23.
Miettinen, M., E. Koivisto, P. Riekkinen and R. Miettinen (1996). "Coexistence of parvalbumin and GABA in nonpyramidal neurons of the rat entorhinal cortex." Brain research **706**(1): 113-122.

Miettinen, M., E. Koivisto, P. Riekkinen Sr and R. Miettinen (1996). "Coexistence of parvalbumin and GABA in nonpyramidal neurons of the rat entorhinal cortex." Brain research **706**(1): 113-122.
Miettinen, M., A. Pitkänen and R. Miettinen (1997). "Distribution of calretinin-immunoreactivity in the rat entorhinal cortex: Coexistence with GABA." Journal of Comparative Neurology **378**(3): 363-378.
Mittmann, W., U. Koch and M. Häusser (2005). "Feed-forward inhibition shapes the spike output of cerebellar Purkinje cells." The Journal of physiology **563**(2): 369-378.
Naber, P. A., F. H. Lopes da Silva and M. P. Witter (2001). "Reciprocal connections between the entorhinal cortex and hippocampal fields CA1 and the subiculum are in register with the projections from CA1 to the subiculum." Hippocampus **11**(2): 99-104.
O'Keefe, J. and J. Dostrovsky (1971). "The hippocampus as a spatial map. Preliminary evidence from unit activity in the freely-moving rat." Brain research **34**(1): 171-175.
Pfeffer, C. K. (2014). "Inhibitory Neurons: Vip Cells Hit the Brake on Inhibition." Current Biology **24**(1): R18-R20.
Pitkänen, A., M. Pikkarainen, N. Nurminen and A. Ylinen (2000). "Reciprocal connections between the amygdala and the hippocampal formation, perirhinal cortex, and postrhinal cortex in rat: A review." Annals of the New York Academy of Sciences **911**(1): 369-391.
Rogers, J. H. (1992). "Immunohistochemical markers in rat cortex: co-localization of calretinin and calbindin-D28k with neuropeptides and GABA." Brain research **587**(1): 147-157.
Scoville, W. B. and B. Milner (1957). "Loss of recent memory after bilateral hippocampal lesions." Journal of neurology, neurosurgery, and psychiatry **20**(1): 11.
Shepherd, G. and S. Grillner (2010). Handbook of brain microcircuits, Oxford University Press.
Soriano, E., A. Martinez, I. Fariñas and M. Frotscher (1993). "Chandelier cells in the hippocampal formation of the rat: the entorhinal area and subicular complex." Journal of Comparative Neurology **337**(1): 151-167.
Stevens, C. F. and A. Zador (1995). "Neural coding: The enigma of the brain." Current Biology **5**(12): 1370-1371.
Stuart, G., N. Spruston, B. Sakmann and M. Häusser (1997). "Action potential initiation and backpropagation in neurons of the mammalian CNS." Trends in neurosciences **20**(3): 125-131.
Tomioka, R., K. Okamoto, T. Furuta, F. Fujiyama, T. Iwasato, Y. Yanagawa, K. Obata, T. Kaneko and N. Tamamaki (2005). "Demonstration of long-range GABAergic connections distributed throughout the mouse neocortex." European Journal of Neuroscience **21**(6): 1587-1600.

van Elburg, R. A. and A. van Ooyen (2010). "Impact of dendritic size and dendritic topology on burst firing in pyramidal cells." PLoS computational biology **6**(5): e1000781.
van Groen, T., P. Miettinen and I. Kadish (2003). "The entorhinal cortex of the mouse: organization of the projection to the hippocampal formation." Hippocampus **13**(1): 133-149.
Van Strien, N., N. Cappaert and M. Witter (2009). "The anatomy of memory: an interactive overview of the parahippocampal–hippocampal network." Nature Reviews Neuroscience **10**(4): 272-282.
Vetter, P., A. Roth and M. Häusser (2001). "Propagation of action potentials in dendrites depends on dendritic morphology." Journal of neurophysiology **85**(2): 926-937.
Witter, M. P. and F. G. Wouterlood (2002). The parahippocampal region: organization and role in cognitive function, Oxford University Press.
Witter, M. P., F. G. Wouterlood, P. A. Naber and T. Van Haeften (2000). "Anatomical Organization of the Parahippocampal-Hippocampal Network." Annals of the New York Academy of Sciences **911**(1): 1-24.
Wouterlood, F. G., W. Härtig, G. Brückner and M. P. Witter (1995). "Parvalbumin-immunoreactive neurons in the entorhinal cortex of the rat: localization, morphology, connectivity and ultrastructure." Journal of neurocytology **24**(2): 135-153.
Wouterlood, F. G. and H. Pothuizen (2000). "Sparse colocalization of somatostatin- and GABA-immunoreactivity in the entorhinal cortex of the rat." Hippocampus **10**(1): 77-86.
Wouterlood, F. G., J. van Denderen, T. van Haeften and M. P. Witter (2000). "Calretinin in the entorhinal cortex of the rat: Distribution, morphology, ultrastructure of neurons, and co-localization with γ-aminobutyric acid and parvalbumin." Journal of Comparative Neurology **425**(2): 177-192.
Xu, X., K. D. Roby and E. M. Callaway (2010). "Immunochemical characterization of inhibitory mouse cortical neurons: three chemically distinct classes of inhibitory cells." Journal of Comparative Neurology **518**(3): 389-404.